Rheological characterization of polymer melts with bimodal distributions

Shadrach kwakye-Nimo

A Thesis
in
The Department
of
Mechanical Engineering

Presented in Partial Fulfillment of the Requirements
for the Degree of
Doctor of Philosophy (Mechanical Engineering) at
Concordia University
Montréal, Québec, Canada

August 2022

CONCORDIA UNIVERSITY
School of Graduate Studies

This is to certify that the thesis prepared

By: **Mr. Shadrach kwakye-Nimo**
Entitled: **Rheological characterization of polymer melts with bimodal distributions**

and submitted in partial fulfillment of the requirements for the degree of

Doctor of Philosophy (Mechanical Engineering)

complies with the regulations of this University and meets the accepted standards with respect to originality and quality.
Signed by the Final Examining Committee:

_____ Chair
Dr.

_____ External Examiner
Dr. Savvas G. Hatzikiriakos

_____ External to Program
Dr. Zhibin Ye

_____ Examiner
Dr. Mehdi Hojjati

_____ Examiner
Dr. Martin Pugh

_____ Supervisor
Dr. Paula Wood-Adams

Approved by _____
Dr. Ivan Contreras, Graduate Program Director

_____ 2022

_____
Dr. Mourad Debbabi, Dean Gina
Cody School of Engineering

Abstract

Rheological characterization of polymer melts with bimodal distributions

Shadrach kwakye-Nimo, Ph.D.
Concordia University, 2022

Polymer melt exhibits complex relaxation and flow behaviors when subject to some form of deformation. The ensued stress experienced by the melt depends on the entire deformation history and not just the deformation rate or the magnitude. To better anticipate the response of melts to deformations, an understanding of their molecular structure is essential. This understanding helps not only in optimizing the process conditions, which turn to be big cost savers, but also enables the production of end-products with controlled and desirable properties.

The research presented here establishes correlations between the features of the molecular weight distributions (MWD) and the rheological behavior of broadly distributed bimodal HDPE and well tailored distributions of polybutadiene. We start by characterizing a set of high-density polyethylene (HDPE) materials which possess very high levels of polydispersity. Then, using statistical learning, the most important features influencing the rheological behavior are identified. We show that by using just the shape features of the MWD the relaxation behavior of the melt can be inferred. We proceed to investigate the behavior of polymer melt at the interface. Using the simple shear flow experimental setting, we eliminate the possibility of contributions from flow induced fractionation and show for the first time that surface segregation could occur in the absence of bulk shear gradient. We additionally show that apart from the surface enrichment being shear-rate dependent, the enrichment-depletion transition point also occurs at a much lower molecular weight value than predicted in literature. We then proceed to show the key role played by the short chain in surface fraction. By using bi-disperse polybutadiene designed to vary in both short chain length and volume, an enhanced relaxation of the melt was shown to positively improve the polymer surface fraction.

Dedication

This thesis is dedicated to my family. I am grateful for the tremendous efforts and sacrifices put in by each and everyone.

Acknowledgments

I would like to render special thanks to my supervisor, Prof. Paula Wood-Adams, for her immeasurable support throughout my journey as a PhD student. This research would also not have been productive without contributions from my main collaborators. To Dr. Yongwoo Inn and Dr. Youlu Yu I say a big thank you for providing me with such immense scientific inputs. I would also like to show my appreciation to my evaluation committee: Dr. Savvas G. Hatzikiriakos, Dr. Zhibin Ye, Dr. Martin Pugh and Dr. Mehdi Hojjati for sacrificing some time out of their busy schedule to undertake this evaluation process. I am also grateful for the assistance I received from the technical staffs, especially from Harriet Laryea who also happened to be a big sister. My group members at various stages supported this journey in diverse ways. Hence to Mohammadali, Milad, Bianca, Keroles, Mina and Cindi, I say a big thank you.

To my mum, thank you for always reminding me of my pledge of not returning home without the PhD. I can now say "I am coming home". To: Claudia, Jedidah, Rachel, Yaw and Akwasi, you have always been my lifeline under all circumstances. Thank you for standing by me. To my Friends: Ivy, Edmond, Martha, Aminat, the role you played as up-lifters will never be forgotten. I appreciate it.

A special appreciation to Chevron Phillips Chemical Company for funding this research. Without this enormous support my dream would not have been realized.

Contributions of authors

Chapter 3 is an articles that I co-authored with Prof. Paula Wood-Adams, Dr. Yongwoo Inn and Dr. Youlu Yu. I have conceptualized the project, designed and executed the experiments, and wrote the manuscript all with the guidance of the listed co-authors.

Chapter 4 is an article that I co-authored with Prof. Paula Wood-Adams, Dr. Yongwoo Inn and Dr. Youlu Yu. I have conceptualized the project, designed and executed the experiments, and wrote the manuscript all with the guidance of the listed co-authors. GPC data used in this work was provided by Chevron Phillips Chemical Company.

Chapter 5 is a draft manuscript that is yet to be submitted to an academic Journal. It is co-authored with Dr. Mostafa Sabzevari and Prof. Paula Wood-Adams. Dr. Mostafa Sabzevari designed and performed the experiment. I performed the simulations, carried out all data analysis, interpreted the results and wrote the paper all with the guidance of Prof. Paula Wood-Adams.

In preparation: a draft manuscript on the non-linear rheological behavior of bimodal HDPE is currently under preparation. This article is co-authored with Prof. Paula Wood-Adams and Dr. Yongwoo Inn. I have conceptualized the project, performed the simulations and drafted the manuscript all with the guidance of Professor Wood-Adams.

Contents

List of Figures

List of Tables

Chapter 1

Introduction

Rheology describes and assesses the deformation and flow behavior of all kinds of deformable materials. Its focus is on materials that do not obey Newton's law of viscosity; in other words, non-Newtonian fluids. Newtonian fluids are defined as fluids whose viscosity is unaffected by a change in shear rate, water serves as a perfect example. Non-Newtonian fluids however exhibit a wide range of behaviors referred to as viscoelastic behaviors ranging from, i.e. the theoretical sense, ideal viscous to ideal elastic.

Rheology serves as a useful tool in several domains. For example, in paint manufacturing it helps determine whether a wall paint would dry up too quickly thereby leaving behind traces of the brush or dry up too slowing thereby showing sagging. In the food industry, it is used to ensure that food and beverages maintain their consistency; that a yoghurt for instance would not sediments into its component after a while on the supermarket shelves. In this study however, focus would be on polymer melts.

In polymer processing a good understanding of rheological processes is key in determining not only the processability of the polymer but also in predicting the physical properties of the end-product. In fact, choosing the right shear-rate at which a melt is

extruded saves the enterprise a lot of money. The plastic industry is an integral component of the manufacturing sector, with a total revenue of $27.7B in 2019 according to Statistics Canada (StatisticsCanada, 2022). In this research the two polymer materials that were used are high density polyethylene (HDPE) and Polybutadiene.

1.1 Scope of study

The scope of this study was to highlight the important information contained in the features of the MWD when investigating the rheological behavior of polymer melts and to also study polymer fractionation at the interface. The structure of the thesis is as follows: the materials were first characterized and the influence of the features of their distributions on the rheological behavior was determined. The focus in this part was on linear viscoelastic properties of the material with the aim of obtaining information about the molecular structure of the material (Article I). The flow behaviour of the melt at the interface was next studied and the effect of the shear rate on the material's ability to have a surface enriched by short chains was established (Article II). The effect of both short chain length and their volume on a polymer's ability to enrich the surface was then determined and the effect of the MWD on the enrichment-depletion transition was investigated (Manuscript III). Finally, non-linear rheological studies were carried out with the influence of the features of the bimodality investigated (Manuscript IV). This thesis touches on different aspects of rheology and highlights the important role it plays in understanding the behavior of polymers.

Chapter 2

Polymer rheology: an overview

This chapter discusses the fundamental rheological principles, experimental methods upon which subsequent chapters are based and briefly reviews literature.

2.1 Basics

Polymer melts are composed of macromolecules which are made up of atoms linked through covalent bonding (Krevelen and Te, 2009). Those molecules could be composed of chains that are either linear, branched or even forming networks and greatly influence the rheological properties of the melt such as the viscosity. Polymers are mostly characterized by their molecular weights and that can be done by either their number average molecular weight (M_N) or their weight average molecular weight (M_W). There are also higher moments such as the z-average of the molecular weight (M_Z). The distribution of molecular weights in a polymer is referred to as the molecular weight distribution (MWD) and its breath is classified by the polydispersity index (PI) parameter defined as the ratio of two consecutive moments, expressed in a form such as $PI = M_W/M_N$.

The distribution of the molecular weights of the chains could be monodisperse or composed by a mixture of two monodisperse distributions which would then be referred to as bimodal distributions. In this study all our MWD are bimodally distributed.

The properties exhibited by a polymer greatly depends on its molecular weight distribution and the presence of branched chains. The effect that the presence of branches would have on the properties of the polymer would depend on both the length and quantity of branches in the material. Short chain branches are considered to have approximately 40 or less carbon atoms. Their presence in a melt influences the mechanical and thermal properties of the material. Long chain branches on the other hand are considered to have more than 40 carbon atoms and are known to greatly affect the melt's rheological behavior especially during processing.

In a polymer melt, the chains are entangled among themselves by varying extents. This results in an internal resistance when subjected to flow which is caused by the ensuing internal friction. Viscosity is a quantitative measure of that internal friction and is expressed as the force per unit area resisting the flow between adjacent layers of the fluid.

There are a lot of variables which affects the viscosity of a material- namely: temperature, pressure and shear rate. The higher the temperature, the lower the resistance to flow. Viscosity is extremely sensitive to temperature, hence when comparing different materials and to also have reproducible experimental results it is of greater importance to have the experimental temperature well under control. Viscosity also increases with increasing pressure, since a rise in pressure results in an increase in internal friction. For most practical purposes, the effect of pressure is not given much attention since most experiments are assumed to be performed under atmospheric conditions. With an increase in shear rate, a decrease in viscosity is observed. The shear rate dependence of viscosity is so crucial from a practical perspective as it dictates the energy required in processing

a melt.

The complex viscosity function is another measure of the viscoelastic flow resistance of a sample. Its absolute value is of importance since it can directly be related to the steady shear viscosity curve through the well-known Cox-Merz rule. The Cox-Merz rule states that the shear rate dependent viscosity function which is obtained from a rotational test would have an identical shape of curve to the complex viscosity curve obtained through an oscillatory test over a broad range of values. That is:

$$\eta(\dot{\gamma}) = |\eta^*(\omega)| \tag{1}$$

In Fig. 2.1, a shear-rate dependent viscosity curve is illustrated, it highlights two important regions:

(i) one in which the viscosity is observed to be independent of shear-rate which is the zone-referred to as the Newtonian plateau, the zone from which the zero-shear viscosity [discussed in subsection 2.1.1] is evaluated and

(ii) a part which is shear rate dependent.

The structure of the polymer has a great influence on the linear viscoelastic behavior of the melt and is discussed next.

2.1.1 Linear viscoelasticity

Determining the linear viscoelastic (LVE) behavior of a material is extremely useful in providing molecular details about the material. A test performed in the linear viscoelastic range entails subjecting the material to a form of disturbance; a disturbance small enough as to only disturb the molecules from their equilibrium position to a negligible extent. Test performed in the LVE thus serves as a probing technique. Such tests are based on

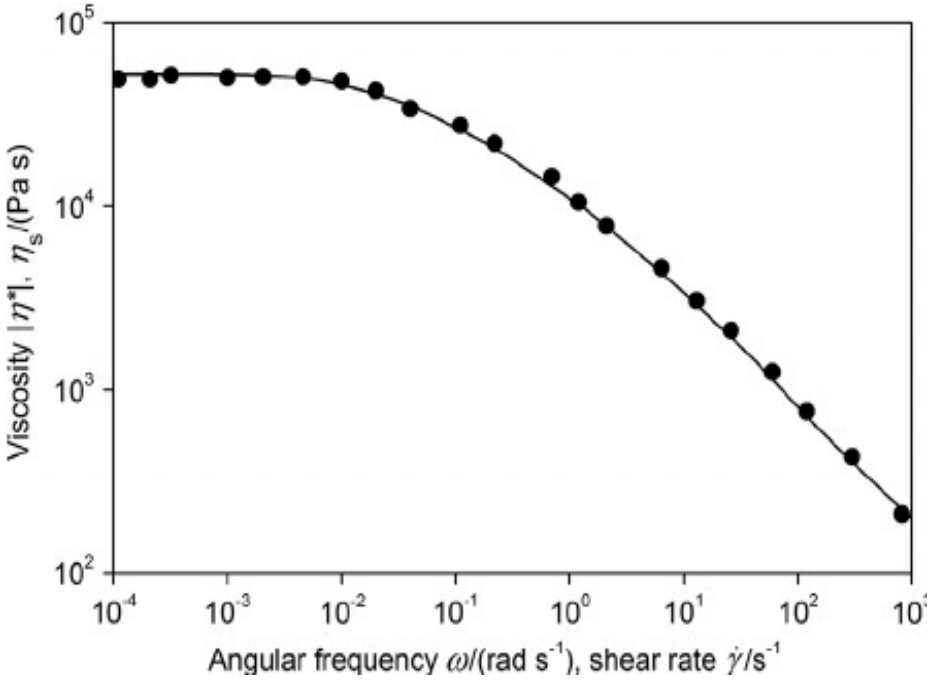

Figure 2.1: Viscosity curve (Laun et al., 2014)

the linearity principle which considers the stress experienced by a material at a current time as only depending on the strain at the corresponding time and those at previous times in an additive manner. This means that the longer the time elapsed between the current and past, the smaller the effect of the strains contributed from past times. This principle is referred to as Boltzmann superposition principle and it highlights the concept of "fading memory". The Boltzmann superposition principle holds not only for small deformations but also for very slow deformation. The following expression is one way of mathematically describing this principle:

$$\sigma(t) = \int_{-\infty}^{t} G(t - t^{'}) d\gamma(t^{'}) \tag{2}$$

where γ is the strain input, σ is the linear viscoelastic stress response and G is the relaxation Modulus (Tanner, 2000; Dealy and Larson, 2006). A corresponding expression

exists where σ is the stress input and γ is the linear viscoelastic response. The response of the viscoelastic materials to any form of deformation can be modeled by making use of a simple mechanical spring-dashpot analogies. Here the spring component represents the material's elastic response to the deformation while the dashpot component represents the viscous part.

There exist two models based on this analogy, the Maxwell and Kelvin model. The Maxwell model has the dashpot and springs connected in series and serves as a simple model in describing viscoelastic fluids, i.e. fluids which can be deformed indefinitely with no possibility of crosslinking. The Kelvin model on the other hand describes viscoelastic solids and is represented by a parallel connection of the dashpot and spring. By making use of several combinations of the above mentioned two models it is sometimes possible to estimate the expected response of a polymer melt under certain experimental conditions such as creep and small amplitude oscillatory shear (SAOS). The next section discusses the behavior of polymer melt in the LVE region.

Zero-Shear viscosity

As mentioned earlier, the viscosity of a melt changes with shear rate. A melt will flow readily at higher shear rate than at a lower value. As the shear rate approaches zero, the viscosity becomes independent of the shear rate; that is in the Newtonian plateau zone. The value of the viscosity in that zone is called the zero-shear viscosity (η_0) which is a material constant and serves as a useful indicator of the polymer molecular weight. There are two main factors affecting the zero-shear viscosity of a material, they are long chain branching and the weight average molecular weight. They both have significant impacts on the zero-shear viscosity, it is therefore empirical in the evaluation of the zero-shear viscosity of a material to ensure that the melt does not contain long chain branching, and this can be achieved through a size exclusion chromatograph equipped with a multi angle

light scattering (SEC-MALS). To obtain the zero-shear viscosity one has to extrapolate the complex viscosity curve, a method which is mostly not reliable, or perform a creep experiment until a steady state is reached and evaluated it from its slope in the steady state region.

The expected relation between the zero-shear viscosity and the weight average molecular weight is given by $\eta_0 = KM_W^{\alpha}$, with $\alpha = 3.5 \pm 0.2$. Any upward deviation of α from that range is mostly assumed to be due to the presence of long chain branching. Wasserman and Graessley (1996) indicated that such upward deviation could also be attributed to high level of polydispersity; an observation which has later been made by several other researchers (Ansari et al., 2011; Szántó et al., 2019; Kwakye-Nimo et al., 2022a).

Crossover modulus

When a polymer is subjected to a form of oscillatory deformation, it is possible to measure its elastic and viscous response. The storage modulus $G^{'}(\omega)$ measures the elastic response while the loss modulus $G^{''}(\omega)$ measures the viscous response. The point where $G^{'}(\omega) = G^{''}(\omega)$ is called the crossover modulus (G_c) and the frequency at which it occurs is the crossover frequency (ω_c). It separates the elastic portion from the viscous part.

The occurrence of ω_c at a lower value can serves as an indication of a system with a high molecular weight or a higher level of entanglements. The crossover modulus is also influenced by the polydispersity of the melt, its magnitude decreases with increasing polydispersity (Utracki, L. A., Schlund, 1987; Ansari et al., 2011) due to the effective release of constraint associated with an increase in polydispersity. In chapter 3 of this study, we show that the weight fractions of the two populations and the ratio of the peaks of the high molecular weight (HMW) to that of the low molecular weight (LMW) could also serve as good predictors of the evaluation of the crossover modulus (Kwakye-Nimo et al., 2022a), a method which does require only knowledge of the MWD.

Time-temperature superposition (TTS)

The experimental window within which a rheological behavior can be investigated is limited, a limitation imposed by the instrument. A way to circumvent that limitation is sometimes is by making use of the time-temperature superposition principle (Cho, 2016). Even though it is an empirical relation it has been very successful in predicting viscoelastic responses at either the short-time or long-time portion in both linear and non-linear viscoelastic regions. It is based on the phenomenon that the relaxation behavior of a melt has the same temperature dependence. Hence by changing the temperature at which a measurement is taken, it becomes possible to shift the data along the time or frequency axis by a shift factor a_T.

A material is termed as thermorheologically simple if the shifting results in an overlap of the experimental data. Polymers containing branched chains usually do not exhibit thermo-rheological simplicity, hence TTS can serve as a first step in ascertaining whether the polymer has a linear architecture or not. This is a necessary step since as described in earlier paragraphs, LCB and polydispersity both affects the zero-shear viscosity. Wood-Adams and Costeux (2001) in their study of LCB materials, used multiple shift factors at different time instead of a single one, a method which provided a better representation of the effect of temperature.

Molecular modeling

Various molecular models have been developed to capture the behavior of polymers at various length scale i.e., atomistic, macromolecular and mesoscopic scale. Examples of such models are reptation dynamics, coarse-grained molecular dynamics, and self-consistent field dynamics. This section will focus on reptation dynamics.

One of the greatest strengths of reptation based models is the ability to relate the molecular weight distribution of polymers to their rheological behavior. This allows

quantitative predictions of rheological behaviors. One such model is the tube model and was first proposed by De Gennes (1971) and Doi and Edwards (1986). The tube model describes the stress relaxation of a test chain. The test chain is restricted in its movement by its surrounding, a surrounding which is considered to acts as a tube in which the test chain finds itself. Thus, the test chain is considered as trapped in a tube, out of which it would have to escape so as to relax the imposed stress on it. This phenomenon of the presence of a tube allows the simplification of the topological interactions into a single mean field approximation instead of a many-body problem. The lateral movement of the tube is restricted to a characteristic diameter called the tube diameter which is independent of the chain architecture and rather depends on the type of material being considered.

The tube actively constrains a test chain at time scales larger than the equilibration time (Van Ruymbeke et al., 2007) and as such the test chains is only able to undergo lateral movements where its center of mass displaces itself through some back and forth movements along the curvilinear axis of the tube in order to escape it. This kind of mechanism is known as reptation (De Gennes, 1971) and is well captured by the diffusion equation. Theoretically the longest reptation time scales with the molecular weight through the expression $\tau_d \propto M^3$; experimental observations however show a relatively higher power law dependency of approximately 3.4. This difference in power law exponent indicated the existence of additional relaxation mechanism that needed to be accounted for, such as contour length fluctuation (Milner and Mc Leish, 1998; Likhtman et al., 2002) which captures the fluctuating movements of the end segments of the chains.

Another important mechanism is constraint release and tube dilation. In the initial considerations the tube was considered immobile but in actual fact it is not. It also moves relative to the moving test chain. When the motion of the tube is slower than the lateral motion of its internal segments it enhances relaxation of the test chain, a

mechanism known as constrain-release (Klein, 1986; Rubinstein et al., 1987; Masubuchi et al., 2008). Constraint release is captured mathematically by implementing a double reptation, that is by squaring the survival probability of the test chain. On the other hand, if the tube's motion is relatively faster than the test chain, it produces the effect of widening the tube, leading to an acceleration of both reptation and contour length fluctuation. This mechanism is referred to as tube dilation (Marrucci, 1985; Ball and McLeish, 1989).

There are several versions of the tube model which were built upon the original version of De Gennes and Doi and Edwards and accounts for these various additional mechanisms. In chapter 4 we employ the model as specified by Pattamaprom et al. (2000) while in chapter 5 the basic version from De Gennes (1971) work is used.

In this work we show that both the relaxation behavior of a melt and its material constants can be estimated from the shape features of their molecular weight distributions.

2.1.2 Non-linear viscoelasticity

In the non-linear viscoelastic range, neither the deformation rate nor its magnitude is small enough to allow the elements of the fluid to return to their initial equilibrium state. This makes the material's response to the deformation a function of both the deformation rate and amplitude. In this region of viscoelasticity, the deformation causes the chains to stretch and orient themselves in the flow direction. Characterizing a melt in the non-linear viscoelastic region has a lot of practical benefits since it is closer to industrial processing conditions.

Works performed on investigating the non-linear viscoelastic behavior of polymers have been diverse. Medium amplitude oscillatory shear (MAOS) and large amplitude oscillatory shear (LAOS) studies on polymers have shown the possibility of generating chain stretching using rotational rheometers (Wagner et al., 2011; Hoyle et al., 2014).

The default option of generating chain stretching though is by extensional flow and in this work, attention would be given to uniaxial extensional flow [see section B.3].

Polymers containing long chain branching are peculiarly known to exhibit strain hardening behaviors in extensional flow (Münstedt and Laun, 1981) but their linear counterparts do not; especially if they have a unimodal molecular weight distribution. On the other hand, distributions that were bimodally distributed with the HMW portion having a high weight average under some circumstances showed strain hardening (Gabriel and Münstedt, 2003; Szántó et al., 2021).

2.1.3 Standard flow

Polymer flow can be broadly grouped under shear and elongational flow. Most often a flow type can also be termed as viscometric if it attains some form of steady state as in tests such as creep and start-up flow.

Viscometric Flows

For a flow to be classified as viscometric, the shear rate of each of its constituent particles must be independent of time (Fridtjov Irgens, 2014). This type of flow is also called steady flow, in effect, the distance between two particles finding themselves on the same streamline remains unchanged throughout the deformation. Viscometric flow can be grouped into drag flow and pressure driven flow. Drag flows are generated when the fluid confined between two parallel surfaces is deformed by having only one of the surfaces moving while the other is stationary. In pressure driven flow on the other hand, the pressure gradient in the channel is the driving force in the shearing or deformation. In pressure driven flow the velocity profile is parabolic if Newtonian, but the fluid would exhibit a curved but non-parabolic profile if non-Newtonian. Drag flow on the other hand has a linear velocity profile. In Fig. 2.2 a schematic of the velocity profile generated by

drag (in simple shear) and pressure flow is shown respectively.

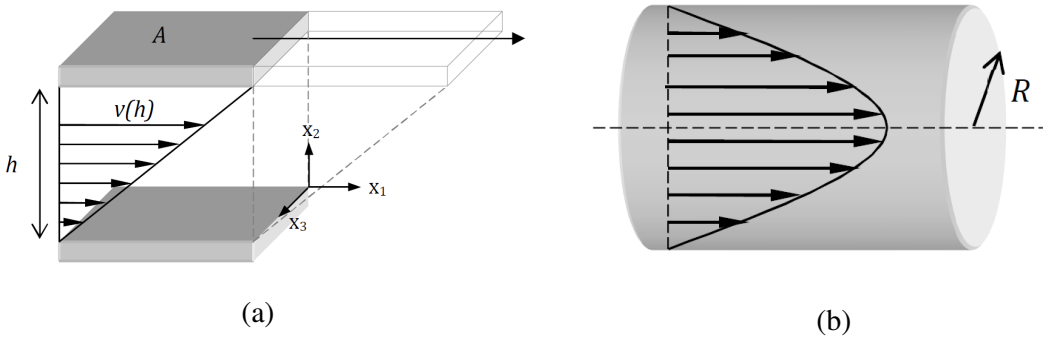

Figure 2.2: velocity profile (a) drag flow (b) Pressure driven flow

A material's response to deformations can be described by the measuring its stress. For non-Newtonian fluids the in-built stress is not only in the direction of flow but also in the perpendicular directions. Hence, three viscometric functions are used to fully describe a material's response; namely - the viscosity, the first and second normal stress coefficients. The first and second normal stress coefficients are used instead of the absolute stresses because non-Newtonian fluids are incompressible and as a result exhibits isotropic stress values thereby making the absolute stress values meaningless.

Extensional flows

In extensional flow the distance between particles that find themselves on the same streamline changes with time. Extensional flow can be classified into uniaxial, biaxial and planar extension. In uniaxial extension the material is elongated in a single direction. This results in a contraction in the other two directions (Dealy and Wang, 2013). The biaxial extension produces a flow type in which the material is stretched radially, and this is achieved by ensuring that there is no expansion along the axis of symmetry. The planar extension on the other hand generates a flow type in which the material is stretched in one direction, allowed to extend in the second direction but compressed in the third

direction. In Fig. 2.3 the schematic of the three extensional flow type is presented

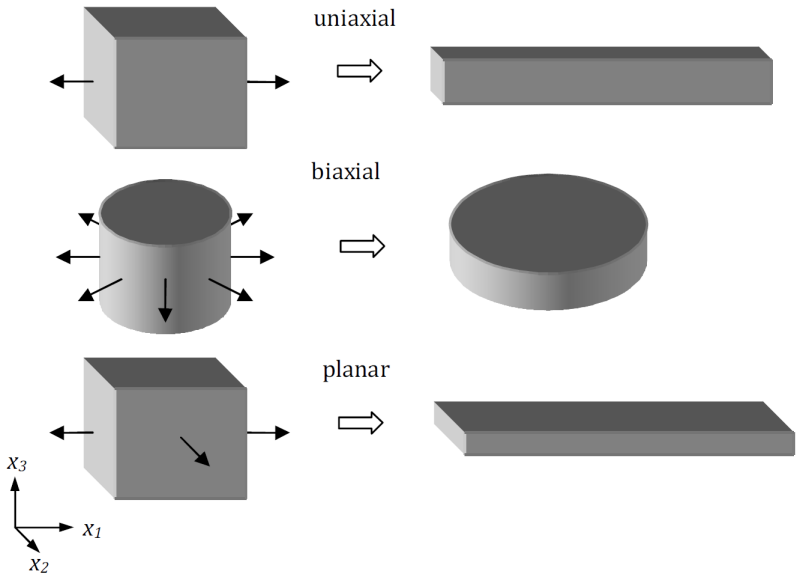

Figure 2.3: Uniaxial, biaxial and plater extension flow (Aho, 2011).

In this work, drag flow and uniaxial extensional flow are used to study the broadly distributed bimodal materials.

Material functions

Material functions are functions that relates the stress components to those of deformation during flow. They are usually expressed in terms of parameters such as stress, rate of stress, rate of deformation. An example of such functions is viscosity. Attention would be given to small amplitude oscillatory shear (SAOS), creep and uniaxial extension in subsequent subsections.

Viscosity function: The viscosity function describes the change in internal resistance during flow as a function of shear rate and it is given by the expression:

$$\eta = \frac{\tau}{\dot{\gamma}} \tag{3}$$

Creep compliance: Creep tests are very useful when studying the linear viscoelastic long-time behavior of materials. Such tests involve subjecting a material which is initially at rest to a constant stress and monitoring its strain response over time. The material function is called the creep compliance and it is defined as

$$J(t) = \frac{\gamma(t)}{\tau} \tag{4}$$

For a melt, over time the rate at which its strain changes become constant given a slope which is equal to the inverse of the zero-shear viscosity. The creep compliance could then be expressed as:

$$J(t) = J_s^0 + t/\eta_0 \tag{5}$$

Uniaxial Extension: Two material functions mostly used to describe extensional flow are the tensile stress growth coefficient and the tensile creep compliance. The tensile stress growth coefficient is obtained from a start-up of steady simple shear where a sample initially at rest is subjected to a constant Hencky strain rate (ε) and its stress response (τ_E) is monitored over time. The stress growth coefficient (η_E^+) is expressed as

$$\eta_E^+(t) = \tau_E(t)/\dot{\varepsilon} \tag{6}$$

The tensile creep compliance is also given by the expression

$$D(t) = J_e^0/3 + t/3\eta_0 \tag{7}$$

which is obtained by applying a constant stretching stress on the sample which was initially in equilibrium and monitoring its Hencky strain response.

Small amplitude oscillatory shear (SAOS): In SAOS, the deformation is sinusoidal. It involves dynamically loading the material at a predefined strain amplitude and a changing frequency. The amplitude is chosen to have a small value to keep the deformation in the linear viscoelastic region. During the deformation of a viscoelastic material there exist a phase lag between the applied stress and the strain response. If the strain is the preset variable in the rheometer, then it would have the mathematical form

$$\gamma = \gamma_0 sin\,\omega t \tag{8}$$

with ω being the angular frequency, γ_0 the strain amplitude. Differentiating Eqn. 8 with respect to time gives

$$\dot{\gamma} = \dot{\gamma_0} cos\,\omega t \tag{9}$$

The variable $\dot{\gamma}$ is the strain rate and $\dot{\gamma_0}$ is the strain rate amplitude. The corresponding stress response would have a lag since the material is viscoelastic. That lag is represented as δ hence the stress would be of the form

$$\tau = \tau_o sin(\omega t + \delta) \tag{10}$$

The above trigonometric function can be expanded to give

$$\tau = \tau_o(sin\,\omega t cos\,\delta + sin\,\delta cos\,\omega t) = \tau_o^{'} sin\,\omega t + \tau_o^{''} cos\,\omega t \tag{11}$$

The first component is in-phase with the strain and relates to the elastic response

while the out-of phase component relates to the viscous response. Dividing Eqn. 11 by the strain amplitude gives us the material function for SAOS

$$\frac{\tau}{\gamma_0} = G^{'} cos\,\omega t + G^{''} sin\,\omega t \tag{12}$$

The parameter $G^{'}(\omega)$ is called the storage modulus and represents the amount of energy stored in the material and $G^{''}(\omega)$ is called the loss modulus and represent the amount of energy dissipated. The relationship between the two viscoelastic moduli is called the loss factor expressed as

$$tan\delta = \frac{G^{''}}{G^{'}} \tag{13}$$

The complex viscosity can also be derived from the storage and loss modulus using the expression

$$|\eta^*| = \sqrt{\left[\left(\frac{G^{'}}{\omega}\right)^2 + \left(\frac{G^{''}}{\omega}\right)^2\right]} \tag{14}$$

2.1.4 Flow related instabilities in rheometry

Rheological data can sometimes be marred by flow related perturbations such as slip, migration, melt fracture. To correctly interpret rheological data, one would have to consider such factors. The subsequent two subsections would discuss two of such phenomena: slip and migration.

Wall slip

Slipping between sample and the wall is known to occur under almost all circumstances (Hatzikiriakos, 2012). For smooth surfaces, i.e. surfaces with a lower value of surface energy, the chains detached themselves directly from the surface to join the flow.

This is known as true slip or an adhesive slip failure. On a high energy surface on the other hand, the chains prefer to detach themselves from a layer close to the surface rather than the surface itself and is referred to as apparent slip or cohesive failure. The slip zone is a layer of thickness relatively smaller when compared to the bulk fluid. In our work we show that it is a layer which is relatively rich in short chains as compared to the bulk (Kwakye-Nimo et al., 2022b). Wall slip affects the velocity profile given an impression of the existence of a discontinuity in speed especially at higher shear rate.

Studies involving slip has touched on several aspects. The effect of the molecular weight and molecular weight distribution on wall slip was studied by Ansari et al. (2013). They found slip to strongly depend on both the weight average molecular weight (M_W) and the molecular weight distribution. An increase in M_W had the effect of decreasing the slip velocity while an increase in polydispersity had the converse effect on the slip velocity.

Using tracer particle velocimetry in a simple shear flow experiment to investigate the effect of short chains content on slip, Sabzevari et al. (2014b) worked on binary blends materials with varying short chain contents incorporated in highly entangled monodisperse melts of polybutadiene. They observed a substantial increase in slip velocity for blends whose short chains component had length smaller than that of the molecular weight between entanglement.

Inn (2015) studied wall slip and melt fracture and the relation they had to flow induced fractionation. By comparing unimodal samples to bimodal sample of similar molecular characteristics, the slip velocity of the bimodal samples was observed to be higher than that of the unimodal samples in the regions just before slip-stick sets in. The authors attributed this observation to the high level of short chain content in the bimodal samples.

By accounting for entropic contributions to surface fractionation in a capillary flow

system, Ebrahimi et al. (2016) used the double reptation model to predict the slip behavior of both unimodal and bimodal samples. This resulted in predictions that were closer to experimental observations, thereby highlighting the possible effect that slip has on molecular fractionation. Najm and Hatzikiriakos (2020) improved the model by incorporating the effect of shear rate.

Sattari et al. (2022) used HDPE materials tailored to show a systematic change in their molecular weight distribution with the aim of studying wall slip in bimodal HDPE with a sliding plate rheometer (SPR). Slip velocity is known to be independent of the MWD at higher stress values (Ansari et al., 2013). In their work, Sattari et al. (2022) observed that, the stress value from which slip velocity is independent of the molecular weight distribution was a function of short chain content and the value lowered by higher short chain content.

In our work, we sought to understand the relationship between surface migration and slip and in chapter 4 it will be shown that wall slip suppresses surface migration.

Migration

Migration effects could occur in a fluid when the elements of the fluids are exposed to some form of force imbalances. In suspension for example the constituent elements of the fluid would not have the same density, and this could lead to migration when the fluid is deformed. In polymer melts, especially in the case of pressure driven flows, migration is driven by disparity in chain length (Van der Gucht et al., 2002a) coupled with the fact that the shear rate at the wall is relatively lower than that in the mainstream flow. This disparity in shear rate results in a flow-induced fractionation where chains of smaller sizes migrate towards the wall (Hariharan et al., 1991). It is believed that in the absence of bulk shear gradient, surface migration is not expected to occur (Dorgan and Rorrer, 2015).

A system is said to be in thermodynamic equilibrium if there is no net macroscopic flow of either matter or energy within itself or between it and the external environment. This is hardly the case during polymer processing, especially for materials with longer relaxation times or for processing conditions that are carried out at elevated temperature. In our work, our system was not in thermodynamic equilibrium; yet useful information could still be obtained as shown in previous studies (Ebrahimi et al., 2016).

Entropic segregation is another factor which drives surface segregation at the interface. Shorter chains will preferentially adsorb themselves to the surface since they do possess more chain end segments per unit volume which allows them to easily compensate for the entropic penalty (Van der Gucht et al., 2002a). The thickness of the segregated region was shown not to be constant but to depends on the width of the surface profile and increases with the chain stiffness (Mahmoudi and Matsen, 2016, 2017).

The pioneering works of Tanaka et al. (1997) involved using a scanning force microscope to investigate the surface mobility of binary, ternary blends and polydisperse polystyrene films. They observed in all cases that, the surface of their materials was in the glass-rubber transition state even at room temperature. This they attributed to the excess free volume which according to them was induced by the surface segregation of the chain end groups. They later on made similar observation by developing another technique to investigate the surface mobility which did not require chemical labeling but instead employed the Gordon-Taylor mixing rule (Tanaka et al., 2002). The surface enrichment observed in this second study was higher than what has been theoretically predicted by Van der Gucht et al.

Another study involved the use of surface layer matrix-assisted laser deposition time of flight technique to study surface fractionation, performed by Hill et al. (2018). This technique also helped them distinguish species with no need of chemical labelling. Their

study was performed on polystyrene and poly(methyl methacryalate) with low polydispersity. They did also observe an entropically driven surface enrichment of short chains after sample annealing.

Musil and Zatloukal (2011) studied die drool of linear HDPE. The collected drool was observed to comprise of relatively shorter chains and was narrowly distributed as compared to the bulk distribution. This, they attributed to flow induced fractionation which they believed occur only at a region near the die wall. They further observed that, the onset of drool and its magnitude correlated with the onset and intensity of slip. Inn (2015) observed that the mid-plane section of a melt from a capillary extrusion was composed of high molecular weight chains while the section near the wall had much shorter chains. Flow induced fractionation was proposed as a key contributing factor to such observations.

Most of the experimental works were carried out using a capillary rheometer, which had flow induced contributions as a result of the shear rate gradient; nevertheless in all those studies, surface enriched by short chains was observed (Schreiber and Storey, 1965; Schreiber et al., 1966; Shelby and Caflisch, 2004; Inn, 2015; Ebrahimi et al., 2016). Accessing the interfacial layer has been challenging, attempts were made using a microtome to slice out a thin layer of the extrudate of a melt from an extruder (Schreiber and Storey, 1965; Schreiber et al., 1966; Shelby and Caflisch, 2004; Inn, 2015; Ebrahimi et al., 2016). By using a microtome to cut a thin sample of the extrudate, the section of the melt which was obtained and analyzed was the layer close to the bulk at the plane of failure and not the layer on the surface. In this work we circumvented these challenges by obtaining debris from a simple shear flow experiment and collected the resulting debris directly on glass substrates.

One of the specific contributions to knowledge of this work was not only to obtain

reliable experimental data on surface segregation but also showing that, contrary to theoretical predictions surface fractionation still occurs with slip even in the absence of a bulk shear induced gradient. This is addressed in chapter 4 and 5.

2.1.5 Experimental methods

Rheometers are instruments design to measure the viscoelastic responses of materials and can be broadly grouped into three categories: pressure flow (e.g. capillary rheometer), drag flow such as in a rotational rheometer (e.g. parallel plate fixture), rectilinear flow (e.g. SPR) and extensional flow (e.g. SER fixture). This section would focus on shear and drag flow since pressure flow-based instruments were not used.

Drag flow-based instruments

Drag flow-based instruments have the advantage of providing a high torque resolution and accurate temperature control. Their limitation is in the maximum deformation rate that can be attained. The two drag flow types of interest to this study are those generated with a parallel-plate of a rotational rheometer and the sliding plate rheometer.

Parallel plate rheometry The parallel-plate fixture was used for three major experiments in this work, creep, SAOS and the preliminary test for the linearity region. A schematic of the parallel-plate fixture is shown in Fig. 2.4.

In the parallel plate fixture the strain rate varies along the distance from the rotation axis. The shear rate is obtained from the expression:

$$\dot{\gamma} = \frac{\Gamma r}{H} \tag{15}$$

The parameter Γ is the angular speed, r the location of any point on the disk and H

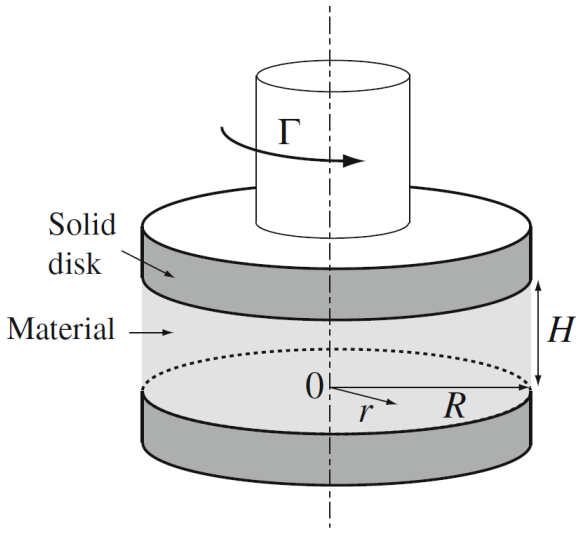

Figure 2.4: Parallel-plate rheometer geometry (Philippe, 2014)

the gap between the plates. The stress is given by the expression:

$$\tau = \frac{3M}{2\pi R^3} \tag{16}$$

with M being the torque and R the radius of the plate. With the stress and shear-rate, most other material functions can be obtained.

Rectilinear flow

The sliding plate rheometer comprises of two parallel plates between which the sample is placed [see Fig. 2.5]. One of the plates (8) would move relative to the other one fixed (4) to subject the sample to rectilinear flow.

At the center of the fixed plate is attached a transducer (7) which records the local stress as the material is deformed. With the stress measured at the center of the sample, the SPR provides the benefit of producing experimental results that are free from edge effects. The moving part is equipped with Teflon rails which not only prevents secondary

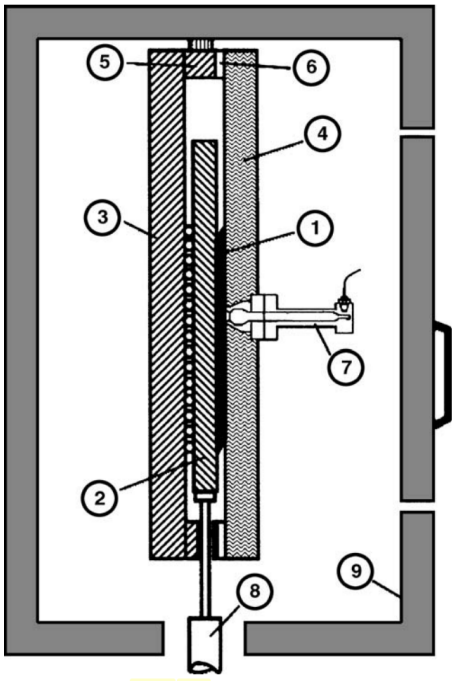

Figure 2.5: Schematic representation of the sliding plate rheometer (Xu et al., 2007)

flow but also helps reduce the possibility of oxidative degradation.

In the sliding plate rheometer, the nominal shear rate is obtained from the velocity of the moving plate (V) and the gap between the two plates (h) through the following relation:

$$\dot{\gamma}_n = V/h \tag{17}$$

The actual deformation experienced by the melt happens to be different from the nominal shear rate since polymer melts slip when flowing over surfaces. To obtain the true shear rate, the effect of slip is subtracted for the nominal shear rate to give the expression:

$$\dot{\gamma} = \dot{\gamma}_n - \frac{2u_s}{h} \tag{18}$$

with u_s being the slip velocity. The slip velocity is assumed to be the same for both plates. From the above expression a plot of the nominal shear rate versus the gap between the plates taken at different values gives a straight line with a slope of equal to $2u_s$.

The sliding plate rheometer was original design to measure the shear stress during experiments which required a large and rapid shear deformation of polymer melts. This made it an ideal instrument to measure non-linear viscoelastic properties of polymer melts and has been used extensively in studies involving wall slip (Hatzikiriakos and Dealy, 1991; Park et al., 2008; Sabzevari et al., 2014b; Sattari et al., 2022) and even in the determination of the normal stress differences (Xu et al., 2007). In this study, the SPR was used to generate rectilinear flow from which the debris left behind was collected and analyzed and detailed in chapter 4 and 5.

Extensional flow

Uniaxial extensional experiment There are several types of fixtures available, design to carry out elongation measurement. The fixture is mounted in the heating chamber of a rotational rheometer. In this work we used the Sentmanat extensional Rheometer (SER). SER can be used to carry out experiments such as start-up of steady shear, simple extension, creep and stress relaxation.

The SER comprises of two drums with either one of them rotating or both counter rotating. The generated force in the sample is calculated from the torque. The test specimen is molded as in the form of a thin rectangular strip and attached to the drum through clamps [see Fig. 2.6].

A limitation of the SER is in attaining steady state flow during experimental measurements, since upon one full rotation of the drum the test sample would start winding up upon the clamp thereby introducing unexpected results. Hence most extensional rheological measurements are performed using unsteady start-up extension. Upon stretching

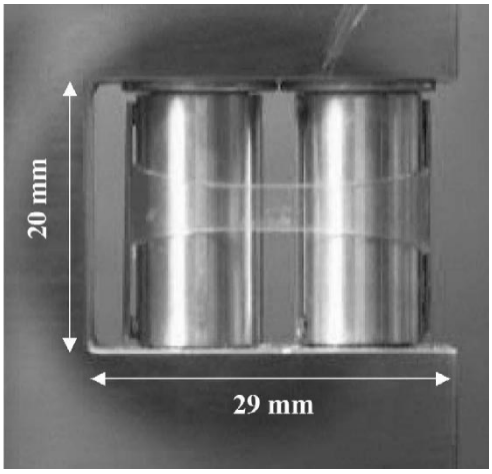

Figure 2.6: SER fixture. Sample attached to counter rotating drums (Sentmanat et al., 2005)

the material, the strain rate called the Hencky strain rate is giving by the expression:

$$\dot{\varepsilon}_H = \frac{2\Omega R}{L_o} \tag{19}$$

with R being the drum radius, L_o the initial length and Ω the drum rotation speed. At very low Hencky strain rate, that is under conditions in which the deformation rate is small, the material is being probed in the LVE. The curve obtained in that zone is called the linear viscoelastic envelop and is used as a reference from which an upward deviation is understood as an exhibition of strain hardening by the material while a downward deviation is an exhibition of strain softening.

2.2 Literature review

Research works involving polymers has touch on different aspects of the field of rheology. A few are discussed next. Zang et al. (1987) calculated the recoverable compliance

of blends by making use of a blending law which was based on knowledge of the respective recoverable compliance of its components, their zero-shear viscosities and its power law dependence on the respective weight average molecular weight. The blending law was in good agreement with experimental data and was extended to account for polydisperse samples.

Creep experiments are very useful in revealing relaxation features that can escape dynamic tests. Gabriel et al. (1998) made use of creep recovery in shear to observe the influence that the molecular structure of the melt has on the rheological behavior. Their materials were composed of LDPE which had long chain branches and LLDPE which had short chains. The LCB that were contain in LDPE were observed to be responsible for the relative low melt elasticity and short relaxation times. A striking difference observed between LDPE and LLDPE was that LDPE unlike LLDPE obeyed the time-temperature superposition in both creep and recoverable compliance. Further investigation using DSC revealed that the non-superposition behavior of LLDPE could be attributed to the immiscibility of the linear molar mass components with the short chain contents resulting in two separate relaxation mechanisms.

The effect the weight average molecular weight and the polydispersity of a MWD had independently on the rheological behavior of a melt was studied by Kazatchkov et al. (1999). They used two sets of LLDPE materials. The first set was made of nine materials which were designed to have the breadth of their MWD varying from 3.3 to 12.7 while the M_W remained approximately constant. In the second set, the materials had their polydispersity constant at an approximate value of 4 while their M_W varied. They observed that an increase in polydispersity resulted in an increase in the zero-shear viscosity, flow activation energy, degree of shear thinning and extrudate melt swell. The melt fracture performance was rather deteriorated by an increase in polydispersity. A critical polydispersity value was observed to give an optimal processing conditions for

the materials they studied. The influence that increasing the value of M_W had on the rheological behavior was to increase the zero-shear viscosity and extrudate swell while resulting in a decrease of the shear rate value for the onset of melt fracture.

Vega et al. (2003) showed that the physical entanglement of a melt can be affected by the polymerization processes during synthesis. Using twelve materials made of metallocene polyethylene (m-PE) and metallocene-Polypropylene (m-PP) having M_W ranging from 25-185 kg/mol with confirmed linear architectures, they calculated the material's respective plateau modulus using the expression:

$$G_N^0 = \frac{2}{\pi} \int_{-\infty}^{+\infty} G''(\omega) dln\omega \tag{20}$$

The values of G_N^0 obtained for m-PP fell within the expected range specified in literature while those of m-PE were lower than expected. The tube model was used to ascertain the validity of the experimental data before reaching to the conclusion that the physical entanglement of the melt can be affected by the polymerization processes during synthesis.

The effect of M_Z on the linear viscoelastic behavior of a melt was illustrated by Vega et al. (2012). Making use of polymers with M_Z/M_W two order of magnitude higher than M_W/M_N enabled them to study the effect of having chains of higher molecular weight at the tail end of the MWD on rheological behaviors. Their results were compared with narrowly distributed MWD polymers with the same M_W. They observed that even at a constant M_W value the zero-shear viscosity of a melt is greatly influenced by the third moment of the molecular weight distribution.

In another related study, the influence of incorporating small amount of very high M_W tails on the melt's linear viscoelasticity was studied by Otegui et al. (2013). They remarked that the polydispersity in terms of M_W/M_N is not enough to judge the effect

of MWD on the zero-shear viscosity. They observed an increase in both the Newtonian viscosity and steady state recoverable compliance when compared to predictions for linear chains. They concluded that, not only was the width of the distribution of importance when it comes to the elastic properties of a melt but also the third (M_Z) and fourth moment (M_{Z+1}).

Szántó et al. (2019) studied the linear viscoelasticity of HDPE materials which had up to 50% of its distribution composed of ultra-high molecular weights and polydispersity as high as 1000. The expected power law dependence of the zero-shear viscosity with M_W for linear polymers which is 3.6 was recovered when the data was corrected for polydispersity. Additionally, the tube model was able to recover the MWD from dynamic measurements for even this type of materials with extremely high polydispersity index.

A lot of work has also been done in quantitatively predicting rheological behaviors. Those studies can be grouped into two: direct and inverse problem. In the direct approach, the linear viscoelastic property of a melt is predicted by using parameters such as the plateau modulus, the value of the molecular weight between entanglement and the scaling law for the zero-shear viscosity. These parameters can mostly be obtained from literature and with the addition of knowledge of the molecular weight distribution, linear viscoelastic properties can be inferred. In the inverse problem on the other hand, the MWD is predicted from the rheological parameters.

Several researched were conducted which involve the use of the direct approach to predict rheological responses of material. Cloizeaux (1990) provided a solution to the diffusion equation representing the motion of the chain in the tube that accounted for contributions from fluctuations. It was of the form:

$$F(t, M) = \frac{8}{\pi^2} \sum_{p_o dd} \frac{1}{p^2} exp(-p^2 U(t)) \tag{21}$$

where $U(t)$ is given by

$$U(t) = \frac{t}{\tau_{rept}} + \frac{1}{H} g\left(\frac{Ht}{\tau_{rept}}\right) \tag{22}$$

The first term in $U(t)$ represents the relaxation by reptation as specified by Doi and Edwards and the second term accounts for the contributions of fluctuations. An empirical modification to the solution provided by Cloizeaux was provided by Van Ruymbeke et al. (2002a) to slow down the relaxation of short chains; chains of length lower than four times the value of the molecular weight between entanglement so as to improve the quantitative prediction of the linear viscoelastic response.

Vega et al. (2004) used the reptation model to investigate the dynamics of a melt having ultra-high molecular weights. The model accurately predicted the linear viscoelastic response in the contour length fluctuation region which is the region where the theoretical number of entanglement in the material is less than 100 ($M_r/M_c = 100$). The experimental values of M_r/M_c for their materials were in the range of 15-220, out of which the calculated value for the molecular weight at which pure reptation (M_r) is expected for polyethylene was obtained to be 800,000. This Mr value was higher than theoretical predictions for polybutadiene and polystyrene. The authors concluded that existing model needs modification to be able to account for differences in chemical composition.

den Doelder (2006) tested the single exponential double reptation (DRSE) (Doi and Edwards, 1986) and the modified time-dependent diffusion (DRmTDD) double reptation model (Van Ruymbeke et al., 2002a) on a set of simulated MWD with the aim of determining how the zero-shear viscosity and the recoverable compliances were related to the moments of the MWDs. The observations made based on the application of the DRSE model was that for the zero-shear viscosity apart from its dependence on M_W had an additional slight dependence on M_Z/M_W while in the case of the DRmTDD

the dependence of the zero-shear viscosity on M_W was different for different M_W with the strongest dependence observed to be at 100000 g/mol. Regarding the steady state compliance, the DRSE model was found to depend on the combination of both the first (M_Z/M_W) and second polydispersity index (M_{Z+1}/M_Z) while being constant in M_W whereas the DRmTDD showed some dependence on M_W. He therefore recommended that for full analysis the use of the DRSE was preferable.

Several other works involved the use of the inverse approach, some of which are discussed next. Carrot and Guillet (1997) predicted the average molecular weights and polydispersity index of several materials by provided a solution to the "inverse" problem. They made use of a simplified molecular dynamic method. They avoided getting an ill-posed solution by limiting their analysis to distributions that had bell-shaped Wesslau MWD. They stated that at least 3 to 4 decades of data from dynamic measurements was needed for an optimal performance of the model. This would enable the model to fully account for tube renewal process and constraint release. Additionally, they proposed that the ratio of the minimum frequency attainable in a dynamic test to the crossover frequency need to have a value lower than 10^{-3}.

Van Ruymbeke et al. (2002b) modified Cloizeaux model in finding solution to the inverse problem. They dealt with the ill-poisedness of the problem by using a non-parametric approach. Their MWD function were specified by using the generalized exponential function (GEX) unlike the Wesslau function used by Carrot and Guillet (1997). The GEX function had the advantage of being able to represent bimodal distributions. Van Ruymbeke et al. (2002b) remarked that the minimum range criterion specified by Carrot and Guillet (1997) did not under all circumstances represent their data well and that the ratio of the minimum frequency attained in a dynamic test to the crossover frequency as specified by Carrot and Guillet seemed to be a decreasing function of the polydispersity of the material. They also remarked that the high frequency range limits

of the dynamic test cannot be neglected especially in cases were the MWD contains a sizable number of short chains so as not to ignore the region of tube fluctuation dominated frequencies which had a greater contribution coming from the short chains.

Pattamaprom et al. (2008) also provided a solution to the inverse problem from a dual-constraint inversion scheme. Their model had the advantage of providing solutions for both linear and branched chains.

A whole lot of works also focused on polymers with different architectures. Wood-Adams et al. (2000) worked on both linear and branched m-PE. They investigated the effect of M_W, MWD and short chain branch (SCB) on the linear viscoelastic behavior of their materials. They reported that with an increase M_W, there was an increase in the zero-shear viscosity and a decrease in the shear rate value at which shear thinning started. An increase in the breadth of distribution led to a broadening of the transition region between the Newtonian plateau and the shear thinning zone. Also, an increase in LCB content resulted in an increase in the zero-shear viscosity, the breadth of the relaxation spectrum, the level of shear thinning and a broadening of the zone between the Newtonian plateau and the power law. It can be said from their study that the effect of LCB on rheological behavior were the same as those of M_W and polydispersity combined. SCB however had no effect on the linear viscoelastic properties.

Trinkle and Freidrich (2001) showed the effectiveness of the use of Van Gurp-Palmen plot in determining polydispersity and distinguishing between molecular architectures. For linear polymers with narrow MWD, the Van Gurp-Palmen plot superposed irrespective of the M_W of the material but with an increase in the Polydispersity then, the complex modulus (G^*) decreased linearly for $\delta \leq 60$. García-Franco et al. (2008) showed however that the above mentioned relation does not hold for LCB because of the combined effect of the LCB and polydispersity.

Hussein et al. (2006) made observations similar to those of Wood-Adams et al. (2000).

They studied the influence of the molecular structure on both rheology and thermorheology of m-PE. They additionally observed that the flow activation energy was sensitive to both the weight average molecular weight and branching content.

Morelly and Alvarez (2020) Studied four HDPE materials with unknown polydispersity and level of branching. They investigated the sensitivity of extensional flow behavior to polydispersity and LCB. Using Van Gurp-Palmen plot they related trends observed in extensional viscosity to the polydispersity and LCB of the materials. Their results showed that Van Gurp-Palmen plot was sensitive enough to LCB and was able to quantitatively distinguish the degree of LCB in industrial polymer. They concluded that LCB has a much greater effect on non-rheological behavior than polydispersity.

Musil and Zatloukal (2011) studied die drool from two materials with identical M_N and M_W and were interested in investigating the effect of long chain branching, shear viscosity and melt elasticity on die drool. They observed that with an increase in LCB, shear viscosity, M_W and melt elasticity came an increase in the formation of drool. The drool sample for all the materials studied was observed to be composed of lower M_W as compared to their respective bulk distribution leading to the conclusion that die drool represents low Molecular weight fractions of their bulk. As shear rate increased, the drool specimen had their M_N and M_{Z+1} parameter moving to lower values while M_W and M_Z remained unchanged implying that the amount of short chains polymer fractionated increased as the flow intensity increased. Die drool was also observed to correlate with slip. The onset of drool occurred at the transition slip-stick region and the higher the slip-stick intensity the higher the amount of drool produced.

While a lot of work has been done on the rheological behavior of melts. The influence that the features of the molecular weight distribution have on the rheological behavior of melts is yet to be addressed. Additionally, no experimental data on polymers fractionation near a surface has ever been produced for simple shear flow systems. In this study

we address that.

We show in chapter 3 that the linear viscoelastic response of a melt can be inferred from the features of its molecular weight distribution.

In chapter 4 the interfacial layer is accessed for the first time. We show that surface fractionation has some shear rate dependency, that the enrichment-depletion transition point occurs at a value lower than theoretical predictions. We also show that contrary to the long-standing believe of having a single slip mechanism based on the surface energy of the wall, that both adhesive and cohesive slip could occur at the same time.

In chapter 5 we further show that polymers relaxation influences surface fractionation and hint on the possibility of the enrichment-depletion transition point not to being constant as initially expected but being a function of the MWD.

2.3 Objectives of this study

The objectives of this work are as follows:

(1) to show that, the shape features of the MWD can be used to infer both rheological and relaxation behaviors of melts

(2) to show that, surface fractionation occurs in simple shear with slip even in the absence of bulk shear rate gradient

(3) to show that, during surface fractionation, contributions from the intermediate chains are the most significant.

Chapter 3

Linear viscoelastic behavior of bimodal polyethylene

In this chapter we characterized all the bimodal high-density polyethylene studied. The influence of the breadth of the distribution on the value of the zero-shear viscosity is shown. We also introduce ways of characterizing the bimodality of the molecular weight distributions and show that features of the distributions could be used to predict rheological behaviors of melts.

The chapter is based on the following publication: *Kwakye-Nimo, S. et al. Linear Viscoelastic Behavior of Bimodal Polyethylene. Rheol. Acta 2022, 61 (6), 373–386*

3.1 Introduction

Linear viscoelasticity (LVE) is an important tool in characterizing the rheological behavior of polymer melts (Ferry, 1980; Dealy and Larson, 2006). It has been used in that regard in several different ways. A few examples are: obtaining insight into the branching structure and the effect that long chain branching (LCB) has on both the zero

shear viscosity and the breadth of the relaxation spectra (Wood-Adams et al., 2000) or even determining the molecular weight distribution of a polymer from knowledge of its LVE properties (Ramkumar and Wiest, 1996; Van Ruymbeke et al., 2002a; Pattamaprom et al., 2008). Experiments performed in the LVE range probe the rheological response of the material without disturbing its internal structure retaining useful structural information (Dealy and Larson, 2006). This non-invasive probing approach of the molecular structure is possible due to the linearity principle. The linearity principle states that the stress in a material at a current time, depends not only on the strain at that time but also on those at previous times in an additive manner. An underlining assumption here is that the longer the time elapsed between the current and past times, the smaller the effect of the strains contributed from past times. This principle is referred to as Boltzmann superposition principle and it highlights the concept of "fading memory".

The most used LVE experiment is oscillatory shear, due to its straightforward implementation. But to access the LVE properties of materials having high molecular weights with very broad molecular weight distributions (MWD), i.e. materials having very long relaxation times, creep experiments become very helpful (Inn and Rohlfing, 2012). Every LVE experimental techniques has its inherent limitation (Morrison, 2001). It is therefore a common practice to interconvert material responses using known mathematical formulas (Ferry, 1980); or to perform a test repeatedly at different temperatures and shift the output to a reference temperature of interest. This technique is known as time-temperature superposition (TTS) and it is very useful in extending experimental data past the frequency limit of the instrument. LVE can be used to investigate the molecular structure because it relates to the dynamics of the polymer chains. For the materials used in this study which have high molecular weights and very broad, bimodal MWDs, both creep experiment and oscillatory shear experiments are used to probe the material's response.

The distribution of relaxation times after a polymer melt is subjected to a step shear strain is captured in its relaxation modulus (Ferry, 1980) and can be described in terms of the relaxation spectrum $H(\lambda)$. There exists also the retardation spectrum which is linked to the creep compliance (Dealy and Larson, 2006; Cho, 2016). In effect, the relaxation and retardation spectra can be described as fundamental characteristics which generalize the viscoelastic properties of a polymer and can be used as an alternative way of visualizing the LVE behavior of polymer melts (Briedis and Faitel'son, 1976; Ferry, 1980; Gramespacher and Meissner, 1992; Dealy and Larson, 2006; Stadler, 2010). An advantage of characterizing a melt using its relaxation spectra is that experiments performed under different flow conditions can be combined through their spectra enabling an LVE investigation spanning over a much broader range.

The relaxation spectrum has been used to effectively investigate different rheological aspects of many different types of polymeric materials. Apart from linear polymers, star polymer melts of varying functionality and arm molecular weights have been characterised in this way (Hatzikiriakos, 2000). It has been also observed in randomly branched chains that an increase in LCB leads to a rise in the slow relaxation modes (Stadler and Mahmoudi, 2013). It has also been successfully applied in the study of interfacial phenomenon (Gramespacher and Meissner, 1992; Shaayegan et al., 2012), and in more challenging materials such as clay suspensions (Shukla et al., 2020). The use of the spectra as a means of characterizing a wide range of materials is thus very robust. Here we use the relaxation spectra to characterize the LVE properties of the polyethylene with very broad MWDs.

Polyethylene comprises a major portion of the plastics market due to its relative low cost, good processability and excellent physical properties. A 2019 market research on plastic production, which involved 17 different categories of plastics, estimated a yearly global production of 359 million tonnes with polyethylene making up 27% of

that market; highlighting the important role polyethylene plays in the plastic industry (Senet, 2021). There are several different types of polyethylene, each type presenting different molecular characteristics and structures (Liu et al., 2002; Stadler et al., 2007; Szántó et al., 2019) . Here we are concerned with linear, bimodal HDPE which has specific behaviors associated with the breadth of the molecular weight distribution and the bimodality.

Bimodal HDPE is known to show peculiar rheological properties (Ansari et al., 2013; Inn, 2013). Such as a stronger power law dependency of the zero shear viscosity on the weight average molecular weight (Munoz-Escalona et al., 1999; Ansari et al., 2011) and longer relaxation times than their unimodal counterparts (Munoz-Escalona et al., 1999; Inn and Rohlfing, 2012).

The effect of the breadth and shape of the MWD of a polymer on the relaxation behavior is enormous. The effect of the breadth of the distribution is seen in the transition between the plateau and terminal region of the relaxation modulus. Narrowly distributed unimodal distributions have narrower relaxation time distributions resulting in a well defined and distinguishable plateau region (Graessley, 1974) and they show a shorter characteristic relaxation time. Their zero-shear viscosity plateau will extend to higher frequencies for lower M_W. As the breadth of the distribution increases, the plateau modulus region becomes less pronounced, the characteristic times shift to higher values and the zero-shear viscosity plateau ends at a lower frequency (Kazatchkov et al., 1999). Additionally, a broader MWD is known to generally have the following effects: it leads to a decrease in the crossover modulus which is the point separating the viscous from the elastic time scale of a melt. Coupled with the influence of the molecular weight it leads to higher zero-shear viscosity (Kazatchkov et al., 1999; Hatzikiriakos, 2000; Szántó et al., 2019). In the viscosity curve, the transition zone from the Newtonian to power law behavior smears out (Hua-feng et al., 2016) and the optimum processing performance of

a polymer melt is also known to be a function of the breadth of the MWD (Kazatchkov et al., 1999). There are however few experimental studies looking in detail at the effect of very broad MWDs and particularly bimodal MWDs of polyethylene on the relaxation spectrum.

While studies involving the relaxation spectra of polymers have touched on several aspects, none has yet addressed the influence of the features of a bimodal distribution on the relaxation behaviors of HDPE. In this article, the linear viscoelastic properties of a set of broadly distributed bimodal metallocene HDPE are studied. We establish correlations between features of the MWD both in terms of the moments and the bimodal parameters to those of the relaxation spectra. This approach of probing the rheological response of different materials by making use of the shape features of the molecular weight distribution, could be useful during the material designing process and could serve as a first step before running computationally expensive simulations.

3.2 Materials and Methods

All materials were supplied by Chevron Phillips Chemical Company (CPChem). Two types of HDPEs are used in this study. The first type is a set of metallocene HDPE, all bimodally distributed and are referred to as HDPE-1 to HDPE-9. These materials were synthesized through a dual-metallocene catalyst system in a single loop-slurry reactor at CPChem and possess a very broad polydispersity index (M_W/M_N) ranging from 7.1 to 32.8 in addition to having large weight-average molecular weights (M_W). Their number-average molecular weights (M_N) also vary from 8.6 to 35.7 kg/mol, a range far broader than those studied by Ansari et al. (2011) whose samples were tailored to have M_N essentially constant. The second type is a unimodally distributed material and is referred to as HDPE-10. It was produced using CPChem's proprietary MarTECH®Loop Slurry

Process technology with Cr-catalyst at CPChem. HDPE-10 is broadly distributed and is used in this study for comparison with its bimodal counterparts. These materials are hexene-ethylene copolymers with densities ranging from 0.935 to 0.957 g/cm^3. For the materials with bimodal MWDs, their HMW components have higher SCB level than their LMW components by a factor ranging from 3 to 6.

Our bimodal materials can be grouped into three different sets. In the first set we have 2 materials: one with predominantly a single large mode of low molecular weight (LMW) chains with a very small fraction of high molecular weight (HMW) chains while the second material has an approximate equal population of LMW and HMW chains [Fig.3.1a]. In the second set, the breadth of the MW distributions is constant with only the peak heights changing [Fig.3.1b]. In the last set the materials have distributions with the LMW component decreasing with a corresponding increase in HMW component [Fig.3.1c]. This affords us the opportunity to explore in more detail how the MWD influences the relaxation behavior of the polymers. Table 3.1 lists the various molecular parameters of the samples used in this study, and the graphs of the MWDs are presented in Fig.3.1.

The measurement of MWD of our bulk and debris samples were obtained using a SEC-MALS system following the method described by Yu et al. (2005). The SEC-MALS system was equipped with a GPC system, an IR-5 infrared detector (Polymer Characterisation SA, Spain) and a multi-angle light scattering photometer detector, DAWN®(Wyatt Technology, CA). The DAWN® MALS detector is an eighteen-angle light scattering photometer that is attached to the GPC-IR® system through a hot-transfer line controlled at $150^o\,C$. Polyethylene solution with a nominal concentration of 1.5 mg/mL was prepared by the auto-sampler at $150^o\,C$ for 5 hours before injection. Degassed TCB mobile phase containing 0.5 wt.% BHT was pumped through an inline filter before going through the SEC columns in an oven set at $150^o\,C$. The fractionated polymer solution was first eluted

through the MALS photometer where its light scattering signal was recorded before passing through the IR-5 detector where its concentration was quantified.

The DAWN ® MALS detector was calibrated using neat toluene that had passed through a 0.02 μm Whatman filter (Sigma Aldrich) at room temperature. The system was normalized using narrow MWD polystyrene (PS) standard (American Polymer Standards) of a M_W of 30 kg/mol with a concentration of 5-10 mg/mL in TCB; at the given chromatographic conditions, the radius of gyration (Rg) of the PS standard was ca. 5.6 nm using the Fox-Flory equation coupled with its Mark-Houwink exponent under the chromatographic conditions (Flory and Fox, 1951) . Refractive index increments dn/dc used in this study was 0.097 mL/g for PE dissolved in TCB at $135^o\,C$. At each chromatographic slice, both the absolute molecular weight (M_W) and the radius of gyration were obtained from the Debye plots (Wyatt, 1993). A high-density PE with broad MWD, Marlex™ HiD9640 (Chevron Phillips Chemical, TX) was used as the linear PE control.

Table 3.1: Molecular parameters of polymers studied

Sample	M_N (kg/mol)	M_W (kg/mol)	M_Z (kg/mol)	M_W/M_N	M_Z/M_W	Density g/cc	Modality *
HDPE-1	35.7	352.6	1932.3	9.9	5.5	0.956	B
HDPE-2	11.09	266.1	998.7	24.0	3.75	0.953	B
HDPE-3	25.9	202.6	624.2	7.8	3.1	0.943	B
HDPE-4	25.8	203.1	547.3	7.9	2.7	0.936	B
HDPE-5	27.2	192.7	517.3	7.1	2.7	0.935	B
HDPE-6	8.6	283.2	1034.9	32.8	3.7	0.952	B
HDPE-7	9.5	211.0	901.8	22.2	4.3	0.956	B
HDPE-8	9.5	225.5	827.2	23.8	3.7	0.953	B
HDPE-9	10.8	202.0	922.0	18.6	4.6	0.957	B
HDPE-10	15.18	232.10	1733.0	15.3	7.5	0.950	U

*B refers to bimodal samples and U refer to unimodal samples.

The Zimm-Stockmayer approach (Zimm and Stockmayer, 1949; Zimm and KILB, 1969) was used to determine the amount of LCB in ethylene homopolymers. The curves

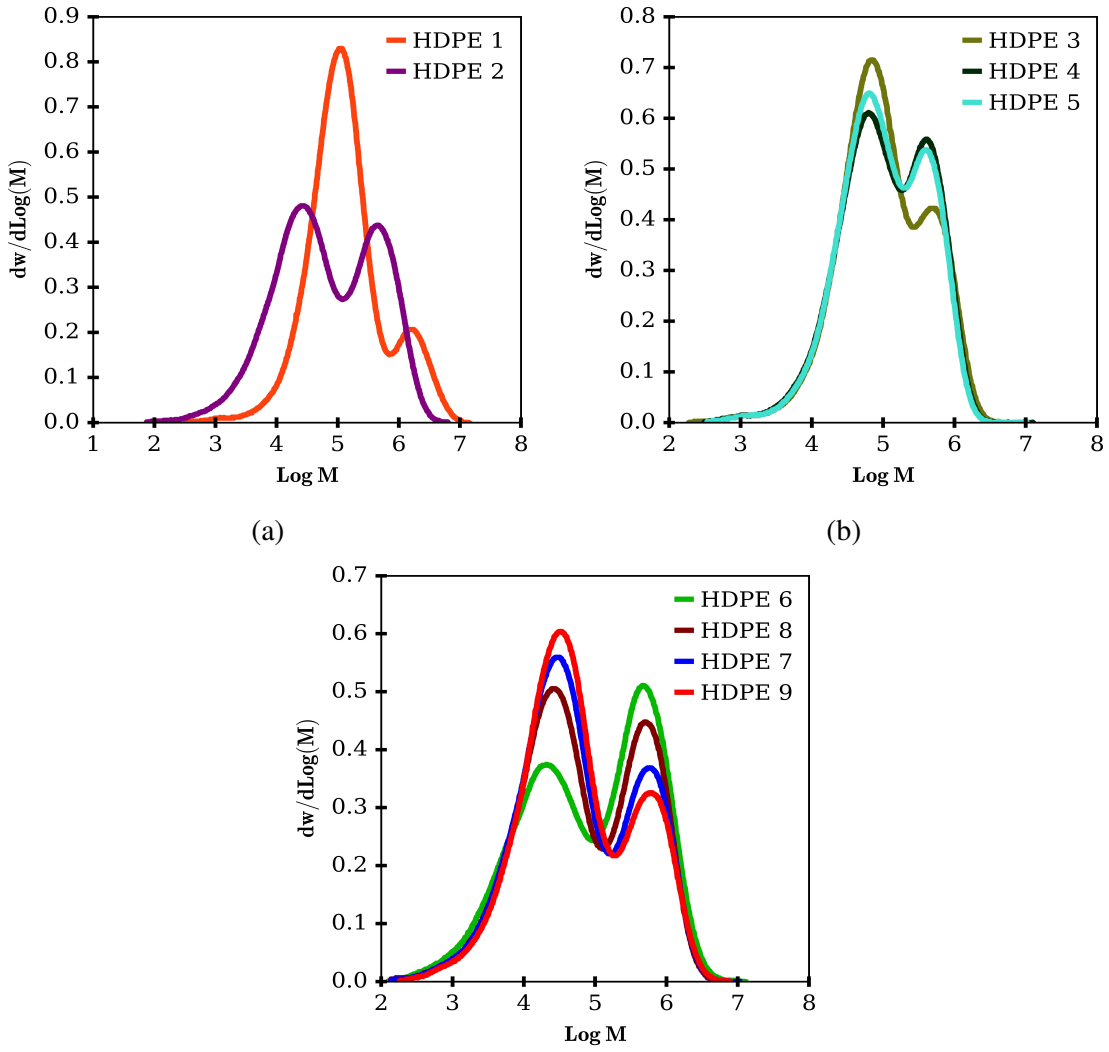

Figure 3.1: Molecular weight distributions of the materials studied

in Fig.3.2 show no negative deviation from the linear control resin, therefore we conclude that no detectable long chain branching is present in our materials.

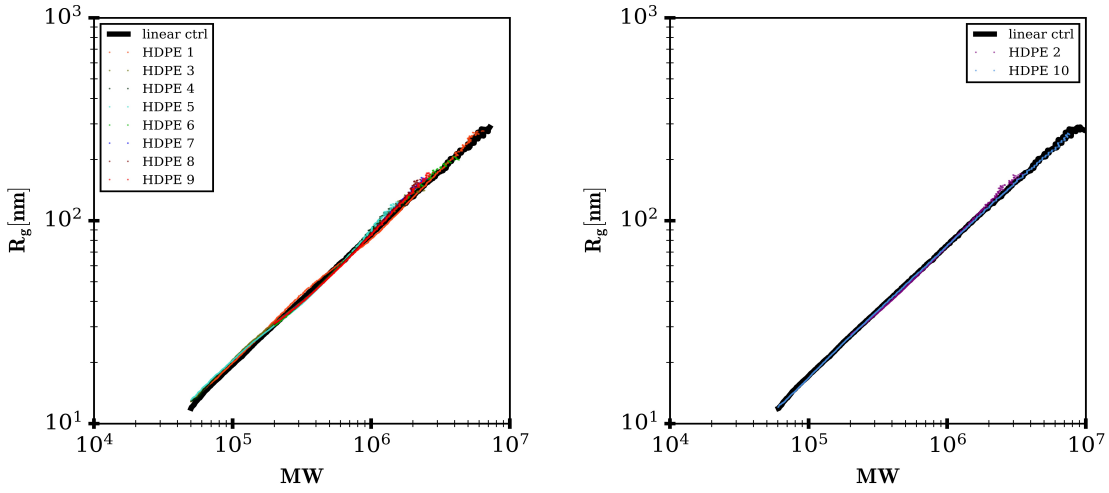

Figure 3.2: Plot of R_g versus M_W for all experimental materials showing no negative deviation from the linear control.

LVE properties of the bimodal materials were measured using Anton-Paar's MC502 rheometer with a plate-plate geometry of 25 mm diameter at a 1 mm gap. Our specimens were prepared by compression molding at a pressure of 15 tons and temperature of $190^o\,C$ for 4 minutes, they were then allowed to melt for an extra 2 minutes after which they were quenched. All rheological measurements were carried out in nitrogen atmosphere after a 45-minute period for stress relaxation after sample loading. Time sweeps experiments were performed at an angular frequency value of 0.1 rad/s and a strain value of 1% for hours ranging from 8 to 28 hours depending on the material, to ensure no change in material functions during the creep experimental window. No thermal degradation was observed. The LVE properties of the unimodal sample was measured at CPChem, using Anton Paar's MCR 501 rheometer at a temperature of $190^o\,C$ with 25 mm diameter and a 1.6 mm gap.

To ensure the shear oscillation experiments were performed in the linear viscoelastic region, strain sweep experiments were performed on all the materials to enable us to choose an appropriate strain amplitude under which the shear oscillation experiments would be performed. The shear oscillation experiments were performed at temperatures ranging from $170^o\,C$ to $210^o\,C$ and the data was shifted to a reference temperature of $190^o\,C$ following the $G^{'}$ method present previously (Wood-Adams and Costeux, 2001). All the samples were thermo-rheologically simple [see section A.2] and the flow activation energies in Table 3.3.

Preliminary creep experiments were performed to determine the stress level that will keep the experiment in the linear viscoelastic region. That was achieved by performing the creep experiment at different stresses (40, 60 and 80 Pa) for between 8 to 28 hours. The creep compliance curves from these experiments superposed indicating linearity. Therefore, for all the materials studied, the creep experiments were performed at a stress level of 40 Pa for time durations ranging from 8 to 28 hours, that is, until steady state was reached, as determined by a constant slope of the creep compliance curve at long times. We note that this does not correspond to reaching the terminal zone in the SAOS behavior. The creep experiments were carried out under nitrogen atmosphere at a temperature of $190^o\,C$. The data used for our analysis is the average of 5 repeated experiments using different specimens.

3.3 Determination of the relaxation spectra

There are several experimental methods for determining the relaxation spectra. One of them is by the use of stress relaxation after cessation of incomplete constant shear rate flow, a technique especially useful when material stability is an issue (Meissner, 1978). It can also be obtained indirectly from a creep experiment (Kaschta and Schwarzl, 1994a,b;

Kraft et al., 1999), or from the complex modulus measured under small amplitude oscillatory shear (SAOS) (Marin et al., 1975; Montfort et al., 1984; Vega et al., 1996). The measured LVE properties are linked to the relaxation $H(\lambda)$ and retardation $L(\lambda)$ spectra with the following expressions:

$$J(t) = J_g + \int_{-\infty}^{+\infty} L(\lambda) \left[-e^{-t/\lambda}\right] dln(\lambda) + t/\eta_o \tag{23}$$

$$G^{'}(\omega) = \int_{-\infty}^{+\infty} H(\lambda) \frac{\omega^2\lambda^2}{1+\omega^2\lambda^2} dln(\lambda) \tag{24}$$

$$G^{''}(\omega) = \int_{-\infty}^{+\infty} H(\lambda) \frac{\omega\lambda}{1+\omega^2\lambda^2} dln(\lambda) \tag{25}$$

J_g is taken as zero for polymer melts.

Inverting the integral in the above equations to obtain the spectra from experimental data is an ill-posed problem, meaning that any small experimental errors can greatly deteriorate the physical meaningfulness of the spectra (Stadler and Mahmoudi, 2013). Several techniques exist to deal with the ill-posed nature in obtaining the spectra (Ramkumar et al., 1997; Kraft et al., 1999; Kontogiorgos, 2010; Stadler, 2010; Shaayegan et al., 2012). In this study we use the methods and software developed by Honerkamp and Weese (1993) and follow the approach of He et al. (2004), to infer the continuous spectra from experimental data.

Melts of HDPE are known to have long relaxation times (Vega et al., 1996; Kraft et al., 1999; Inn and Rohlfing, 2012) making it difficult or impossible to rely only on SAOS to give us access to a broad enough range of time scales to capture all the material structure information. For this reason it is useful to combine SAOS data with creep data in order to access the full range of relaxation behavior (Ramkumar et al., 1997; Kraft et al., 1999;

Stadler, 2010; Shaayegan et al., 2012). This involves the following steps.

(i) The SAOS and creep experiments are performed. In Fig.3.3 we present such data for one of the materials.

(ii) Both the creep compliance and the complex modulus are converted into retardation spectra [shown by open symbols in Fig.3.4a].

(iii) The combined spectrum is obtained by using the creep data-derived spectrum for the long-time and that derived from the complex modulus for the short-time [represented by the solid line in Fig.3.4a]. The overlap between the SAOS and creep derived spectra tells us that both experiments were performed in the LVE region and also serves as a first indication that the spectra obtained are likely physically meaningful.

(iv) The range of validity from the spectrum derived from the SAOS data used in this study is as specified by Davies and Anderssen (1997); their long time limit is taken as the switching point to the spectrum derived from creep. An alternative approach is determining the reliability of the spectrum in certain time domain using relevant factors as indicated by Stadler (2010).

(v) Using the combined retardatation spectrum obtained at a temperature of $190^o\,C$, we then converted it into a combined relaxation spectrum (Ferry, 1980; Dealy and Larson, 2006). In Fig.3.4b we present the weighted relaxation spectra of selected materials.

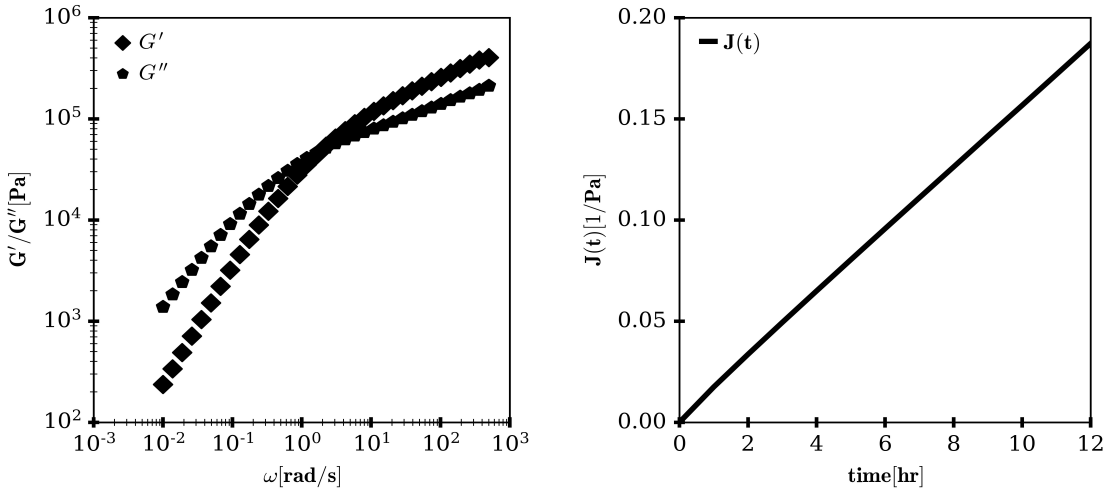

(a) (b)

Figure 3.3: Storage and loss modulus as function of frequency and (b) creep compliance curve of HDPE-3

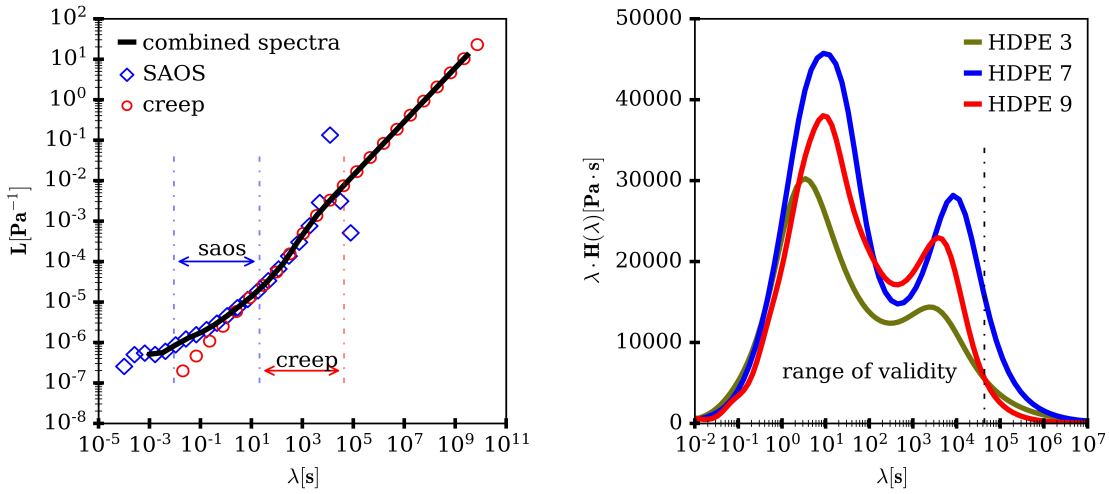

(a) (b)

Figure 3.4: Retardation and relaxation spectra: (a) retardation spectra of HDPE3 showing good overlap between spectra obtained from creep and oscillatory shear experiments; and (b) weighted relaxation spectra of selected materials showing different shape features

3.4 Bimodal parameters

The concept of bimodal distributions occurs in many areas of natural sciences occurring mostly as a result of the mixture of two unimodal distributions (Gezeck et al., 1997; Sambrook Smith et al., 1997). A bimodal MWD can be expressed by the equation:

$$w(logM) = \phi_{LM} w(logM)_{LM} + (1 - \phi_{LM}) w(logM)_{HM} \tag{26}$$

with ϕ being the weight fraction and $w(logM)$ the probability distribution of each population. Several statistical indices exist designed to describe bimodal distributions. In this study, we quantify the bimodality of the MWD using two of the known indices: the bimodal separation (S_B) and the bimodal ratio (R_B) (Zhang et al., 2003).

The variable S_B is defined as the distance between the means of two log normal distributions, i.e. in this case the LMW and HMW populations, taking the breadth of the individual distributions into account. An $S_B > 1$ means that the two distributions do not overlap. For the materials studied here, all S_B were less than 1, indicating that the two distributions overlap. This implies that the interaction effects between the two distributions will also have to be accounted for in our analyses, especially in terms of the relaxation mechanisms. S_B is expressed mathematically as:

$$S_B = \frac{log\bar{M}_{p,H} - log\bar{M}_{p,L}}{2(\sigma_{p,H} - \sigma_{p,L})} \tag{27}$$

where $\bar{M}_p$, is the respective mean value (i.e. the peak M_W) of each population and σ_p is the standard deviation defined as

$$\sigma = \sqrt{\frac{1}{N-1} \sum_{i=1}^{N} \left(log\bar{M}_i - log\bar{M}_p\right)^2} \tag{28}$$

The bimodal ratio, R_B, on the other hand is the ratio of the amplitude of the peak of

the HMW to that of the LMW:

$$R_B = \frac{A_{p,H}}{A_{p,L}} \tag{29}$$

where $A_{p,H}$ and $A_{p,L}$ are the amplitudes of the HMW and LMW peaks respectively. The dominant chain population in the bimodal distribution is indicated by R_B. A bimodal distribution with $R_B < 1$ represents a LMW dominated bimodality while $R_B > 1$ represents a bimodality dominated by HMW. To obtain the indices of interest, the bimodal distributions were resolved into unimodal Gaussian distributions and the six parameters: the two means, standard deviations and amplitudes were determined. The values of the bimodal parameters for our materials are listed in Table 3.2 and the resolved peaks used in their estimations are presented in the supplementary information [A.3]

Table 3.2: Bimodal parameters of the experimental materials

Sample	$\mathbf{S_B}$	$\mathbf{R_B}$
HDPE-1	0.97	0.23
HDPE-2	0.75	0.90
HDPE-3	0.71	0.50
HDPE-4	0.63	0.76
HDPE-5	0.64	0.68
HDPE-6	0.73	1.37
HDPE-7	0.85	0.67
HDPE-8	0.83	0.91
HDPE-9	0.86	0.54

3.5 Results and Discussion

3.5.1 Linear viscoelasticity

Using the combined relaxation spectra, the dynamic material functions were back calculated over a frequency range equivalent to the inverse of the maximum creep experiment time to the maximum frequency values attainable in the SAOS tests. This helped us extend the dynamic properties into a lower frequency range which is of interest to us due to the fact that it possesses molecular structural information.

In Fig.3.5, the dynamic properties of selected materials are presented. The symbols represent experimental data and the lines were obtained from the combined spectra. We note that the dynamic properties do not reach the terminal zone within our window even though our creep experiments did reach steady state [see Fig A.1 in supplementary information]. A closer look at the storage [Fig.3.5b] and loss modulus curves [Fig.3.5c] in the frequency range $10^{-2} - 10^{-4}$ reveals a relaxation mode [small bump] which was not captured by the SAOS experiment alone but was captured by the creep experiment.

All measured linear viscoelastic constants are presented in Table 3.3. The zero-shear viscosity for the bimodal materials was obtained from experimental creep compliance data by taking the inverse of the slope of the creep compliance curve at long times when steady state was reached [see section A.1]. For the unimodal materials on the other hand the zero-shear viscosity was obtained by fitting Carreau–Yasuda model to the SAOS data. The crossover modulus was determined from SAOS data at the point where $G^{'}(\omega) = G^{''}(\omega)$. The flow activation energies were determined from the $G^{'}$ dependent shift factors as detailed by Wood-Adams and Costeux (2001). The need for a vertical shift along the modulus axis was assessed using the Cole-Cole plot (Hatzikiriakos, 2000) indicating that vertical shifts were not needed as is typical for linear polyethylene (Otegui et al., 2013; Derakhshandeh et al., 2017). The materials were also confirmed to be thermo-rheological simple [see Fig. A.4]. Viscoelastic constants are discussed in the following sections.

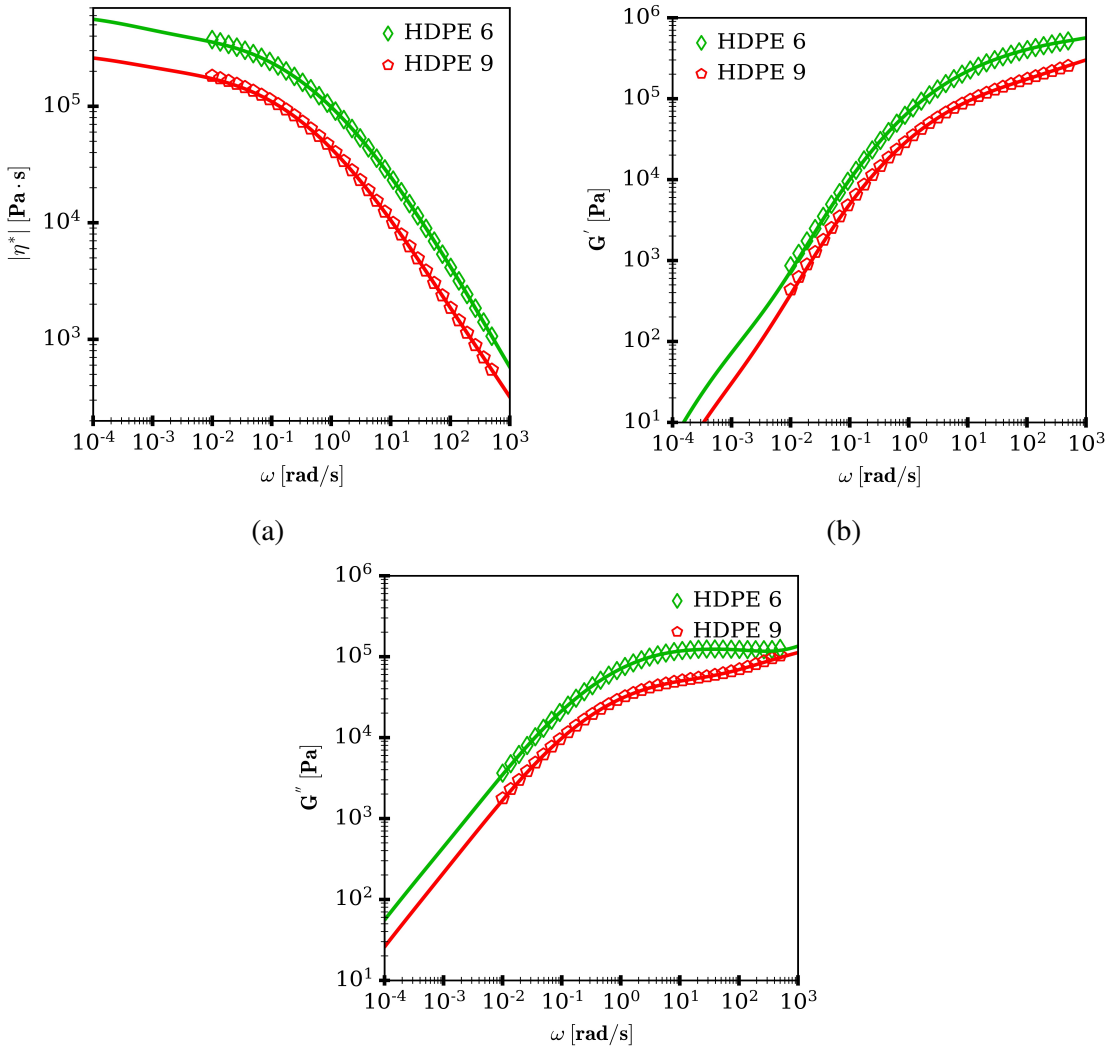

Figure 3.5: Dynamic linear viscoelastic properties of HDPE-6 and HDPE-9. Symbols are from experimental data obtained at $190^o\,C$, lines are calculated from combined relaxation spectra: (a) complex viscosity curve as a function of frequency, (b) Storage modulus as a function of frequency, and (c) loss modulus as a function of frequency

Table 3.3: Linear viscoelastic constants of the experimental materials

Sample	$\mathbf{E_a}$ $(\mathbf{kJ/mol})$	$\eta_\mathbf{o}(\mathbf{kPa.s})$	$\mathbf{G_c}(\mathbf{kPa})$	$\omega_\mathbf{c}[\mathbf{rad/s}]$
HDPE-1	29.02	4575	10.5	0.0352
HDPE-2	29.16	397	49.4	1.2053
HDPE-3	27.56	236	49.6	1.9847
HDPE-4	29.15	231	73.9	2.6309
HDPE-5	30.21	175	64.5	2.8693
HDPE-6	30.64	694	73.3	1.1052
HDPE-7	31.44	311	37.2	0.9292
HDPE-8	30.66	540	53.4	0.9916
HDPE-9	27.94	279	29.1	0.8707
HDPE-10	——	2293	32	1.3600

3.5.2 Zero Shear Viscosity

The zero-shear viscosity, which is related to the number of entanglements, is of course strongly dependant on the chain length. The dependence of the zero-shear viscosity on M_W is generally accepted to obey a power law relation expressed in the form $\eta_o = KM_W^\alpha$, with an α value usually ranging between 3.4 to 3.7 (Ferry, 1980; Dealy and Larson, 2006) for linear chains. The dependency of the zero-shear viscosity on polydispersity or higher moments of the MWD is a topic with no clear answer in the literature. In some studies it has been shown that the breadth of the MWD increases the values of the zero-shear viscosity (Wasserman and Graessley, 1996; Kazatchkov et al., 1999; Vega et al., 2012; Szántó et al., 2019). Wasserman and Graessley (1996) established the following relation for the zero-shear viscosity using M_Z/M_W as a measure of the breadth of the MWD:

$$\eta_o = KM_W^\alpha \left(\frac{M_z}{M_w}\right) \tag{30}$$

In previous studies involving bimodal m-HDPE, a stronger dependence of the zero-shear viscosity on M_W from that expected for more narrowly dispersed chains has been reported (Vega et al., 1996; Ansari et al., 2011). Ansari et al. (2011) for instance, reported an exponent value of 4.5 while Vega et al. (1996) reported a value of 4.2. In this study, when not correcting for polydispersity, we find a power-law exponent of 4.7 characteristic of very broad MWD (Hepperle et al., 2005). A good agreement between the evaluation of zero shear viscosity from creep experiment and through the relaxation spectra was obtained [see Fig. A.2].

For linear chains of HDPE with very broad MWD, the flow activation energy can be expected to fall within the range 25.10 – 35.56 kJ/mol (Hatzikiriakos, 2000). Our flow activation energies values [27.56 - 31.44 kJ/mol], fell within this range and are comparable to those obtained by Derakhshandeh et al. (2017) who obtained values ranging from 27.2-31.9 kJ/mol with their HDPE materials evaluated by shifting the entire curve using time-temperature superposition (Dealy and Larson, 2006) and those of Ansari et al. (2011) [22.97 – 29.41 kJ/mol], who worked on m-HDPE with different molecular characteristics than the ones used in this study.

To account for the influence of the breadth of the MWD on the zero-shear viscosity, Eqn. 30 is used as specified by Wasserman and Graessley (1996) and our results are plotted in Fig. 3.6.

In Fig. 3.6 we compare our values to those of the linear polyethylene materials studied by Stadler et al. (2006) and the unimodal HDPE of Wood-Adams et al. (2000) , and we find a good agreement between their data and ours. Once the effect of M_Z/M_W is accounted for, the η_0 vs M_W power law exponent is 3.6 as expected for linear HDPE (see Fig. 3.6). Note that the data from our study has been shifted to a reference temperature of $150^o C$ before making the comparison. It is also worth noting that in other studies Eqn. 31 was found to give a better representation for the influence of the MWD on the

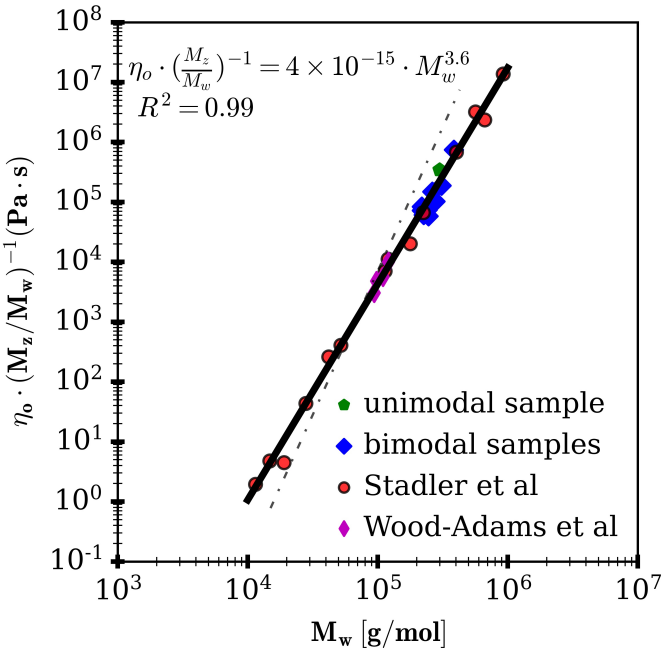

Figure 3.6: Zero-shear viscosity at $150^o\,C$ as a function of molecular weight accounting for polydispersity (M_Z/M_W). A comparison of our data with those from the literature showing good agreement. Correlation was generated using all data plotted in the graph.

zero-shear viscosity.

$$\eta_o = K M_W^{\alpha} \left(\frac{M_W}{M_N}\right)^a \left(\frac{M_z}{M_w}\right)^b \tag{31}$$

For instance Szántó et al. (2019) accounted for polydispersity in their zero-shear viscosity values with the exponents a and b equal to -0.12 and 0.68 respectively, while den Doelder (2006) proposed 0 and 0.9.

Stadler et al. (2006) on the other hand argued that the zero-shear viscosity does not depend on MWD, since correcting η_0 for polydispersity in their study did not lead to a more accurate correlation and the power law exponent on M_W was 3.6 independent of the correction. This is likely related to the narrow range of M_Z/M_W values in their study: 1.6 to 3.8 with a spread of 0.5 around the mean of 2.3 in terms of the interquartile range (IQR)]. This can be compared to an IQR of 1.15 in our study for values ranging from 2.7 to 5.5 and a mean of 3.8. In our study, if we fit our zero shear viscosity versus M_W without the correction, we find a power law exponent of 4.7. Similarly Ansari et al. (2011) observed a more accurate correlation for η_0 when correcting for M_Z/M_W, with a change in power law exponent moving from 4.5 to 3.6. The zero-shear viscosity was found not to significantly correlate with any of the bimodal parameters defined in our experimental methods section (Fig. A.8).

3.5.3 Crossover Modulus

The crossover modulus (G_c) is the point at which the polymer transitions from primarily viscous behaviour to primarily elastic behaviour. The frequency at which the crossover modulus occurs, and the magnitude of the crossover modulus are greatly influenced by the molecular structure, i.e., the molecular weight averages and the breadth of the MWD. An increase in the breadth of the MWD results in a lowering of the crossover

modulus due to the release of the constraints imposed by the LMW chains. It also leads to an increase in the characteristic time which is defined as the inverse of the crossover frequency (Kazatchkov et al., 1999); the characteristic time dependence on M_W is very similar to that of the zero-shear viscosity. Such observations made with unimodal MWD were also observed for our bimodal distributions with broad MWD.

The features of the distributions with greater impact on the crossover modulus were determined through statistical analysis. A total of 9 different features from the MWD were considered, which included the moments of the MWD, the ratio of the area under each curve, the various polydispersity indices and the bimodality features. The data are then scaled and transformed by taking its logarithm, a step necessary to, not only linearize the relationships but also to bring the values within the same order of magnitude. A filter method based on statistical correlation (Pearson's correlation) from supervised machine learning is then used to score and return the most correlated MWD features in relation to the target variable (i.e. the crossover modulus, see Fig. A.9). To account for confounding effects the Generalized Linear Model (GLM) technique is used to determine the influence of the most correlated parameters obtained from the feature selection on the crossover modulus. The number of features used in the model was based on the impact their addition had on the performance of the model, which was determined by observing the adjusted R-squared when new features are added to the model and the associated p-values of the selected features [see Table A.1]. The obtained expression is given by:

$$G_c = K\Phi^{-10.69}R_B^8 \tag{32}$$

where Φ is the weight fraction of HMW population. From Eqn. 32, the crossover modulus is negatively correlated with Φ. This can be understood as a reduction in crossover modulus as the breadth of the HMW portion increases. A similar decrease

in crossover modulus with other measures of the breadth of distribution is reported in literature (Utracki, L. A., Schlund, 1987; Vega et al., 1996; Ansari et al., 2011).The trend observed for the materials we studied is plotted in Fig. 3.7.

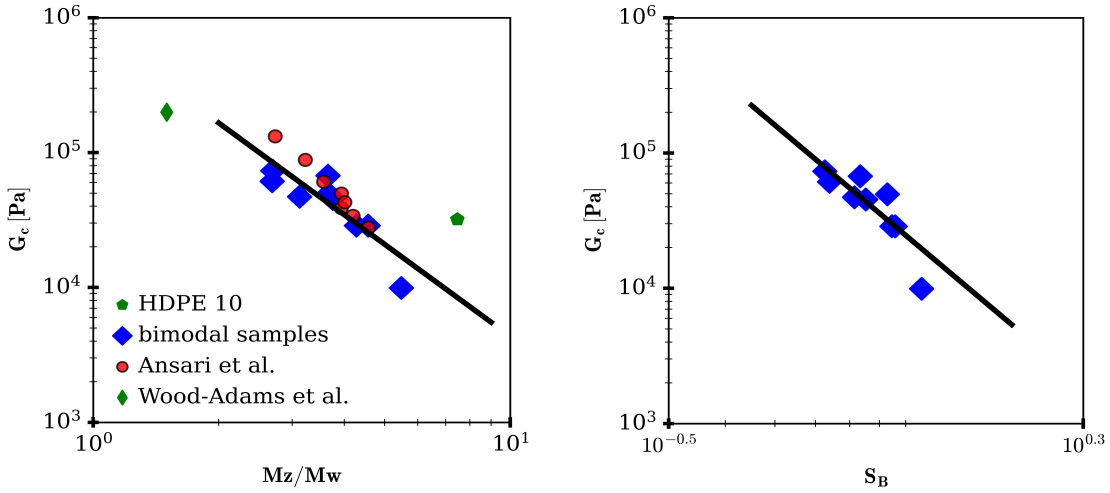

(a) (b)

Figure 3.7: The crossover modulus as a function of the breadth of the molecular weight distribution. (a) crossover modulus vs M_Z/M_W (b) crossover modulus vs the bimodal separation. Lines are to guide the eye

In Fig. 3.7a the crossover modulus is seen to exhibit a power law dependence on the breadth of the MWD as represented by (M_Z/M_W). In that figure, we also plot, for comparison, the values obtained by Ansari et al. (2011) and Wood-Adams et al. (2000) and our unimodal sample HDPE-10. Interestingly the unimodal samples appear to follow a different trend from the bimodal samples. The trend observed for the bimodal samples agrees with results of Ansari et al. (2011). While in our work and that of Ansari et al. (2011), no significant dependency of the crossover modulus on M_W/M_N was obtained, in other works such a dependence was observed (Utracki, L. A., Schlund, 1987). In Fig. 3.7b, the crossover modulus is plotted as a function of S_B for the sole purpose of highlighting how the shape features of the distribution are able to also accurately capture rheological responses. The trend observed in Fig. 3.7b supports the observations made

in Fig. 3.7a. Both parameters M_Z/M_W and S_B represent an aspect of the breadth of the distribution. It is worth nothing that, the negative correlation of S_B with the crossover modulus signifies that with a wider difference between the two peaks in the MWD, constraint release due to the relaxation of the LMW component is enhanced resulting in the lowering of the crossover modulus. The power law correlation here is very useful especially in comparing qualitatively the rheological response of two different materials during the material design process.

R_B is a measures of the high molecular weight end of the MWD. An increase in HMW content, R_B, results in an increase in the degree of entanglement leading to slower relaxation and thus an increase in the crossover modulus. This behavior is accurately captured in Eqn. 32.

3.5.4 Relaxation Processes

The relaxation mechanisms can be observed by plotting the weighted relaxation spectra as a function of the relaxation time. For bimodal distributions at-least two relaxation peaks can be expected. The first peak at low values of λ corresponds to the relaxation of the LMW population and the second peak at higher values of λ corresponds to the relaxation of the HMW population. Simply put, the LMW population chains reptate releasing their constraints on the HMW population and thus speeding up their reptation.

In the following analyses, we use the bimodal parameters to explore this phenomenon. We begin by normalizing both the MWD [Fig. 3.8a] and the relaxation spectra [Fig. 3.8b] placing all distributions within the same order of magnitude. From Fig. 3.8 we note that not only do all the distributions exhibit 2 peaks but also, they present different shape properties such as peak location, peak size, and full width at half maximum (FWHM).

For the relaxation spectra it can be described in terms of the moments of its distributions (Graessley, 1974; Wasserman et al., 1998). The first (λ_I), second (λ_{II}) and third

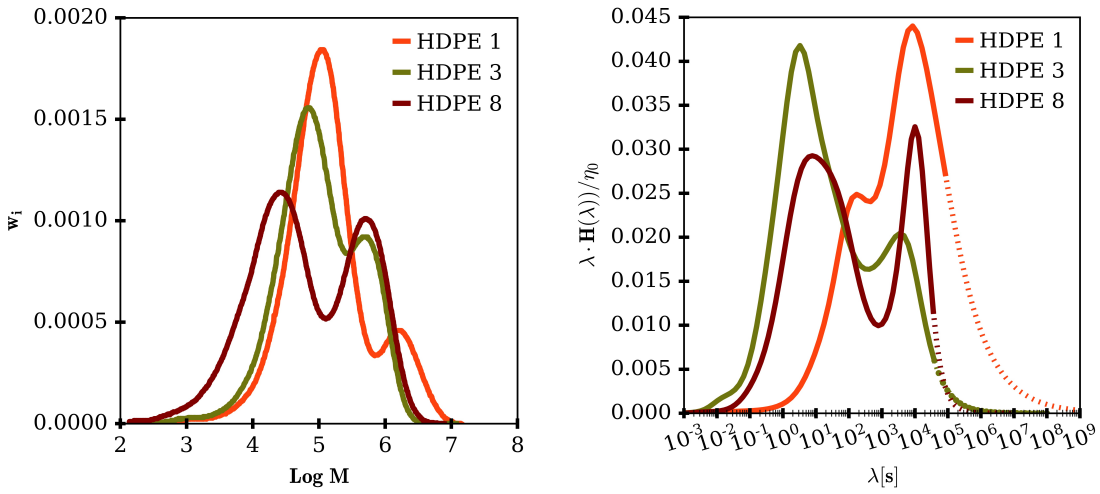

(a) (b)

Figure 3.8: Normalized MWD distributions and spectra of selected samples (a) molecular weight distributions (b) relaxation spectra: dashed line indicates regions where the validity of the spectra has been exceeded. Note that HDPE-1 has the broadest long-time portion in its spectrum out of all experimental materials.

(λ_{III}) moment of the spectra can be expressed as:

$$\lambda_I = \frac{\int_{-\infty}^{+\infty} H(\lambda) dln\lambda}{\int_{-\infty}^{+\infty} [H(\lambda)/\lambda]\, dln\lambda} \tag{33}$$

$$\lambda_{II} = \frac{\int_{-\infty}^{+\infty} \lambda H(\lambda) dln\lambda}{\int_{-\infty}^{+\infty} H(\lambda) dln\lambda} = \frac{\eta_0}{G_N^0} \tag{34}$$

$$\lambda_{III} = \frac{\int_{-\infty}^{+\infty} \lambda^2 H(\lambda) dln\lambda}{\int_{-\infty}^{+\infty} \lambda H(\lambda) dln\lambda} = J_s^0 \eta_0 \tag{35}$$

Using those moments, two measures of the polydispersity of the relaxation spectra can be defined:

$$RSI_I = \frac{\lambda_{II}}{\lambda_I} \tag{36}$$

$$RSI_{II} = \frac{\lambda_{III}}{\lambda_{II}} \tag{37}$$

where RSI_I (Wasserman et al., 1998) and RSI_{II} (Graessley, 1974) are polydispersity indices. In the terminal zone, the moments of the relaxation spectra can be related to the LVE constants such as the steady state compliance and plateau modulus [see Eqns. 34 and 35]. For our samples, the plateau modulus could not be determined since the maxima in the loss modulus curve needed for its estimation could not be reached experimentally and using the mathematical relation provided in Eqns. 24 and 25 require extrapolation pass the range of validity of the underlining technique (Dealy and Larson, 2006; Stadler, 2010). We instead use these moments for the sole purpose of calculating the breadth of the relaxation spectra of our materials.

Values of RSI_I and RSI_{II} for the materials we studied are listed in Table 3.4, along with other previously reported values of RSI_I (Wasserman et al., 1998). Looking at the RSI_I values, we can clearly see that our materials represent broader relaxation spectra than those previously studied. This leads to the difficulties in obtaining reliable values for the steady state compliance, hence it was excluded from this study.

We also define a new parameter RSI_{III} which is the separation between the two relaxation modes; expressed as the ratio of the mean positions of the two-relaxation peaks in the spectrum given by:

$$RSI_{III} = \frac{\lambda_{p,H}}{\lambda_{p,L}} \tag{38}$$

This parameter also captures information about the breadth of the relaxation spectra but uses distinct features rather than the integral of the entire distribution. In some instances, this might be useful, for example, when it is not possible to obtain a reliable

Table 3.4: Relaxation Spectra Indices

Values obtained for our materials		
Materials	$\mathbf{RSI_I}$	$\mathbf{RSI_{II}} \times 10^4$
HDPE-1	2005	377.6
HDPE-2	210	1.303
HDPE-3	1069	64.11
HDPE-4	2489	50.20
HDPE-5	901	61.46
HDPE-6	1655	1.246
HDPE-7	1278	25.01
HDPE-8	2469	0.7714
HDPE-9	6162	2.642
RSI_I Literature values (Wasserman et al., 1998)		
LLDPE	3-5	
HDPE	3-30	
mLLDPE (linear)	1.5-2.4	
mLLDPE (small level of LCB)	25-100	
LDPE (high pressure)	13-126	

relaxation spectrum over the entire range. We proceed by making use of the feature selection method described previously but this time measuring the correlation between the polydispersity of the spectra and the features of the MWD. The 2 most important features as dictated by the summary statistics were the bimodal separation and M_Z/M_W, both being measures of the breadth of the molecular weight distribution [see Fig. A.10].

In Fig. 3.9a, RSI_{II} and RSI_{III} are plotted as a function of M_Z/M_W. RSI_{III} is found to negatively correlate with M_Z/M_W, while RSI_{II} is not correlated with M_Z/M_W. We also note here that for broad MWDs, higher moments of MWD provide better correlation with the relaxation spectrum breadth as can be seen from the feature selection scoring in Fig. A.10. RSI_{II} has been reported to increase with the breadth of MWD (Graessley, 1974), however we observed the opposite. To further investigate this behavior RSI_{III} will be used to examine its relationship with the features of the MWD since it provided

a better correlation with the MWD than did RSI_{II}.

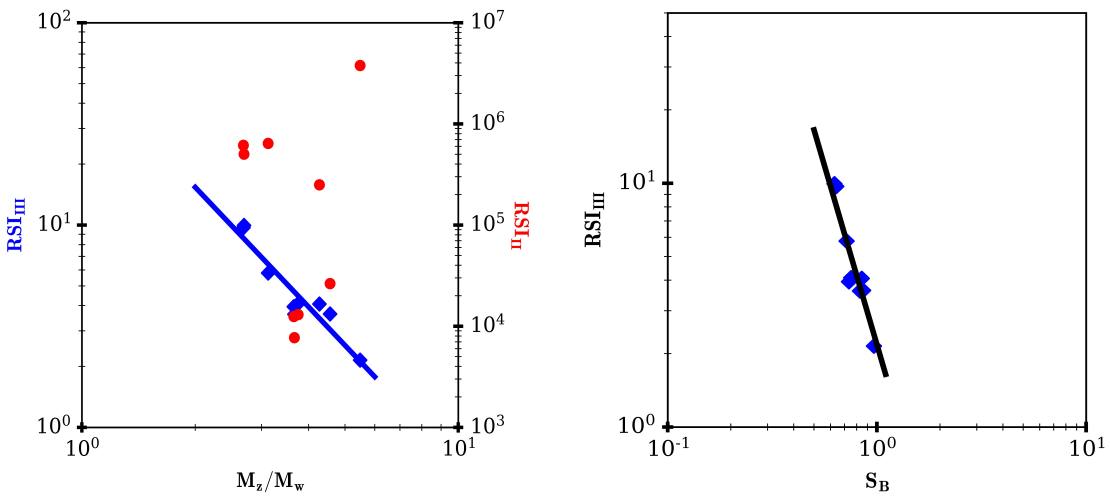

Figure 3.9: Relaxation spectra indices (a) as a function of M_Z/M_W and (b) as a function of S_B . Line is to guide the eye.

Using Generalized Linear Modelling the relationship between RSI_{III} and the selected features is determined to be:

$$RSI_{III} = K \cdot S_B^{-3.91} \cdot \left(\frac{M_Z}{M_W}\right)^{0.38} \tag{39}$$

From Eqn. 39, RSI_{III} is negatively correlated to S_B while its correlation with M_Z/M_W is positive in agreement with that described by (Graessley, 1974) . The trend shown in Fig. 3.9 by M_Z/M_W is due to the confounding effects which must be accounted for when analyzing such correlations from experimental data. Otherwise, we risk presenting interpretations that may not present the complete picture. These observations illustrate the importance of the approach used to determine Eqn. 39.

In Fig. 3.9b, RSI_{III} is plotted as a function of the shape features of the distribution. The decrease in breadth of the relaxation spectra with an increase in the polydispersity of the material is explained as follows, polymer chains have characteristic times within

which they impose constraints on their environment (Struglinski and Graessley, 1985). For short chains, the characteristic time is denoted by T_S and for long chains by T_L. At time scales below T_S the system is in a sort of frozen state with respect to coordinated main chain movements. As the time scale approaches T_S, the short chains begin to reptate thereby removing the constraint they imposed on their surroundings leading to the acceleration of the relaxation of the long chains. A bimodality with a larger value of S_B indicates a distribution with long chains that are much longer than the short chains. In such a situation the time required for a single segment of a long chain to diffuse is far greater than T_S, hence the long chains only fully relax once the short chains have already relaxed. Hence, the breadth of the relaxation spectrum will decrease with an increase in bimodal separation [Fig. 3.9b] if the fraction of long chains is less than the fraction of short chains. In Table 3.2, eight out of nine materials studied have $R_B < 1$, meaning that they meet these criteria.

We note that when $R_B < 1$, broadening the HMW peak also accelerates the relaxation of the melt, because it provides the HMW population an additional range of characteristic times and thus constraint release. The feature that results in a greater decrease in breadth of the relaxation spectrum for the materials we studied is S_B. Note that if R_B is higher than the values we studied (max. 1.37) then the correlations and observations that we have presented will not necessarily hold.

3.6 Conclusion

It was shown that the LVE behavior of a polymer with a bimodal, broad MWD can be probed in an approximate manner by making use of the MWD shape features. The correlations using the bimodality features yield trends that agree with analyses involving relaxation mechanisms. The distribution of relaxation times of broadly distributed

bimodal materials was found to decrease with an increase in the breadth of the MWD highlighting the important role played by the LMW chains in accelerating the relaxation process via constraint release. For our materials a strong correlation between the zero-shear viscosity and the weight average molecular weight was observed. When this correlation is corrected for the effect of breadth of MWD using (M_Z/M_W) we find the expected power law dependency on M_W of 3.6. The crossover modulus was found to be influenced by M_Z/M_W as previously reported, but more closely correlated with the bimodal ratio and weight fraction of the HMW population. The crossover modulus was negatively correlated with weight fraction of the HMW while showing a positive correlation with the bimodal ratio. The breadth of the relaxation spectra was found to be strongly influenced by the separation distance between the two populations of the MWD and M_Z/M_W.

Chapter 4

Polymer fractionation at an interface in simple shear with slip

In this chapter, we investigate the surface fractionation of HDPE by using simple shear flow. We show for the first time that surface fractionation could occur even in the absence of bulk shear gradient and further observe that surface fractionation shows a shear rate dependency.

The chapter is based on the following publication: *Kwakye-Nimo, S. et al. Polymer fractionation at an interface in simple shear with slip, macromolecules 2022,55, 66096619*

4.1 Introduction

The flow of polymer melts near surfaces is of considerable interest to both theorists and experimentalists. An understanding of the polymer's behaviour at the interface is essential in producing materials with desirable properties in various fields of research such as lubricants, coating, adhesives and composite materials (Anastasiadis and Hatzikiriakos, 1998; Hadaeghnia et al., 2020; Zhao et al., 2022). It also helps in suppressing processing related problems such as die drool and melt fracture (Inn, 2013). This of course requires knowledge of the chain length distributions at the interface and the nature and type of the surface (Van der Gucht et al., 2002a).

The wall over which a polymer melt flows introduces anisotropic behaviour on the chains close to it, both structurally and in terms of their dynamics (De Virgiliis et al., 2012). The disturbance created by the solid wall in the melt is complex because of the broad range of chain length scales and the resulting wide range in relaxation time scales (Varnik and Binder, 2009). The amount of material adsorbed onto the wall for monodisperse systems, has theoretically been predicted to depend on the degree of polymerization (Scheutjens and Fleer, 1980; Allal and Vergnes, 2009; De Virgiliis et al., 2012) and on the width of the interface as compared to the thickness (Mahmoudi and Matsen, 2017; Mahmoudi et al., 2018) but to a negligible extent on the adsorption strength (Van der Gucht et al., 2002a). This signifies that for polydisperse polymers the thickness of the adsorbed layer may vary.

A prime contributing factor to anisotropic behaviour at the interface is entropic segregation. Entropic enrichment of short chains at the surface occurs because they have more chain ends per unit volume thus diminishing the entropic penalty (Bouchaud and Daoud, 1987). Van der Gucht et al. (2002b) proposed a simple relation which accounts for the surface excess in terms of the bulk concentration and the chain length for a polydisperse

system. The expression is as follows:

$$\frac{\phi_N^{ex}}{\phi_N^b} = A\left(1 - \frac{N}{N_w}\right) \tag{40}$$

where ϕ_N^{ex} is the integrated surface excess of chain of length N, ϕ_N^b is the bulk composition, N_W is the weight average chain length and the prefactor, A is the amplitude of segregation which was shown to have a constant value of 0.195 for polymer melts. It is worth nothing that in recent studies, the amplitude of segregation was found not to be a constant parameter but to be influenced by the chain's stiffness (Blaber et al., 2019). This model predicts surface enrichment only for chains shorter than the weight average chain length.

For flow systems involving capillary extrusion, the long chains close to the wall acquire higher elastic energy in comparison to the shorter chains counterparts propelling the longer chains away from the wall leaving the wall enriched with shorter chains (Busse, 1964). Dorgan and Rorrer (2015), provided a model which accounts for the entropic balance of a polydisperse melt in capillary flow. In their work, they described two essential driving forces for segregation which are:

(i) the concentration gradient which is present even in the absence of flow and

(ii) a contribution resulting from the shear gradient during flow.

In this work, we will be comparing our results to the model predicted by Van der Gucht et al. (2002b) since in the simple shear flow system used, there is no shear gradient.

The enrichment of the surface by short chains has been confirmed experimentally in several studies involving different materials and different flows. The skin of a capillary extrudate was found to be highly concentrated in low molecular weight (LMW) chains in several studies (Schreiber and Storey, 1965; Schreiber et al., 1966; Shelby and Caflisch,

2004; Ebrahimi et al., 2016), with a possible suggestion that flow induced fractionation occurs only at a very thin layer near the die exit (Musil and Zatloukal, 2011). In two phase polymer flow systems, the less viscous component moved to the outer layer of the extrudate circumference (Schreiber and Storey, 1965; Schreiber et al., 1966). Molecular scale simulation of cross flow migration of polymer melt under various conditions also confirms enrichment of surface by short chains (Rorrer and Dorgan, 2014). Thus, surface enrichment by short chains is observed practically in all situations in which polymer flows over a surface. We note that there is a lack of experimental data for segregation in simple shear. Here we address this issue.

While the entropic contribution to fractionation is thought to have a negligible effect on slip when it comes to narrowly distributed polymers, its effect on polymers with broad molecular weight distribution (MWD) is considerable. By accounting for the ensuing effective MWD at the interface, predictions where presented using a double reptation slip model produced results that were very close to experimental data (Ebrahimi et al., 2016). The double reptation slip model prediction was further enhanced by accounting for flow induced fractionation (Najm and Hatzikiriakos, 2020). In a nutshell the chain composition at the interfacial layer is influenced by both entropic and flow induced segregation, which in turns has a bearing on the manner in which the polymer slips at the wall or vice-versa.

Polymers are known to slip over the surface on which they flow under essentially all circumstances (Wise et al., 2000; Kalyon and Gevgilili, 2003; Hatzikiriakos, 2015; Gustafson and Morse, 2016). In the case of polymer melts, within the first few layers the chains adsorb to the surface resulting in the formation of tails, loops and trains (Scheutjens and Fleer, 1980; De Virgiliis et al., 2012; Sgouros and Theodorou, 2020) which are in turn entangled to various degrees and at multiple sites with the bulk. When subjected to flow, adhesive slip occurs when the polymer chains detach/desorb themselves completely

from the wall. This is typically expected to occur on low energy surfaces. Alternatively, on high energy surfaces, the flowing chains are believed to disentangle from a monolayer close to the wall and is referred to as cohesive failure or apparent slip.

There have been several attempts in the past to experimentally measure both entropic segregation and flow induced segregation. Attempts have been made too measure entropic segregation using neutron reflectivity (Zhao et al., 1993), a method that is known to result in artificial results due to the effect of deuterations on chain fractionation (Hariharan et al., 1993). Experimentally measuring surface segregation has been challenging.

Our goal in this study is to provide experimental data on the extent to which a surface could be enriched by short chains in simple flow involving slip. This, we carry out using the sliding plate rheometer (SPR) (Dealy and Giacomin, 1988). After subjecting the polymer to simple shear at a higher enough rate for slip to occur, a thin layer of debris of polymer remains on the substrate, which we collect and analyze using GPC. We subsequently study the surface profile of the obtained films.

The Couette flow geometry gives us the opportunity to eliminate the possible contribution of flow induced segregation since the gradient in shear required to drive migration is absent at constant shear rate in simple shear flow (Dorgan and Rorrer, 2015). We note that the model of Dorgan and Rorrer (2015) indicates that once slip commences in simple shear, there exists a gradient in shear rate. Our results show not only the occurrence of surface fractionation but also that it occurs with a dependence on the shear rate. We further establish a relationship between slip, fractionation and the surface properties of the films.

4.2 Experimental section

4.2.1 Materials and sample preparation

The bimodal metallocene high density polyethylene (HDPE) used in this study and referred to as "bulk sample" was supplied by Chevron Phillips Chemical Company (CPChem). It was synthesized through a dual-metallocene catalyst system in a single loop-slurry reactor at CPChem and has the molecular characteristics listed in Table 4.1. This material has been described in our previous work (Kwakye-Nimo et al., 2022a) where it was referred to as HDPE 6.

Table 4.1: Molecular weight parameters of the distributions Shear rates

	$\mathbf{M_N}$ $[kg/mol]$	$\mathbf{M_W}$ $[kg/mol]$	$\mathbf{M_Z}$ $[kg/mol]$	$\mathbf{M_W/M_N}$	$\mathbf{R_{g,w}}$ $[nm]$
Bulk	10.93	357.55	1426.3	32.67	26.8
3 s^{-1}	11.48	310.40	1335.6	27.03	24.4
5 s^{-1}	11.67	306.90	1306.3	26.31	24.3
7 s^{-1}	11.62	304.00	1302.7	26.16	24.1
9 s^{-1}	11.97	325.90	1277.5	27.23	25.0

The specimens used for simple shear, slip experiments were prepared by compression molding for 4 minutes at a temperature of $190^o\,C$ and a pressure of 15 tons. They were subsequently allowed to melt for an extra 2 minutes before being quenched. Specimens were of dimensions 75 mm x 50 mm x 1.2 mm

4.2.2 Gel Permeation Chromatography (GPC)

The molecular weight distribution of all our specimens were obtained by using an Agilent 1260 Infinity II High-Temperature GPC System (Agilent Scientific, Santa Clara, CA), equipped with an IR4 infrared detector (Polymer Char, Spain). The GPC system was calibrated using the broad calibration method and a broad polyethylene standard, Marlex® BHB 5003 (CPChem, The Woodlands, TX). The Mark–Houwink constants for

the universal calibration are $K = 3.95 \times 10^{-4}\ dL/g$ and $a = 0.726$ for polyethylene (PE). All GPC measurements were performed at $145^o\,C$. The samples were dissolved in a Blue-M oven set at a temperature of $150^o\ C$ for nominally 5 hours before they were transferred to the GPC instrument for analysis. To prevent degradation, 2 g of BHT was added to one gallon of 1,2,4-trichlorobenzene as the mobile phase. At a flowrate of 1.0 mL/min, 400 μl of the polymer solution were then injected into a set of three (3) Waters HMW6E SEC columns (Waters, MA). In Fig. 4.1, we present the molecular weight distribution of the bulk sample before and after subjecting it to simple shear with slip. We note that the distribution of the bulk is not affected by the shear flow. This indicates that thermal degradation did not occur during the experimental time in the sliding plate rheometer.

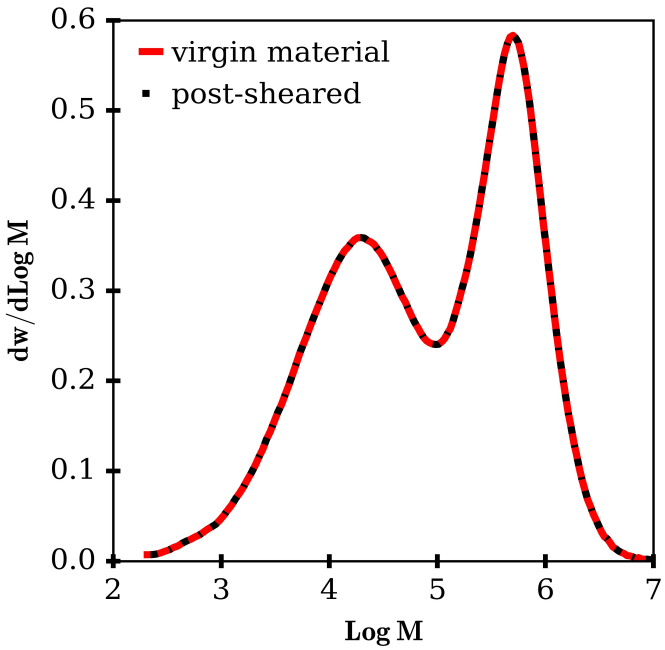

Figure 4.1: Molecular weight distribution of the material studied. A comparison between pre and post-sheared MWD.

4.2.3 Linear viscoelastic properties

In Fig. 4.2, we present the linear viscoelastic properties of the material (Kwakye-Nimo et al., 2022a). In Fig. 4.2a, the storage and loss modulus as a function of frequency from experiment is plotted in symbols, while in Fig. 4.2b, the weighted relaxation spectra as a function of time is plotted. We note here that this material exhibits very long relaxation times.

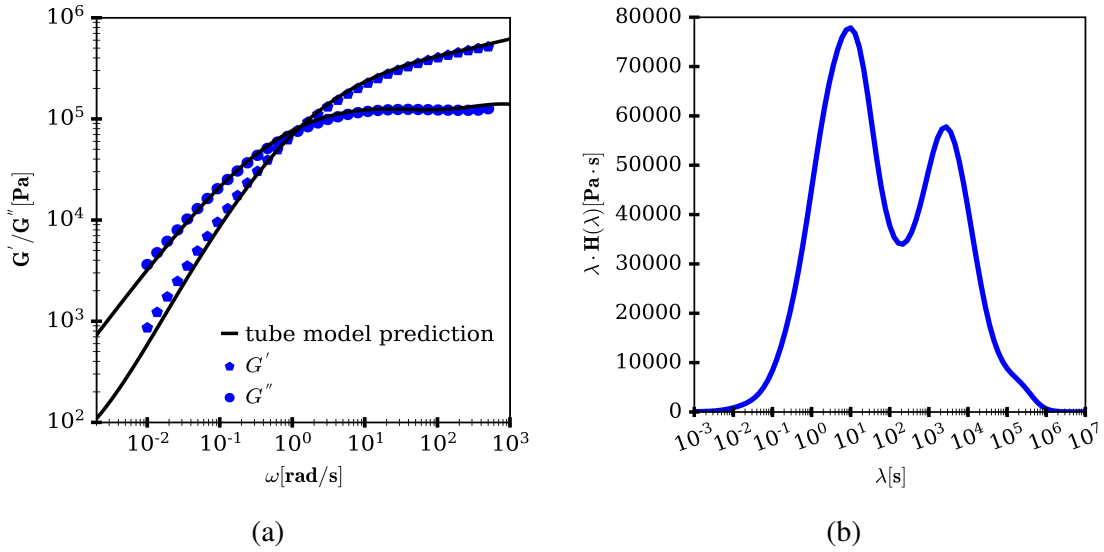

(a) (b)

Figure 4.2: Linear viscoelastic properties: (a) dynamic linear viscoelastic curves (points are experimental data from Kwakye-Nimo et al. (2022a) and (b) combined weighted relaxation spectra Kwakye-Nimo et al. (2022a)

4.2.4 Extensional viscosity properties

Extensional transient viscosity measurement was carried out in order to determine the maximum stress required for the bulk material to break when stretched. These results are compared to the stress experienced by the polymer during the simple shear flow experiment and are discussed in subsequent paragraphs. The test was carried out at CPChem by using an Anton-Paar MCR-500 device which was equipped with an extensional viscosity

fixture, a Sentmanat Extensional Rheometer (model SER-3 universal testing platform, Xpansion Instruments). The specimen was compression molded at $182^o\ C$ into dimensions of 12.77 x 18 mm and subsequently cut out of the molded plaque. Its thickness was subsequently measured. A 30 seconds wait was allowed for the specimen to attain thermal equilibrium prior to carrying out the experiments at a temperature of $190^o\ C$. The following Hencky strain rates were used : 0.1, 0.3, 1, 3, 10 in a nitrogen atmosphere.

4.2.5 Molecular modeling

We extract the tube model parameters (τ_d, τ_R, L) for the material studied using the dual constraint model (Pattamaprom et al., 2000). These parameters are used later to relate the behaviour of chains in the bulk flow to the tethered chains at the surface.

The unusual motion a chain undergoes to relax in a polymer melt can be described by the diffusion equation (De Gennes, 1971; Doi and Edwards, 1978b,a). The chain's surrounding imposes on it constraints which is referred to as a tube, out of which it has to escape through various mechanisms. The diffusion equation is of the form:

$$\frac{\partial}{\partial t}\psi^*(s,t) = \frac{1}{\pi^2\tau_d}\frac{\partial^2}{\partial s^2}\psi^*(s,t) - \frac{1}{\tau^*(s)}\psi^*(s,t) \tag{41}$$

where ψ^* is the probability that the chain will survive the tube, τ_d the reptation time, τ^* is the relaxation time for the contour length fluctuations. The above equation was solved using crank-Nicolson finite-difference method over a space grid $s \in [0,1]$ in 5×10^{-3} steps intervals and a logarithm time stepping. We adopted as boundary conditions those proposed by Stephanou et al. (2010), who using atomistic simulation, argued that the survival probability of the ends of the chains in the tube have some time dependency, hence should not be zero (Stephanou et al., 2011; Stephanou and Mavrantzas, 2013). Thus, the boundary conditions used in this work are as followed:

$$\begin{aligned}\psi^*(s,t=0) =& 1 \\ \psi^*(s=0,t) =& \psi^*(s=1,t) = exp(-t/\tau_e)\end{aligned} \tag{42}$$

where τ_e the equilibration time. The dual constraint model is solved in 2 steps. In the first step the solution of the PDE gives us the overall probability that the chain will survive the tube. A Rouse process is subsequently activated to ensure that the survival probability of the chain does not decrease at a rate faster than the Rouse process. In the second stage the output from step 1 is used to account for constraint release through the late portion of the relaxation time for contour length fluctuation and then the diffusion equation is solved a second time. The Rouse process is again activated to serve the same purpose [see Pattamaprom et al. (2000) for details]

The total relaxation modulus, accounts for both fast and slow processes and is given by the expression

$$G_{total}(t) = G(t) + \sum_i w_i G_{R,i}(t) \tag{43}$$

The solutions of the diffusion equation enter $G_{total}(t)$ through $G(t)$ by the relation $G(t) = G_N \psi(t) \psi^{'}(t)$. In Eqn. 43, $G_{R,i}$ is the contribution from the high frequency Rouse processes. The complex modulus, G^* is then obtained from $G_{total}(t)$ using Schwarzl approximation (Schwarzl, 1971).

The parameters required for the simulation are the molecular weight between entanglement, M_e and the equilibration time, τ_e. The values of M_e reported in literature for polyethylene varies from 1035 to 2340 g/mol (Pattamaprom and Larson, 2001; Van Ruymbeke et al., 2002a; Vega et al., 2003; Touloupidis et al., 2016; Szántó et al., 2019). In this work, we adopt the value of 1250 g/mol (Wasserman and Graessley, 1996). Therefore, $\tau_e = 5.7\ ns$ is the only parameter that was obtained by fitting to

the experimental data. This value falls within the range of values reported in the literature for HDPE at $190^o\ C$ (Balzano et al., 2008; Pattamaprom et al., 2008). Having obtained τ_e, the reptation time (τ_d) was calculated through the relation $\tau_d = 3Z^3\tau_e$ where $Z = M_W/M_e$, while the Rouse time (τ_R) was obtained from the relation $\tau_R = Z^2\tau_e$. The average contour length of the tube was obtained through the expression $L = (Nb^2)/a$ with N being the weight average chain length, b the effective polymer statistical segment length and a the tube diameter. The linear viscoelastic prediction of the dual constraint model on broadly distributed commercial materials is quite remarkable [see Fig. 4.2a]. We note that, to the best of our knowledge, this is the first time that the dual constraint model has been applied to this kind of material.

4.2.6 Simple shear flow experiment with slip

Prior to collecting the debris, a time sweep experiment was performed using an Anton Paar MCR502 rotational rheometer at an angular frequency of 0.1 rad/s and a strain value of 1% under air atmosphere for a period of 1 hour to assess stability. No degradation was observed. This was further confirmed by GPC testing of the bulk after shearing (Fig. 4.1).

Glass slides, 75 mm x 50 mm x 1 mm, are used for the collection of the debris in the SPR experiments. The glass slides are cleaned with tap water and soap and then subjected to a 10 minutes sonification in deionized water and another 10 minutes in acetone. The glass slide is loaded into a specially machined groove in the moving plate of the SPR at the testing temperature ($190^o\ C$). The specimen is then loaded into the SPR by placing it on the glass substrate, and closing the plates to press the sample by 0.2 mm for a final thickness of 1 mm. After this, 45 minutes is allowed for thermal equilibration and stress relaxation before subjecting the polymer to simple shear flow. Fig. 4.3 shows an example of debris collected on a glass slide.

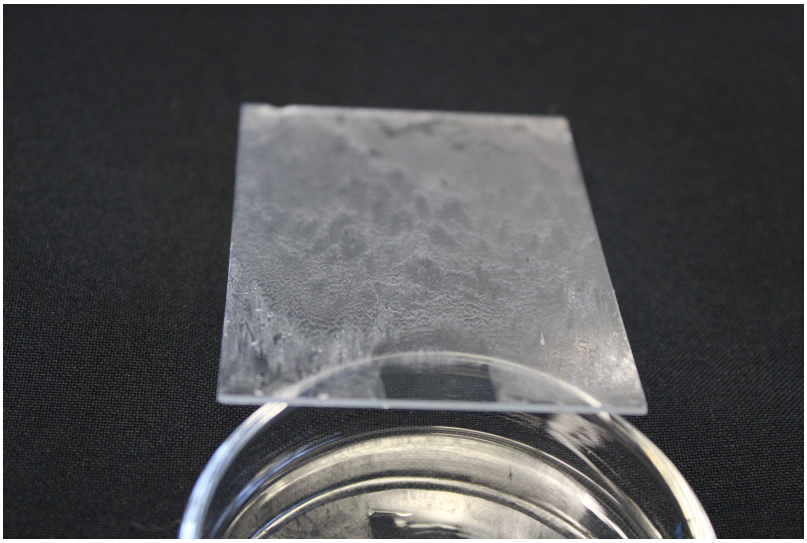

Figure 4.3: Debris on glass substrate collected at a shear-rate of 9 s^{-1} in a simple shear flow experiment using the SPR.

At the end of the simple shear flow experiment which generally last under 25 seconds, the glass slide is quickly offloaded and exposed to liquid nitrogen to prevent oxidative degradation. A test for oxidative degradation is performed on the debris using Fourier transform infrared spectroscopy (FTIR) [Nicolet1S10 in ATR mode]. In Fig. 4.4, the results from the degradation tests are presented. Fig. 4.4a presents the time sweep data which shows no change in material properties over the testing period and in Fig. 4.4b the FTIR data is shown which shows no sign of oxidative degradation which is expected to manifest itself as a peak at a wavelength of $1700\ cm^{-1}$. Note that the FTIR spectrum of the virgin material is the same as those of the debris shown in Fig. 4.4b.

The experiment is carried out at 4 different shear rates, 3, 5, 7, 9 s^{-1}, with multiple repeats (with different specimens) per shear-rate. The harvesting of the debris from the glass slides was performed by scraping the film off of the glass substrate with a blade. For both GPC studies and profilometry studies, 5 repeats were performed.

The tensile strength values of the bulk sample, measured at $190^o\,C$ and at extensional strain rates 3 and 10 s^{-1}, was in the range of 0.58 to 0.73 MPa. Data are presented

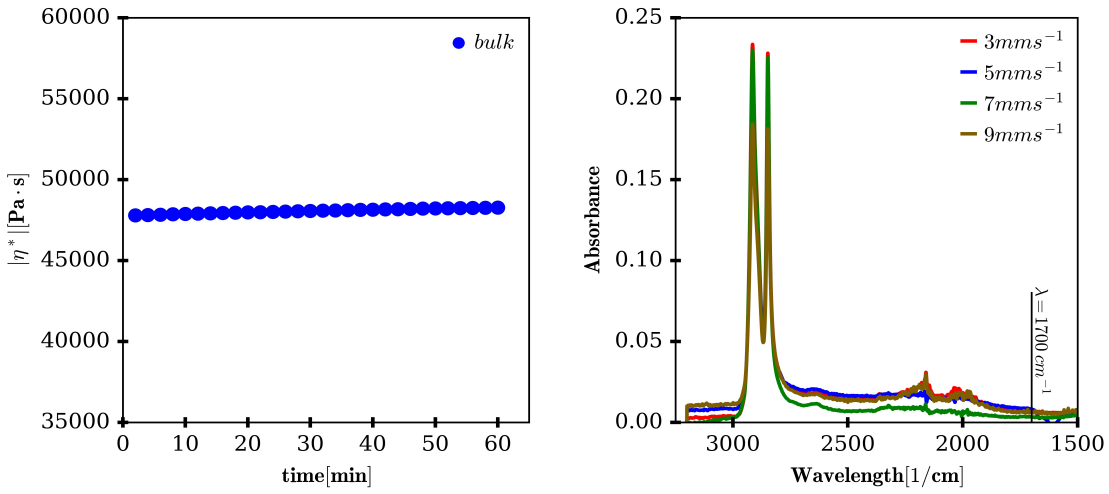

(a) (b)

Figure 4.4: Degradation checks (a) time sweep showing no change in material properties (b) FTIR showing no oxidation peak at around 1700 cm^{-1}

in Fig. B.6. The maximum stress employed during our simple shear experiment was 0.1178 MPa, which is clearly lower than the ultimate tensile strength of the bulk sample. Therefore, the force experience by the chains during flow is not enough to cause a break in $C - C$ hence the enrichment observed can not be attributed to chain scission (Dorgan and Rorrer, 2015).

4.2.7 Surface Profile

The surface profile of the films is measured with a Veeco Dektar 150 stylus surface profilometer. The advantage of using the stylus profilometer in contrast to the optical alternative is that it provides direct contact between the instrument and the surface being measured. The stylus tip was of dimension 12.5 μm and exerted a force of 10^{-5} N during a 30 seconds scan over a distance of 2 mm. For each glass slide, 4 measurements of the surface profile are taken in the flow direction. The average of the 20 measurements of the surface profile per shear rate is used for subsequent analysis. In Fig. 4.5, the surface

roughness taking over an area of 1 mm x 1 mm on one of specimens sheared at 9 s^{-1} is presented. The blue section of the graph is a cut made in the film to serve as a reference from which the thickness of the film was measured. We note that the interfacial layer is not smooth.

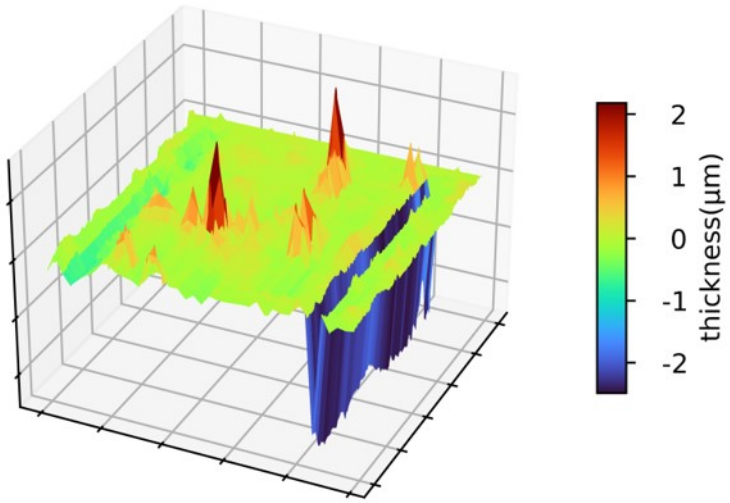

Figure 4.5: Surface roughness of debris obtained from simple shear flow experiment performed at a shear rate of 9 s^{-1}.

4.3 Results and Discussion

The MWD of the debris obtained from the simple shear with slip experiments, performed at different shear rates is presented in Fig. 4.6. The experimental data were very reproducible with an average margin of error in $dw/dlogM$ of ± 0.0021.

From Fig. 4.6, three observations can be made.

(i) Surface fractionation in simple shear flow with slip shows a clear shear-rate dependency.

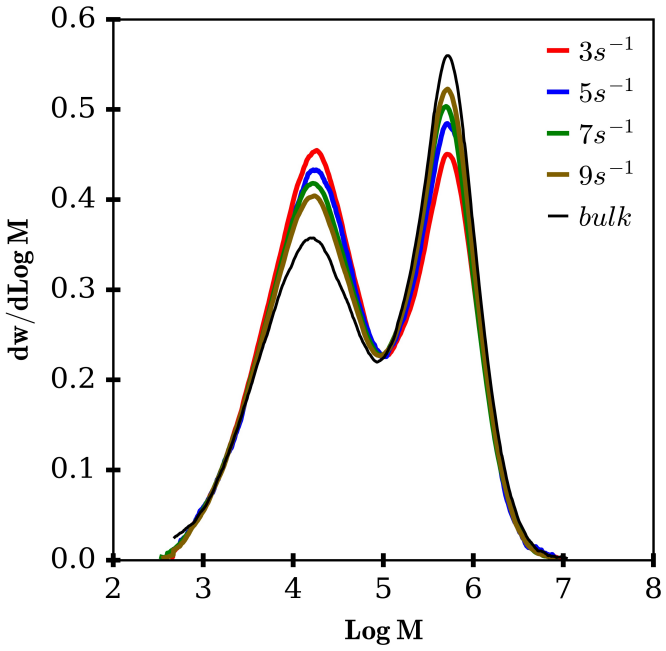

Figure 4.6: MWD of the debris obtained from simple shear flow with slip experiments performed at different shear rates as compared to that of the bulk material.

(ii) Surface enrichment of short chains is higher at lower shear rates. This observation is in sharp contrast to assumptions used in similar studies involving capillary flow (Najm and Hatzikiriakos, 2020).

(iii) The debris MWD approaches that of the parent distribution at higher shear rates.

With regard to the counter-intuitive nature of observation in (ii) and (iii), we remark that the large thickness of the debris [to be discussed in later paragraphs] cannot be ruled out as a possible contributing factor. Before interpreting our results, we ascertain ourselves of two important things:

(i) that the debris MWD is indeed different from that of the bulk and not as a result of experimental artifacts and

(ii) that the debris is indeed shear rate dependent.

This we carry out using statistical tests of significance. With regard to the first point, we perform a permutation test (Boik, 1987) with the following hypothesis:

H_0: there is no significant difference between the bulk sample and debris

H_1: there is a significant difference between the bulk and the debris

We make use of the number average molecular weight (M_N) of the distributions as our test statistic and employ a non-parametric test method. The sample size used for the simulation is 10000, from which the fraction of observations with M_N values less than or equal to that of the bulk distribution gives us the p-value. In Fig. 4.7, we present the outputs of the statistical tests. In Fig. 4.7a, the result of the permutation test is presented. The distribution of our test statistics is clearly normal i.e. the central limit theorem was obeyed. The distribution of M_N values are shown to be no where near the threshold value of the M_N of the bulk [dash line in Fig. 4.7a]. A p-value of 0.00 was obtained from the simulation, which signifies that the probability that our observation was due to random chance is completely zero, hence we fail to accept the null hypothesis. Therefore, we conclude that the MWDs of the debris are indeed different from that of the bulk.

We proceed to test the statistical significance of the shear rate dependency of our experimental results. From the experimental data at each shear rate, we draw 10000 bootstrap samples, perform peak deconvolution on them and use the area under the curve of each population as our test metric. From the standard error of the mean, we calculate the confidence interval at a 95% confidence level. In Fig. 4.7b, the non-overlapping error bars is a confirmation of the shear rate dependency of the distributions. This margin of error is consistent with the evaluation made from experimental data [see section B.1.1].

From the summary statistics of the distributions [See section B.1.2] the median chain length of the debris for all the shear-rates, was observed to be higher than that of the bulk sample. This suggests the loss of short chains in the debris MWD. To investigate this

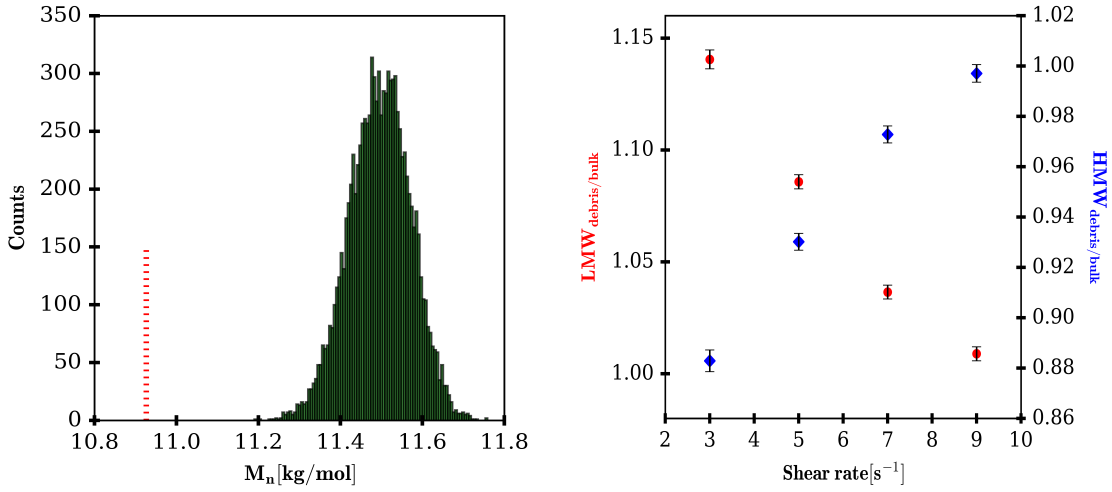

Figure 4.7: Statistical tests: (a) permutation test showing distribution of test statistic (b) deconvoluted peaks vs shear rates, non-overlapping error bars are an indication of shear rate dependence.

further, we account for the entropic contribution to segregation using Van der Gucht et al. (2002b) model while acknowledging that we are not in thermodynamic equilibrium, yet useful information could still be obtained as shown in previous studies (Ebrahimi et al., 2016).

Using Eqn. 40 to evaluate the surface composition, we follow the steps taken by Ebrahimi et al. (2016) by assuming constant density. We divide the distribution into 20 bins, return the ratio of the area under the curve of the debris to the bulk as the surface excess. A bin size of 20 gave the minimal sampling fluctuation and was based on the square root choice of bin width (Ng et al., 2013). In Fig. 4.8a, we plot the surface composition as predicted by the model, and in Fig. 4.8b, we present the evaluated surface excess in the debris as a function of the molecular weight.

From Fig. 4.8b we make four observations:

(i) Depletion of chains with $M < M_e$ in the debris

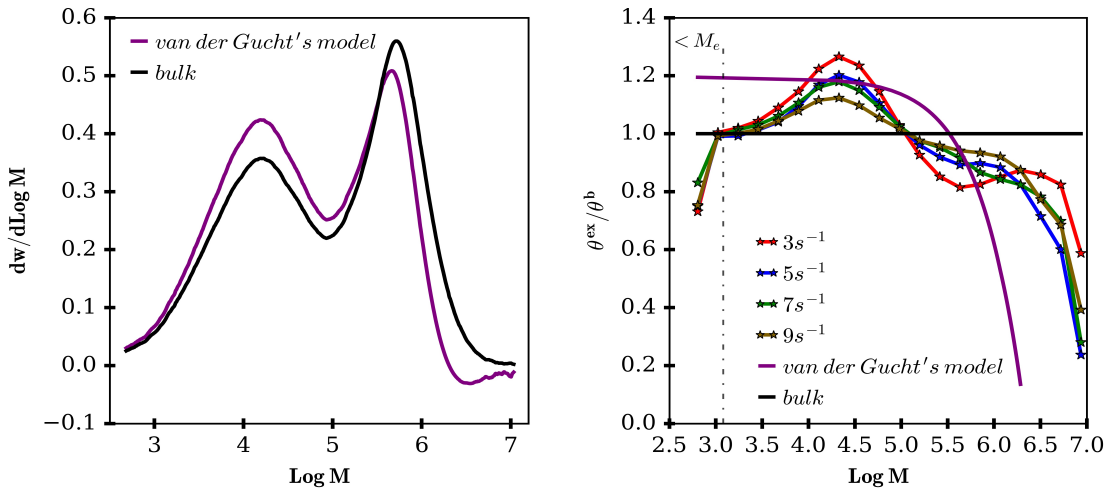

(a) (b)

Figure 4.8: Surface segregation: MWDs (a) of bulk (experimental) and surface as predicted by the Van der Gucht et al. (2002b) model. (b) Surface excess as a function of molecular weight for debris (experimental) and Van der Gucht et al. (2002b) model.

(ii) The enrichment/depletion transition point of the debris occurs at a chain length $M < M_W$

(iii) The enrichment section (above the horizontal dashed line) has a different shape from the model prediction.

(iv) An enrichment which decreases with increasing shear rate.

The higher median chain length of the debris as compared to that of the bulk can be attributed to the depletion of chains whose molecular weights were lower than M_e as seen from Fig. 4.8b. Considering the depletion of unentangled chains, we propose the following. During flow, the bulk chains would have to slide over the tethered chain by a distance equivalent to its tube length (Adjari et al., 1994). The required friction force per sliding chain is given by $f_v = \zeta N \dot{\gamma} D$, with $\zeta, N, \dot{\gamma}, D$ being the monomeric coefficient, the number of monomers per chain, the shear rate and the Pincus blob size respectively (Brochard-Wyart et al., 1996; Colby et al., 2007). When $N > N_e$, f_v can be expressed

in the form $f_v = \eta_o a P (P/N_e)^2 V$ (Brochard-Wyart et al., 1996), where P is the mobile chain of molecular size a having a monomer viscosity η_o, travelling at a speed V. This latter expression makes evident the increase in force required to pull entangled chains along with the flow. Therefore, for unentangled chains at the interface, a much lower force is required to pull them past the tethered chains. This implies that unentangled chains that are not directly adsorbed onto the surface are pulled along with the bulk flow. Hence the observed depletion of chains smaller than M_e.

With regard to the enrichment/depletion transition, a zero surface-excess is predicted by Van der Gucht et al. to occur at molecular weight equal to M_W. We however observe this transition point at a much smaller molecular weight for this particular material. Acknowledging the fact that the enrichment/depletion transition point is independent of the polymer-surface interaction (Van der Gucht et al., 2002a) coupled with the simple shear experimental setting used in this study, leaves us with the nature of the cohesive failure as the only possible reason for this observation. The influence of cohesive failure on segregation will be discussed in later paragraphs.

The ability of a chain to adsorb itself on the surface depends on its ability to compensate for conformational loss at the wall, (Van der Gucht et al., 2002a) which decreases as chain length increases. The possible number of adsorption sites occupied by the chain on the other hand increases with the chain length. For chains of intermediate length that are able to compensate for conformational loss, adsorption to multiple sites is highly probable (Bouchaud and Daoud, 1987). In this regard, the area under the curve of the enrichment section could be viewed as the overall probability that chains would directly adsorb themselves to the wall and be able to resist the force applied by the bulk flow.

Ebrahimi et al. (2016) used a microtome to collect a thin surface layer of polymer from an extrudate exiting a capillary. GPC analysis showed not only an enrichment in short chains but also a high molecular weight (HMW) fraction enriched relative to the

bulk. Their technique provides useful information on the thin layer of polymer adjacent to the debris, which is in effect the layer closer to the bulk and not the debris itself since the debris remained in the die. Hence the enrichment observed in HMW relative to the bulk is an indication that the layer adjacent to it, that is the layer at the wall was depleted of moderately long chains. In Fig. 4.9, we plot the surface excess of the thin layer of segregated polymer accessed by Ebrahimi et al. (2016) as a function of molecular weight. A depletion of moderately long chains is observed. The thickness of the layer accessed by their method is of approximate magnitude as ours. A clear opposite trend as compared to our debris is observed: a depletion of moderately long chains while chains that were relatively shorter or longer were enriched. This is for the layer of chains closer to the bulk than the debris, in other words, at the other side of the plane of failure. This remarkably serves not only as a validation of our results but also highlights the effectiveness of our method in accessing directly the chains adsorbed to the surface.

Besides looking at the MWD of the debris, we also perform an analysis of the morphology of the film. There are several parameters used to describe the morphology of a surface (Sadowski et al., 2016; Abbott and Zhu, 2019). In this study we use the following: the average height of the film (H_{av}); the root-mean square roughness of the film (R_q) which quantifies the deviation of the roughness profile from the mean line; the amplitude of the waviness of the surface (W_p) and the skewness (S_{sk}) which measures the symmetry of the surface profile about the mean. A positive skewness indicates a surface profile with much more peaks than valleys while a negative value is an indication of the converse. Table 4.2 lists the shear rate dependent values of those parameters.

We remark that apart from the surface being made of peaks and valleys [see Fig. 4.5], there were also regions that seemed to be bare glass. A visual inspection of the debris is presented in Fig. 4.10. The top row, taken with a Canon Camera, highlights the presence of holes in the thin film while the row beneath is an optical micrograph obtained at a $5X$

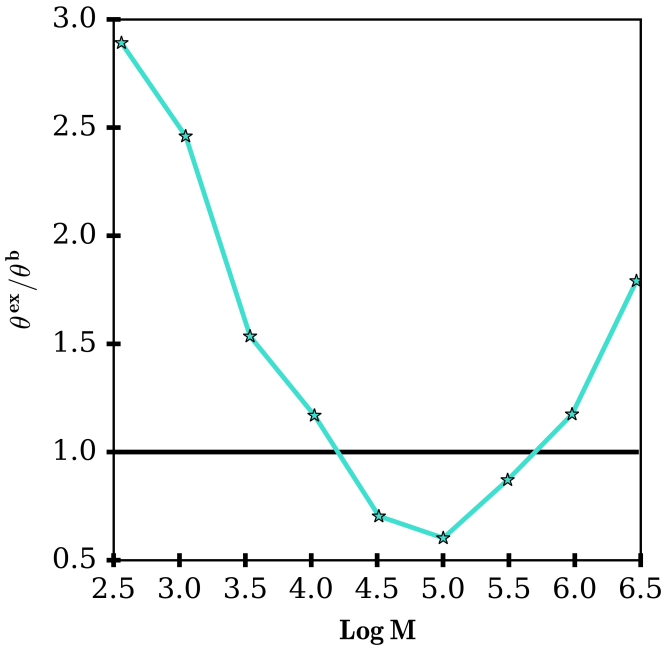

Figure 4.9: Surface excess as a function of molecular weight for debris with M_W=212 kg/mol ($LogM = 5.3$). Data from Ebrahimi et al. (2016) were digitized and analyzed following our approach

Table 4.2: Surface parameters describing thin films

Shear rates	$R_q(nm)$	S_{sk}	$W_p(nm)$	$H_{av}(nm)$
3 s^{-1}	144.7± 94	1.05± 0.3	258.1± 164	786.4 ± 108
5 s^{-1}	16.1± 60	0.92± 0.4	71.3± 31	995.1 ± 149
7 s^{-1}	4.3± 0.40	0.76± 0.5	18.3± 2.6	1287.5 ± 237
9 s^{-1}	6.5± 1.10	1.38± 0.4	32.8± 6.5	1571.0 ± 391

magnification using a Zeiss Axioplan fluorescence microscope, which gives us a close-up view of the holes. The spatial distribution of the holes at any given shear rate was random on the glass slide but their frequency and size decreased at higher shear rates [see section Fig. B.2].

The occurrence of holes in thin molten films can sometimes be attributed to dewetting. Dewetting could potentially occur after slip but before the temperature is cooled as a

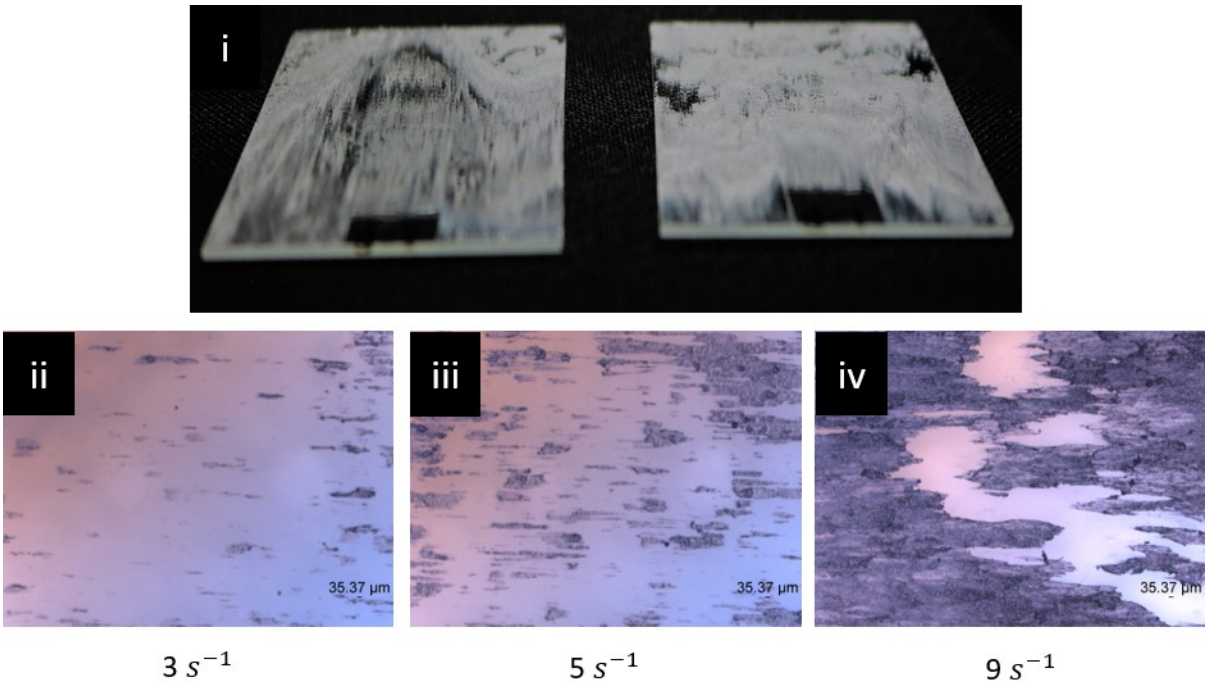

Figure 4.10: Visual depiction of holes in the thin film. Top row is a photograph and bottom row is depiction using optical microscopy.

result of interfacial instabilities. These instabilities typically result in the rupture of the film creating holes at locations where the film is thinner. These holes eventually grow laterally over time resulting in the formation of rims around them (Müller-Buschbaum and Stamm, 1998; Geoghegan and Krausch, 2003; Janiszewska et al., 2020). We rule out dewetting as a possible reason for the holes observed on the films in our study for the following 3 reasons:

(i) the films produced in this study are stabilized by gravity due to their large thickness [Table 4.2] (Xue and Han, 2011);

(ii) the amplitude of modulation of the surface of the film is not equal in magnitude to the thickness of the film, which is required for rupture (Xie et al., 1998); and

(iii) the kinetics of dewetting of a material is influenced by its molecular weight and the

distribution of relaxation times (Liu et al., 2002).

So, in the unlikely event of the rupture of the film due to surface instability, the lateral growth of the holes to form rims would be very slow. Therefore, dewetting is unlikely and a more plausible reason for the observation of holes in our films would be the pulling of chains from the surface during flow.

On a high energy surface, tethered or adsorbed chains are believed to preferentially disentangle themselves from the bulk polymer rather than desorb from the wall. The surface energy of the glass slides used in this study is 50 mJ/m^2 (Sattari et al., 2022), classifying it as high energy (Kuang et al., 2014). We remark that holes were also observed in the debris even on steel plates which has higher surface energy value of 60 mJ/m^2 (Sattari et al., 2022) [See Fig. B.4]. The micrographs suggest that those holes could really be bare glass, and FTIR performed at those regions did not contain peaks expected for HDPE [See Fig. B.5]. The presence of these holes could have an implication on the possible slip mechanism as discussed later. We do however acknowledge the limitation in terms of the resolution of the FTIR device used to confirm that those regions are indeed bare glass, hence the possibility of a very thin undetected layer of polymer at those regions is not ruled out.

The polymer chains adsorbed on the wall have been shown to form tails, loops, and trains. This has been shown theoretically (Scheutjens and Fleer, 1979, 1980), confirmed through simulations (De Virgiliis et al., 2012; Sgouros and Theodorou, 2020) and inferred experimentally (Lyklema and Van Vliet, 1978). The adsorbed amount of chains on the surface, for a monodisperse system, was shown to scale with $\sqrt{N}$ where N is the chain length (Scheutjens and Fleer, 1980; De Virgiliis et al., 2012); hence variations in amount of material adsorbed on a surface could be expected for polydisperse system (Lyklema and Van Vliet, 1978) .

In most experimental studies involving thin films, the adsorption of the polymer onto

the substrate was achieved through careful deposition of the polymer by various means such as spin-coating. In those systems the formation of tails, loops and trains by the chains were also observed (Cosgrove and Griffiths, 1992; Coppée et al., 2011). Our films by contrast were obtained as a consequence of failure at a plane near the wall hence the interface could be expected to be rough. The value of the skewness parameter listed in Table 4.2 indicates a surface dominated by peaks. Considering the scale, the observed thickness of our films, is unlikely to be influenced by contributions from tails, loops and trains. The roughness of the surface of the film (Table 4.2) is however of macromolecular scale. This is likely related to the probability of whether a particular entangled chain would join the bulk flow or not as determined by the side of the plane of failure on which its center of mass is located. The trend in Table 4.2 clearly shows an increase in thickness and a decrease in roughness with shear rate.

The manner in which the materials slips depends on the shear rate and can be broadly categorized into a weak slip followed by a transition zone and then strong slip (Hatzikiriakos, 2012). In each of those regions, one or more dominant relaxation mechanisms of the tethered chains could occur (Mhetar et al., 1998; Joshi et al., 2001). The slip behaviour of the bulk sample was studied by Sattari et al. (2022) and is presented in Fig. 4.11. The red circles are interpolated values corresponding to our experiments. The tube-model parameters calculated for our material are used to calculate the Weissenberg number shown in Table 4.3 and to define the slip regions in which the shear flow experiment was performed as specified by Mhetar et al. (1998) and added as line to Fig. 4.11, which serves as a theoretical demarcation between the transition zone and the strong slip region for this material. Experimental studies have shown that strong slip is independent of the MWD (Ansari et al., 2013; Sattari et al., 2022). We note that the experimental point at 111.35 kPa (Fig. 4.11) falls exactly on at the theoretical boundary between the transition and strong slip zones. In the experimental slip study (Sattari et al., 2022) this

point was identified as the last point in the transition zone; a truly remarkable agreement between theory and experiment considering the very broad MWDs that we are working with.

Table 4.3: Weissenberg number at experimental shear rates

$Shearrate$	$W_{i,\tau_{rep}} = \dot{\gamma}_a \tau_{rep}$	$W_{i,\tau_{rouse}} = \dot{\gamma}_a \tau_{rouse}$
3 s^{-1}	0.959	0.00121
5 s^{-1}	1.60	0.00201
7 s^{-1}	2.24	0.00281
9 s^{-1}	2.88	0.00365

The polymer is subjected to strong flow at $W_{i,\tau_{rep}} \sim 1$ (Kirk et al., 2018; Sgouros and Theodorou, 2020). From Table 4.3, the experimental conditions under which the simple shear experiment were performed caused the chains in the system to experience more of stretching than chain orientation (Robertson et al., 2022) as indicated by the magnitude of $W_{i,\tau_{rep}}$ relative to $W_{i,\tau_{rouse}}$ and reflected by the continuous decrease in surface roughness, R_q.

The relaxation mechanism experienced by the tethered chains can be inferred from the slip region in which the experiment was carried out (Mhetar et al., 1998; Joshi et al., 2001). In the transition zone, that is below the horizontal line in Fig. 4.11, the flow of the bulk chains causes the tethered chains to align in the direction of flow [see Fig. 4.10(ii & iii)]. The tethered chains in this region relax through convective constraint release. In the strong slip region on the other hand, a sudden disentanglement of the layer attached to the wall from the bulk chains is expected to occur once the critical stress for the onset of strong slip is exceeded. Therefore, tethered chains in the strong slip region relax through a combination of fluctuation and retraction. Fig. 4.12a presents the root-mean square of the debris surface roughness as a function of the slip velocity. The exponential reduction in the debris roughness with increasing slip velocity is consistent with the increased

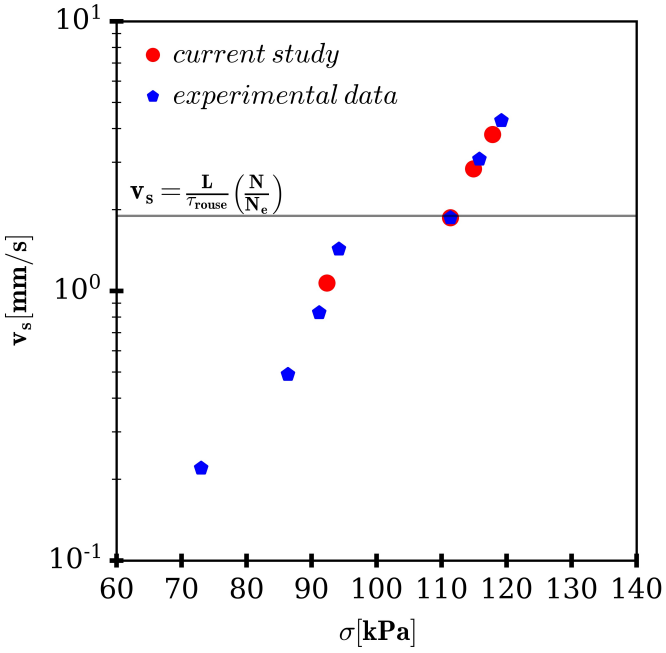

Figure 4.11: Slip velocity as a function of stress. Red circles are interpolated values corresponding to this study and blue symbols are original experimental data from Sattari et al. (2022).

alignment of the tethered chains with the flow in agreement with theoretical predictions (Mhetar et al., 1998; Joshi et al., 2001).

The occurrence of holes on a high energy surface during flow as observed in our experiment suggests that using the surface energy of the substrate as a single indicator to categorize a slip mechanism as either adhesive or cohesive can sometimes have limitations especially at lower shear rates. The reduction and eventual disappearance of holes with increasing slip velocity is as a result of "the chains of the skin being trapped above a threshold slip velocity" as remarked by Brochard-Wyart et al. (1996). The trapping of the tethered chains at higher slip velocity results not only in the MWD distribution of the debris approaching that of the bulk distribution at higher shear rates [Fig. 4.6] but also suppresses the enrichment/depletion process as seen from Fig. 4.12b where the area under the normalized enrichment curve ($\Gamma = \int_{M_e}^{M_{tr}} [\theta^{ex}/\theta^b] dM$) from Fig. 4.8b is plotted

as a function of the slip velocity. Note M_{tr} is the molecular weight at which the debris becomes depleted relative to the bulk.

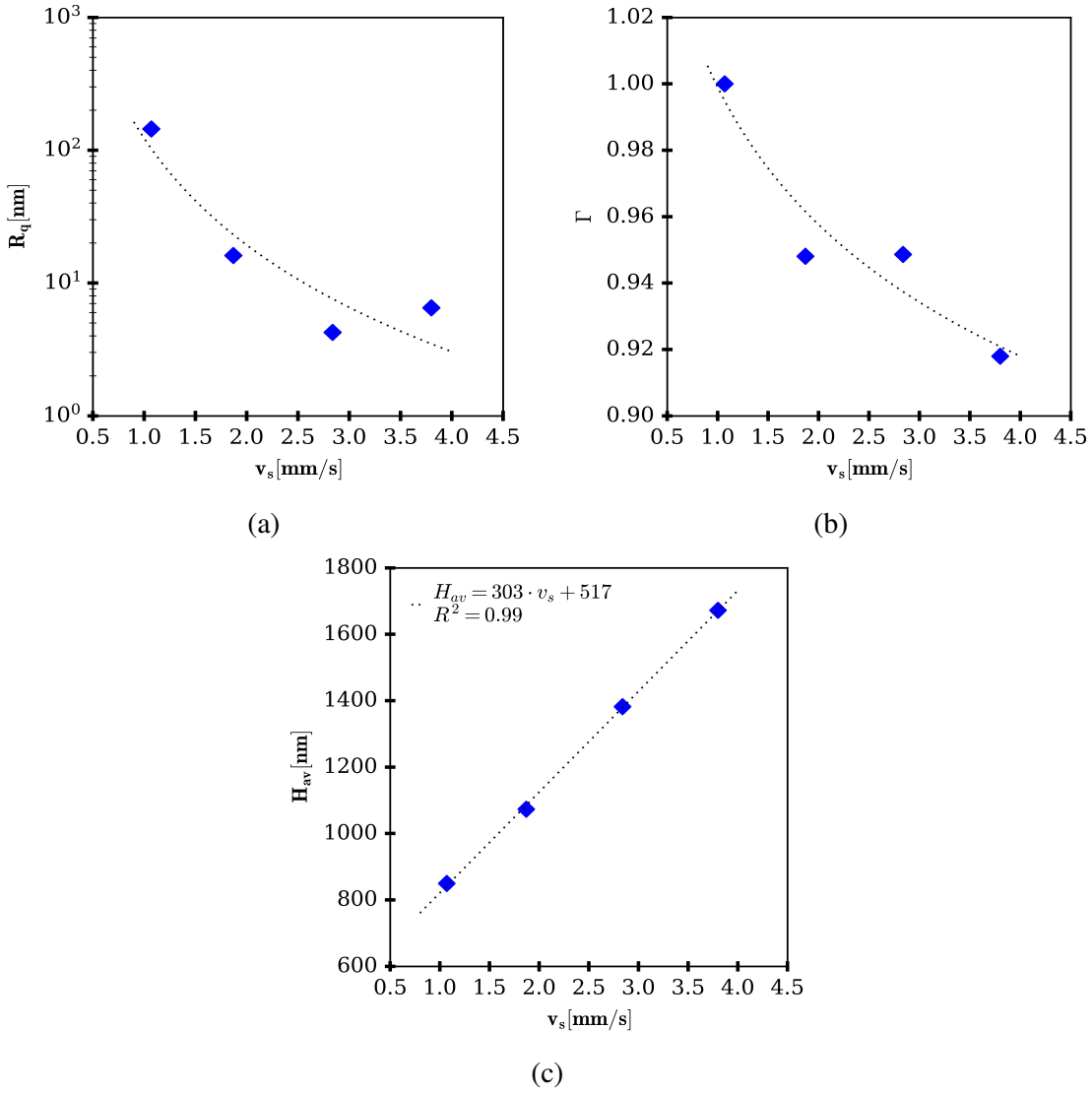

Figure 4.12: Thin film's properties as a function of slip velocity (a) R_q versus V_s (b) normalized enrichment as a function of slip velocity (c) H_{av} versus V_s. Lines in (a) and (b) are to guide the eye only.

Brochard-Wyart et al. (1996) observed a linear relationship between the density of the grafted chains and the slip velocity. A similar relationship is observed in our study [see Fig. 4.10(ii,iii,iv) & Fig. 4.12c]. In Fig. 4.12c, the film thickness is plotted as a

function of the slip velocity showing a correlation of 0.99 as measured by the R-square value. Even though the difference in order of magnitude between the thickness of our films and those studied by Brochard-Wyart et al. is wide and may suggest the presence of additional mechanism, the similarity is nevertheless remarkable. This finding also aligns with observations made in previous studies in which die drool increases with slip velocity (Musil and Zatloukal, 2011). Die drool is thus the capillary flow equivalent of debris from slip in simple shear.

4.4 Conclusion

Surface fractionation was shown to occur even in a flow system without a bulk shear gradient: simple shear flow with slip. The surface fractionation was observed to be shear rate dependent. The enrichment/depletion transition occurs at a value lower than M_W highlighting the depletion of long chains occurring at a chain length lower than the thermodynamically predicted M_W due to slip. Unentangled chains were also observed to be depleted. The root-mean square roughness of the debris film was observed to decrease with increasing slip velocity while the debris thickness linearly increased with slip velocity. The holes in the debris on a high energy surface observed during this study suggests a possible combination of adhesive and cohesive slip mechanism at the shear rates used in this study. Surface fractionation was suppressed at higher shear rates.

Chapter 5

Effect of short chains content and molecular weight on polymer fractionation at the interface in Simple Shear

5.1 Abstract

In chapter 4 it was shown that for short chains to enrich the surface, they must be of length greater than M_e. The role played by short chains in enriching the surface is however undeniably important but the influence of their length and volume fraction in the material is not well understood. In this chapter we address that by making use of monodisperse short chains samples. During simple shear of polymer melts in sliding plate rheometry with highly absorbing substrates, a thin debris of polymer remains on

the substrate after the melt undergoes strong slip. We collect this debris and measure its molecular weight distribution using gel permeation chromatography. Binary mixtures of linear polybutadienes are investigated in a systematic manner. It is observed that the molecular weight distribution of the debris is significantly enriched by short and intermediate length chains with an equivalent depletion of long chains as compared to the bulk. The results are in overall agreement with predictions from thermodynamic segregation theories though the detail of the distribution is significantly different in some cases. Also, since the flow geometry is simple shear, this low molecular weight enrichment at the surface cannot be explained by the shear stress gradient induced fractionation that is believed to occur in capillary flow. These findings are important for a better understating of many polymer flow related phenomena including wall slip, die drool, and extrudate surface instabilities.

5.2 Introduction

Surface enrichment of short chains in polydisperse polymers (Hariharan et al., 1990, 1991; Van der Gucht et al., 2002b; Minnikanti et al., 2007; Inn, 2013; Matsen and Mahmoudi, 2014), has extensive implications in polymer processing and end-product surface characteristics. In polymer processing, wall slip, (Brochard-Wyart et al., 1996; Archer, 2005; Ansari et al., 2013; Sabzevari et al., 2014b,a; Ebrahimi et al., 2015, 2016) wetting/dewetting (Redon et al., 1991; Jones and Richards, 1999; Reiter and Sharma, 2001; Bäumchen et al., 2014; Sabzevari et al., 2015a, 2016) and extrudate surface instabilities including die drool (Gander and Giacomin, 1997; Musil and Zatloukal, 2011) and melt fracture (Denn, 2001) have been related to surface enrichment of low molecular weight (M_W) species at the interface. Also affected are surface/interfacial properties such as

surface tension (Minnikanti et al., 2007; Mahmoudi and Matsen, 2017) and thermal properties such as glass transition temperature (Tanaka et al., 2002) that are important specifically for thin film polymer applications. Understanding of surface segregation hence becomes crucial, specifically in polydisperse systems typical of industrial polymers.

Surface segregation in polymers can be driven by chain disparities due to a combination of entropic and enthalpic factors or by a shear stress gradient across the flow channel. In linear polydisperse polymers, chains are chemically identical differing only in molecular weight. Surface segregation is thus mainly induced from factors motived by chain length disparities. These factors in both flow and static conditions can be entropically driven by the reduced conformational entropy at the surface or enthalpically driven by the surface attraction/repulsion of chain ends. The latter reflects the surface energy difference between the backbone and end groups of the chain (Van der Gucht et al., 2002b; Minnikanti et al., 2007).

Shorter chains suffer less from entropy reduction at a surface than longer chains and hence are thermodynamically driven to the surface (Hariharan et al., 1990; Stark et al., 2007). Van der Gucht et al. (2002b) used a self-consistent field model to derive an equation for the entropically-driven integrated surface excess of each component in a mixture of linear chains. In their model, the integrated surface excess of a chain of length N in the debris relative to the bulk is expressed as: $\theta_N^{ex} = (\phi_{N,d} - \phi_{N,b})$ where ϕ_N is the volume fraction of chains of length N and the subscripts b and d represent the bulk and debris materials, respectively. The integrated surface enrichment relative to the bulk composition is $\theta_N^{ex}/\phi_{N,b} = A(1 - N/N_W)$ in which A is a pre-factor and N_W is the weight average chain length of the polydisperse polymer.

Energetic factors strongly enhance surface segregation when end segments are preferentially attracted to the surface as compared to backbone units resulting in a change in the pre-factor A in the Van der Gucht et al. relation. In a linear system, since all chains

possess two ends, the number of backbone units determines which chains are more affected by the energetic force. This means that the shorter chains are enriched or depleted at the surface (Van der Gucht et al., 2002b; Minnikanti et al., 2007) depending on the relative surface attraction of the chain ends and the backbones (Tanaka et al., 2002).

Under certain flow conditions such as capillary extrusion, surface segregation is believed to be also mechanically driven by the shear stress gradient across the flow channel: this is called the shear induced fractionation (Shelby and Caflisch, 2004; Musil and Zatloukal, 2011; Inn, 2013). Theoretical work (Rorrer and Dorgan, 2014) has indicated that surface segregation of low molecular weight chains occurs under capillary flow due to the shear stress gradient, while in the case of simple shear without slip no such enhanced segregation occurs. It is important to note that slip and die drool in capillary flow have also been linked both experimentally (Musil and Zatloukal, 2011) and theoretically (Schmalzer and Jeffrey Giacomin, 2013).

We have previously studied wall slip of binary and ternary mixtures of short and long chains of polybutadiene (PBD) (Sabzevari et al., 2014b,a) and polystyrene (Sabzevari et al., 2015a, 2016) on different substrates and different flow conditions. We showed that among samples with similar weight average molecular weight (M_W), slip is enhanced in those with lower number average molecular weight (M_N). Also, for slip of polydisperse systems, the size and the content of the largest chains in the mixture is the dominant factor affecting slip when short chains with different content values are present. In accordance with our previous studies, here we investigate the surface enrichment of short chains.

Characterizing the surface composition of a polymer of chemically identical chains has been one of the most challenging aspects of surface segregation studies (Jones and Richards, 1999; Tanaka et al., 2002). The use of molecular weight distribution (MWD) analyses has been hindered by experimental difficulties in collecting samples: the depth of the enrichment layer is so small that it is practically impossible to separate it from the

bulk for Gel Permeation Chromatography (GPC) measurements. Spectroscopic characterization techniques and neutron reflectivity, on the other hand, suffer from the lack of a proper test probe to monitor the enrichment without inducing additional energetic effects, e.g. labeling and deuterating chain (ends) changes its surface energy and induces an energetic driving force (De Gennes, Pierre-Gilles Gennes, 1979; Hariharan et al., 1993; Zhao et al., 1993; Tanaka et al., 2002).

Tanaka et al. (2002) were the first to measure the surface enrichment of short chains in thin polystyrene PS films without chemical labeling. They measured the glass transition temperature, T_g, of the air-polymer surface of binary and ternary mixtures of short and long chains and compared those to the surface T_g of the pure constituents. By using a typical T_g mixing rule, they inferred the surface composition. Their work is indeed interesting, illustrating relative excess of short chains to more significant extents than the maximum value predicted by Van der Gucht et al. (2002b) relation, which only considers entropic effects. As the authors reported in their previous work (Tanaka et al., 2002), preferential attraction of chain ends to the surface was clearly a contributing factor.

Hill et al. (2018) used surface layer matrix-assisted laser desorption ionization time-of-flight mass spectrometry (SL-MALDI-ToF-MS), to distinguish surface species without labeling. They showed that their method provides the entire MWD demonstrating that entropically driven surface enrichment of short chains occurs even in low polydispersity polystyrene and poly(methyl methacryalate) after annealing.

The objective of the present study is to provide the first experimental data on the extent of surface enrichment of short chains in simple shear flow with slip. Our choice of materials affords us the opportunity to investigate the effect of short chain length and content on fractionation. By using simple shear flow in a sliding plate rheometer (SPR) we ensured that flow induced fractionation does not contribute to our observations. During the SPR experiment, a thin debris of polymer remains on the substrate after the

sample undergoes strong slip (Koran and Dealy, 1999; Park et al., 2008; Sabzevari et al., 2015b). We collect this debris and measure its MWD using GPC. Binary mixtures of linear PBDs are investigated in a systematic manner.

This work is the first presentation of the MWD of the interfacial layer at the polymer-solid interface after slip in simple shear. Results indicate significant surface enrichment of short chains at the polymer-solid interface. Findings in this work are important for a better understating of interfacial properties of thin films and wall slip as well as polymer processing issues such as die drool and melt fracture specifically in polydisperse polymers typical of industrial applications.

5.3 Materials and experimental procedure

Two sets of linear 1,4-polybutadienes (PBD) were used, as listed in Table 5.1:

(i) one polydisperse PBD denoted as $336k$ purchased from Sigma Aldrich and

(ii) three monodisperse (narrowly distributed) polymers denoted as $10k$, $44k$, and $90k$ purchased from Polymer Source Inc. Canada.

The molecular weight distribution of all polymers shown in Fig. 5.1 were characterized by GPC relative to linear polystyrene (Waters 1525; THF at $35^o\,C$ with a flow rate of 1 mL/min; Phenomenex column; refractive index detector). Debris and bulk material of all blends listed in Table 5.2 were also subjected to the same GPC analysis. Bulk specimens were collected and analyzed both before and after shear flow to evaluate the impact of shearing on our observations.

Mixtures were prepared in solution ($\sim$ 10% weight fraction ($wt\,\%$) polymer) with dichloromethane (DCM) by mixing for 3 days. The solvent was evaporated at room temperature followed by further drying under $\sim 70\,cmHg$ vacuum for 3 days.

Table 5.1: Molecular weight characteristics of PBD samples used in this study

#	Sym.	$M_N(kg/mol)$	$M_W(kg/mol)$	PI
1	$10k$	9,533	9,959	1.04
2	$44k$	40,260	43,702	1.09
3	$90k$	81,648	90,071	1.10
4	$336k$	169,777	336,158	1.98

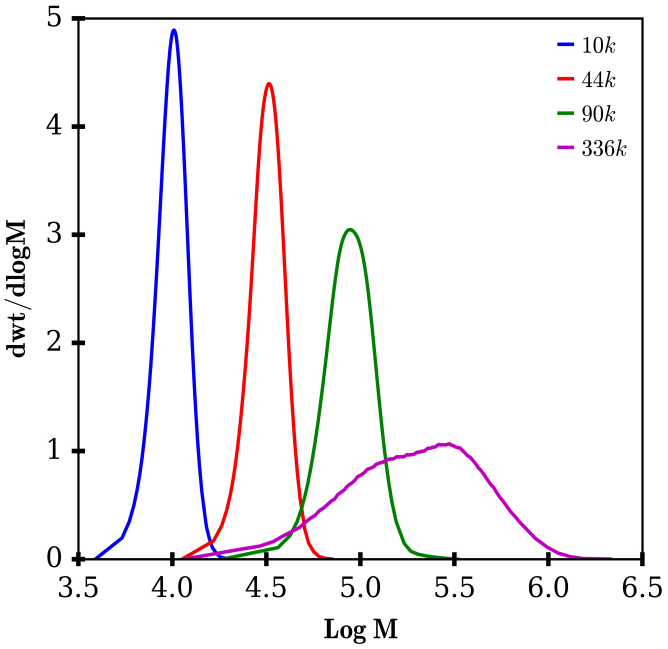

Figure 5.1: Molecular weight distribution of base polymers.

Seven materials were studied in total: the pure PBD $336k$ sample which was used as the reference and 6 binary mixtures made up of the monodisperse polymers and the reference PBD $336k$ material. For each monodisperse polymer, two binary mixtures comprising 10 and 20 $wt\,\%$ were prepared with PBD $336k$. Binary samples were labeled for example as: $336k - 10k(90/10)$ for a blend of $10wt\,\%$ PBD $10k$ in PBD $336k$. Table 5.2 shows the list of binary mixtures. The radius of gyration was calculated from the expression (Dealy and Larson, 2006) $< R_g^2 >_0 = (C_\infty l^2 j/6M_o)M_W$ with the constants

having as value (Strauch et al., 2009) $C_\infty = 4.61, j = 2, M_o = 54.09\, g/mol$ and $l = 1.34 \times 10^{-10} m$.

Table 5.2: List of PBD samples examined in the present work. All molecular weight information obtained using GPC. Indices b and d represent bulk and debris, respectively.

#	sym.	$M_{N,d}$ (kg/mol)	$M_{W,d}$ (kg/mol)	PI_d	$R_{g,b}$ (nm)	$M_{N,b}$ (kg/mol)	$M_{W,b}$ (kg/mol)	PI_b	$R_{g,b}$ (nm)
1	$336k$	125.0	264.1	2.11	11.6	169.8	336.2	1.98	13.1
2	336k-10k(90/10)	50.2	175.7	3.50	9.5	71.8	301.0	4.19	12.4
3	336k-10k(80/20)	33.1	179.4	5.41	9.6	37.1	212.7	5.73	10.4
4	336k-44k(90/10)	100.6	227.0	2.26	10.8	125.7	277.2	2.20	11.9
5	336k-44k(80/20)	75.0	165.2	2.20	9.2	97.3	236.3	2.43	11.0
6	336k-90k(90/10)	122.4	231.5	1.89	10.9	141.9	269.9	1.90	11.7
7	336k-90k(80/20)	104.6	207.5	1.98	10.3	131.9	241.1	1.83	11.1

All SPR experiments were carried out at room temperature. Specimens were prepared by compression molding at a pressure of 15 tons. Pressure on the mold was maintained for 60 minutes to allow for relaxation. The test specimen was then loaded onto the SPR and allowed 30 minutes for stress relaxation after which it was sheared. The gap between the SPR plates was maintained at 1 mm. The nominal shear rate was set at 5 s^{-1} for all the material studied, a choice based on previous PBD slip studies (Sabzevari et al., 2014a). The shear rate was kept constant allowing us to focus on the effect of the short chain length and content on surface fractionation.

Polymers flowing over a surface often slip (Wise et al., 2000; Hatzikiriakos, 2015) and previous studies (Brochardt and De Gennes, 1992; Migler et al., 1993; Awati et al., 2000) have shown that the slip behavior ranges from weak slip through a transition to strong slip. It is greatly influenced by the surface energy of the substrate. In the strong slip regime on a high energy surface the bulk chains disentangle from a monolayer close to the wall. Our choice of nominal shear rate ensured that the experiment was performed in the strong slip region. The travel distance was set at 50 mm. This results in a long

debris trail on the substrate (Fig. 5.2). All systems left a hazy debris behind on both plates confirming strong slip at a nominal rate of 5 s^{-1} (Park et al., 2008).

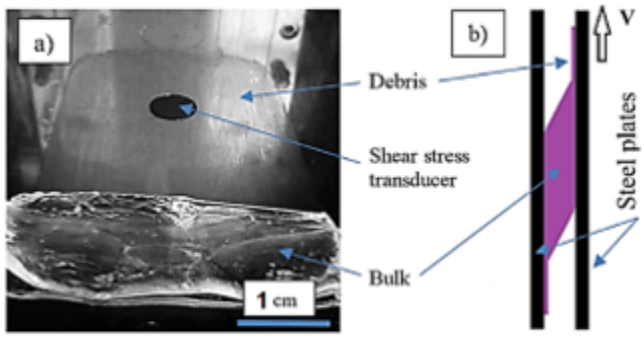

Figure 5.2: Slip and debris in simple shear, a) bulk and debris after slip of PBD and b) schematic of slip in the SPR shear cell (reproduced from Sabzevari et al. (2015b)).

5.3.1 Debris collection procedure

The moving plate of the SPR was modified to accommodate a removable microscopic glass slide on which the debris was collected (see Fig. 5.3). We machined a groove into the moving part of the SPR which was of appropriate dimension to fit a glass slide (40 x 80 x 1 mm). Prior to performing the experiments, the glass slide was thoroughly cleaned by washing with water and soap, and then rinsing with DI water, Acetone, and THF for 10 min each under sonication.

The debris was removed from the glass by submerging the entire slide into a solvent for two hours at room temperature. Two solvents were tested for this purpose: toluene and THF. The effectiveness of the solvent in completely removing the debris from the glass substrate was evaluated via FTIR analysis (ThermoScientific Nicolet iS10 FTIR Spectrometer). In Fig. 5.4 the FTIR spectrum is presented. It is clear from Fig. 5.4 that THF completely dissolved all debris from the glass substrate. THF was also used as the solvent for the GPC analysis, hence our debris solution was directly used for GPC

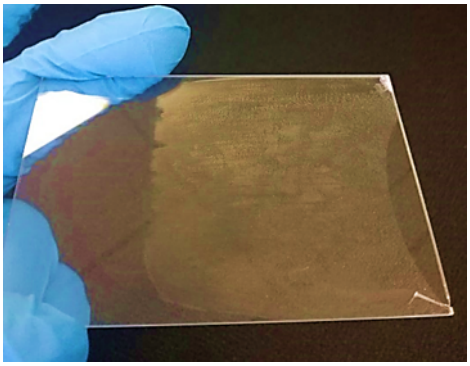

Figure 5.3: Debris on the glass slide after a shear test at 5 s^{-1} in simple shear flow using SPR (PBD $336k$).

analysis. This method ensured that the debris collection method was exhaustive.

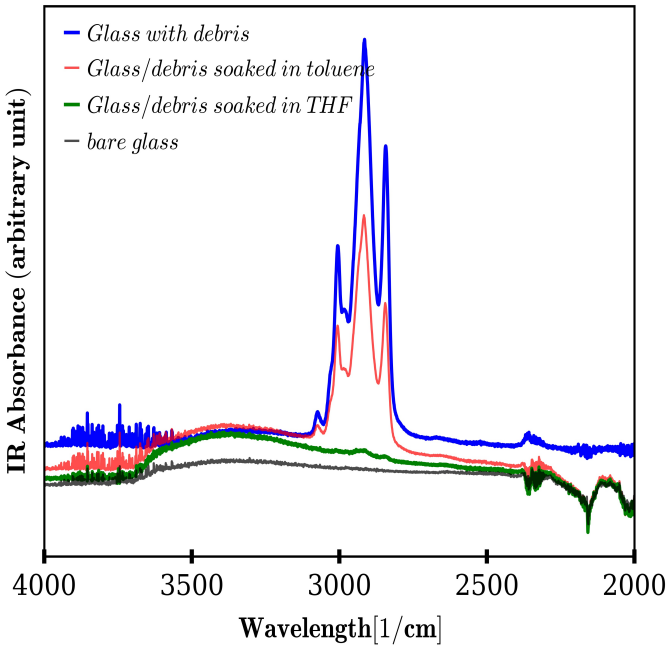

Figure 5.4: FTIR analysis of glass surface including the original clean, bare glass, the glass containing the debris and then the glass/debris after soaking in either THF or toluene. Data are shifted along the vertical axis for better illustration. It is shown that the PBD $336k$ debris can be removed from the glass surface after two hours dissolution in THF at room temperature.

The results from the GPC analysis of the reference material are presented in Fig. 5.5.

The debris MWD is noticeably different from that of the bulk. The possible effect that shearing could have on our results was evaluated by GPC testing the bulk sample both prior and after simple shear flow experiment. The results indicate no change in molecular characteristics. Therefore, simple shear did not cause any significant molecular weight fractionation within the bulk.

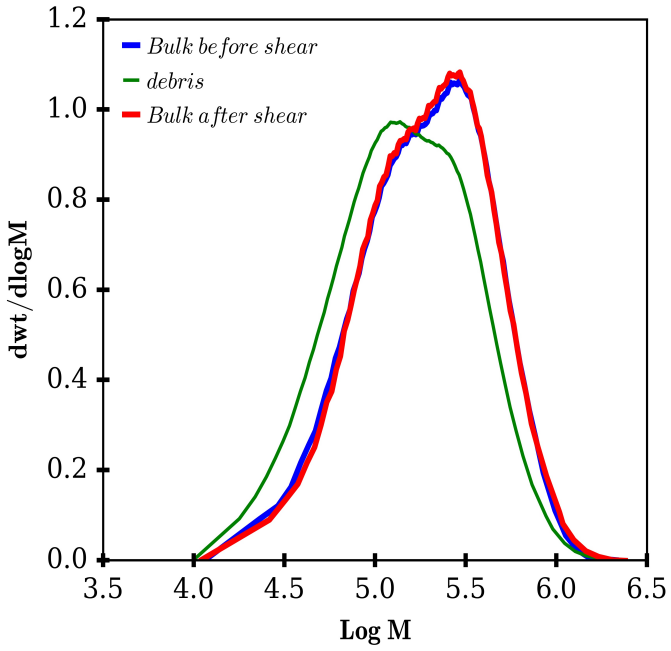

Figure 5.5: Molecular weight distribution of the PBD $336k$ bulk (before and after shear) and its debris.

Fractionation can occur in the absence of flow in response to the thermodynamic driving force (Van der Gucht et al., 2002b). This implies that during the rest period for stress relaxation, fractionation could have occurred. By performing our experiments at room temperature and a constant shear rate on polybutadiene allows us to assume that the contributions from thermodynamic driving forces are negligible in our analyses, leaving the effect of slip and the response of the chains of various lengths as the significant factors.

The average thickness of the debris on the glass substrate was 300 nm, as measured by tapping mode AFM (Nanoscope IIIa MultiMode SPM atomic force microscope). The thickness of the debris was one order of magnitude greater than the radius of gyration (Table 5.2).

5.4 Experimental results

The molecular weight distributions of the debris obtained by subjecting the materials to simple shear flow at a constant shear rate are presented in Fig. 5.6. Also plotted in that Figure is the MWD of their respective bulk material and the expected surface segregation as predicted by Van der Gucht et al.' s model (Van der Gucht et al., 2002b) . In making use of the model we follow the steps employed by Ebrahimi et al. (2016) which assumes constant chain density allowing for the replacement of N and N_W by M and M_W, respectively and the transformation of the expression $\theta_N^{ex}/\phi_{N,b}$ into $\upsilon_{ex}(M)/w_b(M)$. The sum of $\upsilon_{ex}(M)$, integrated surface excess, and $w_b(M)$, bulk weight fraction then gives the MWD function for the model. Minnikanti et al. (2007) also proposed a model for dealing with different species in polydisperse melt while Dorgan and Rorrer (2015) provided a model which accounts for both the concentration gradient present in the absence of flow and contributions emanating from shear gradient during flow. Our choice of model in our analysis was based on the fact that we were dealing with only a single species and had no shear gradient contribution in our flow system.

The MWDs of the debris for all of the materials clearly shows substantial differences from their respective bulk distributions: it has been enriched by short and moderate chains with a corresponding depletion in the content of longer chains. Similar observations in capillary flow had been attributed to flow induced fractionation (Shelby and Caflisch, 2004; Inn, 2013). In simple shear flow however it is thought that the absence of

the gradient in shear rate required to drive migration would make it impossible for such surface fractionation to occur (Dorgan and Rorrer, 2015) while our results clearly show that it happens. There exists two possible reasons for our observation: the first is the contribution from the localized stress gradient existing in the vicinity of the slip plane in simple shear flow (Rorrer and Dorgan, 2014) and the second is the likelihood of chains joining the bulk flow when they are in the vicinity of the slip plane depending on the location of their center of mass and their length.

Table 5.2 lists the M_W and M_N values of the bulk versus debris for PBD $336k$ and the binary mixtures, with the indices b and d representing bulk and debris, respectively. Attention is given to the number average molecular weights in Fig. 5.7.

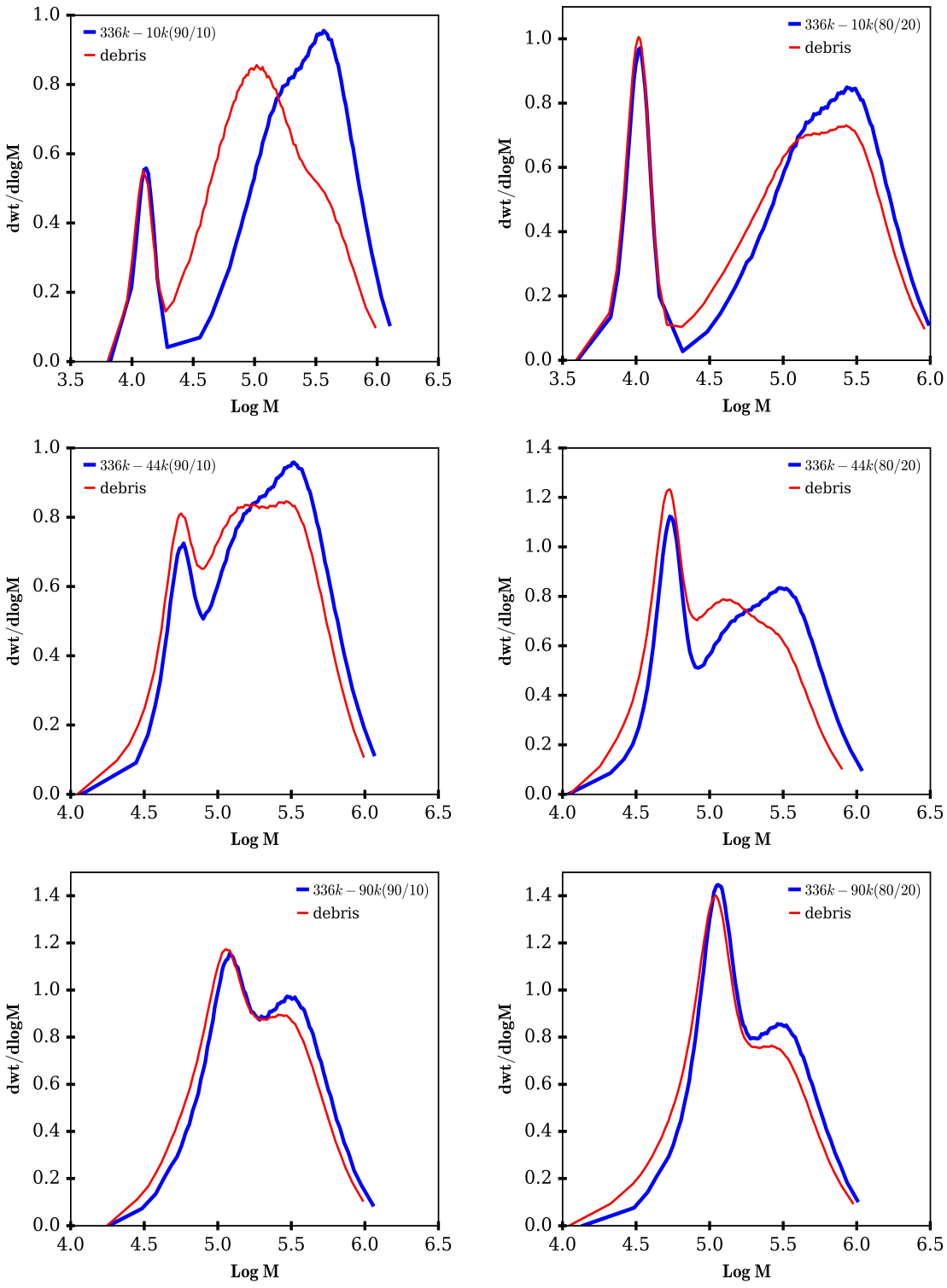

Figure 5.6: Molecular weight distribution of bulk (thick, blue line) and debris (red line, 10 s^{-1} for the binary mixtures)

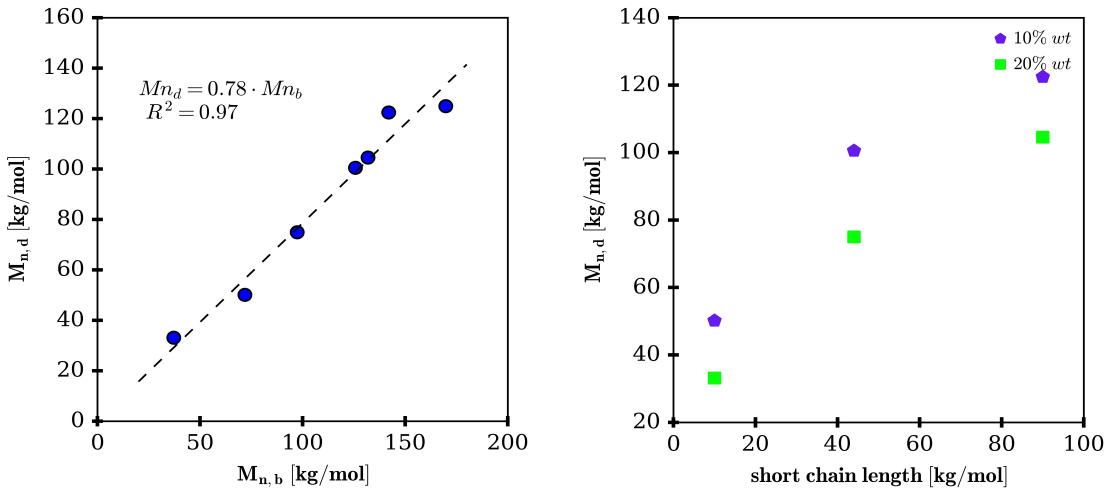

(a) (b)

Figure 5.7: M_N (a): Correlation of $M_{N,d}$ between $M_{N,b}$. Dashed line represents the linear regression fit of the data. (b): Correlation of $M_{N,d}$ with the chain length of the short chains, a reduction in $M_{N,d}$ with increasing weight fraction of LMW observed.

In Fig. 5.7a the M_N of the debris is plotted versus that of the bulk. A very strong linear correlation is observed, indicating that the debris had on average a M_N about 0.78% that of the bulk. This correlation indicates the importance of shorter chains in the molecular weight fractionation. A look at Fig. 5.7b which considers the number averages in terms of the influence of the chain length of the LMW components and their weight fraction however reveals an interesting trend. The M_N increases with the chain length of the LMW component while an increased weight fraction led to a reduction in the M_N. In order words the more the shorter chain content, the lower the M_N. The M_W however did not show such correlations, although all debris M_W are smaller than the corresponding bulk M_W.

To understand the results in Fig. 5.7, we employ the tube model to calculate the relaxation modulus of the materials and obtain their respective zero-shear viscosities. A test chain i in a polymer melt after being subjected to some form of perturbation, relaxes the stressed imposed on it by the use of several mechanisms. The surrounding

constraints are referred to as the tube out of which the test chain would have to reptate. The tube survival probability of the chain i at a specific time t can be determined from the expression (Doi and Edwards, 1986) :

$$P(t,M) = \frac{8}{\pi^2} \sum_{k=odd} \frac{1}{k^2} \left[exp\left(-\frac{k^2 t}{\tau_d} \right) \right] \tag{44}$$

where P_i is the survival probability and τ_d is the longest relaxation time. The effect of contour length fluctuation was incorporated through the longest relaxation time using the expression (Milner, 1996; Milner and Mc Leish, 1998) :

$$\tau_d = 3\tau_e \left(\frac{M}{M_e} \right)^3 \left[1 - \kappa \left(\frac{M_e}{M} \right)^{0.5} \right]^2 \tag{45}$$

where τ_e and M_e are the equilibration time and the molecular weight between entanglement, $1.31 \times 10^{-6}\ s$ and 1850 $g \cdot mol^{-1}$ (Struglinski and Graessley, 1985; Luengo et al., 1997; Pattamaprom et al., 2000; Ebrahimi et al., 2015) respectively [Ferry's (Ferry, 1980) definition was used for the value of M_e] . The relaxation modulus was then calculated using the expression

$$G(t) = G_N^0 \left(\int_{-\infty}^{\infty} w(M) P(t,M) d log M \right)^{\beta} \tag{46}$$

where β accounts for the cooperative constraint release and taken to have a value of 2, G_N^0 was taken to be equal to 1.15 MPa (Van Ruymbeke et al., 2002a; Liu et al., 2006). The calculated relaxation modulus curves are presented in Fig. 5.8.

The effect of the weight fraction of the low molecular weight (LMW) component is illustrated in Fig. 5.8a by presenting the simulated relaxation modulus of the PBD $336k - 10k$ series. At the time scale that the slip experiment was performed ($\sim 0.1\ s$), a depression in the relaxation modulus is observed with the introduction of short chains

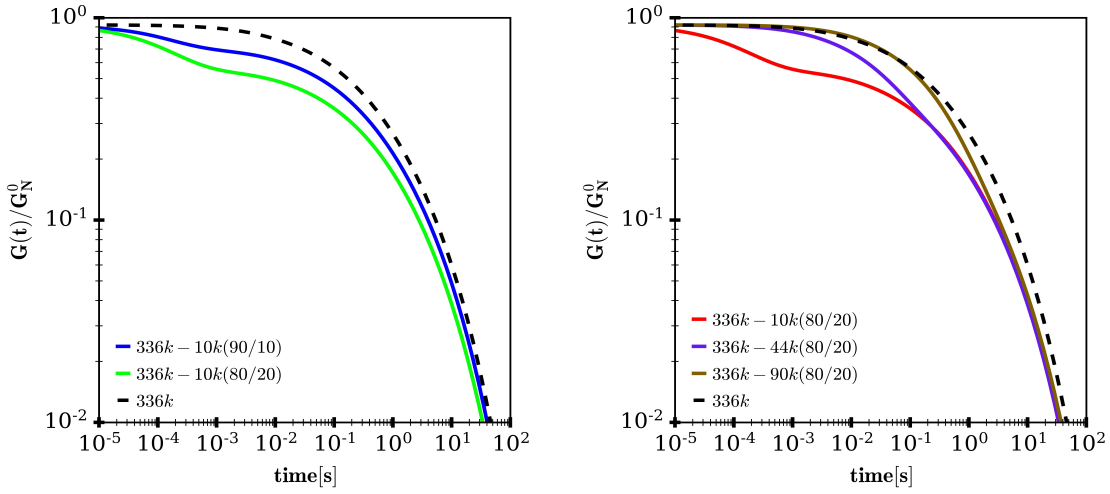

Figure 5.8: Calculated Relaxation Modulus (a): effect of weight fraction of short chains (b): effect of chain length of short chains at 20% weight fraction.

and its magnitude scales with the length and weight fraction of the short chains. In Fig. 5.8b the influence of the short chain length at a constant value of $wt.$ fraction is shown. Shorter chain lengths from the LMW component to more effectively cause a reduction in the modulus at lower and moderate time but had little influence at longer time. These observations were consistent with all the other materials.

A recent study on the effects of the shape features of the MWD on the relaxation behavior of polymers illustrated the manner in which the bimodal ratio and separation of the distributions influences the relaxation of polymer melts (Kwakye-Nimo et al., 2022a). Larger values of the bimodal ratio, which was defined as the ratio of the HMW peak to that of the LMW, were indicative of distributions dominated by the HMW component leading to slower relaxation of the melt. Hence, doubling the $\%wt.$ fraction of the short chains results in a reduction of the bimodal ratio, which leads to faster relaxation as shown in Fig. 5.8a. With regard to the influence of the short chain length in the binary mixture on the relaxation of the melt, the wider the difference (larger values of bimodal

separation), the smaller the time required for the short chains to relax and allowing the longer chains to relax at an early time. The depression of the relaxation modulus when varying short chain length observed in Fig. 5.8b therefore highlights the role played by the short chains in the constraint release process. When relaxed, chains which are not directly adsorbed to the surface but rather entangled with chains that were adsorbed, could be pulled along the bulk flow (or not) depending on which side of the plane of failure their center of mass sits.

We next turn our attention on how an enhanced relaxation of the melt influences surface enrichment, we start by segmenting our MWD into bins ranging from 7 to 10 based on the number of data points available in the MWD, in accord with the square root choice of bin width (Ng et al., 2013). The surface enrichment is then calculated as the ratio of the area under the curve of the debris to that of the bulk distribution and is presented in Fig. 5.9a for the reference material. Note that our method of segmenting the distribution and evaluating the enrichment per segment produces the expected 19.5% enrichment for Van der Gucht et al.' s model (Van der Gucht et al., 2002b). The debris, however, exhibited substantially higher enrichment than that predicted by the model. We additionally observe that the enrichment-depletion transition point occurs at a molecular weight lower than the M_W. This transition point seemed to depend on the details of MWD, which we believe influences the cohesive failure mechanism [see Fig. 5.9b]. In Fig. 5.9b the enrichment depletion curve of the reference material is compared to the two blends of $336k - 90k$, which clearly shows a transition point for the two blends also occurring at a different value other than the reference material and Van der Gucht et al.' s prediction. The enrichment- region was found to negatively correlate with the chain length, which is understood as a reduce probability for longer chains to preferentially want to adsorb themselves to the wall.

For a system which involves simple shear flow such as the one used in this study, the

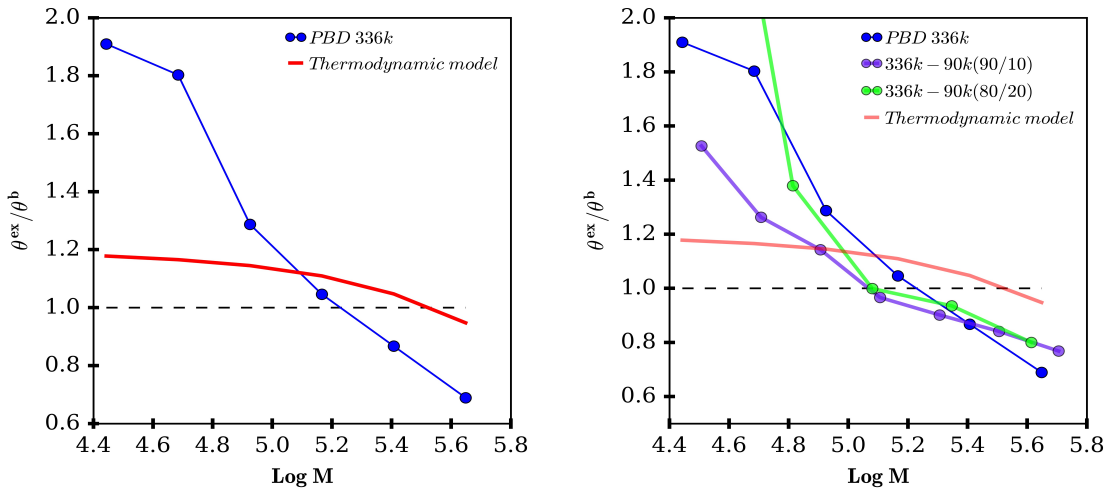

(a) (b)

Figure 5.9: Surface excess as a function of molecular weight for the (a): reference material and Van der Gucht et al. model (b) blends of $336k - 90k$, transition point also occurring at different value other than the reference and M_W

only plausible reason explaining the occurrence of the transition point at a value other than M_W is the nature of the cohesive failure. The failure mechanism at the interface has previously been attributed also to several other observations involving macroscopic phenomenon such as die drool (Musil and Zatloukal, 2011) and melt fracture (Inn, 2013).

To compare the influence that the short chain length and volume fraction had on surface enrichment we convert the MWDs into cumulative distribution functions (CDF). CDFs have the benefit of not only normalization but also allows us to easily compare key quantitative features such as the median from several data sets (Groeneboom and Pyke, 1983). The results for selected materials are presented in Fig. 5.10.

In Fig. 5.10(a & b) the CDF of the debris of the reference material and PBD $336k - 44k(80/20)$ are compared to their respective bulk distributions. The median chain length in the debris is clearly seen to be shifted to lower values as compared to the bulk in both cases. A shift in median to a lower value indicates the depletion of HMW chains and an enrichment of short chains. The median chain length of the debris was lower than

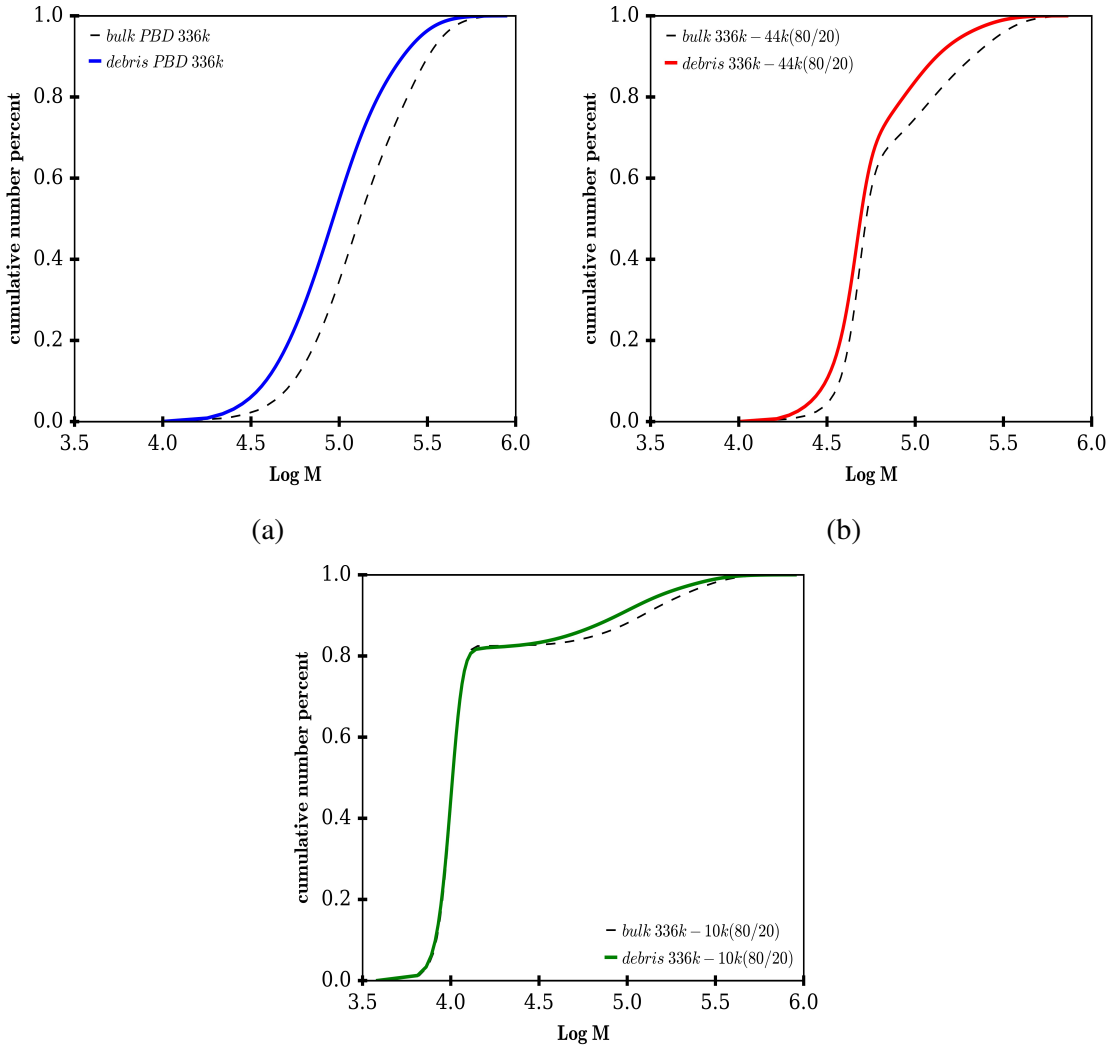

Figure 5.10: ECDFs (a) reference material (b) 336k-44k(80/20) (c)336k-10k(80/20)

that of the bulk in all cases except for those systems containing the lowest molecular weight short chain, $10k$. The CDF of PBD $336k - 10k(80/20)$ is shown in Fig. 5.10c. This system does not have a lower median chain length in the debris, but it is enriched at moderate values of molecular weight.

To determine how the chain length and their volume influenced surface migration, we next plot the ratio of the number average of the debris to that of the bulk as a function of

the chain length, this is shown in Fig. 5.11. We exclude the blend 336k-10k(90/10) from our analysis due to experimental flaws [shown as light purple].

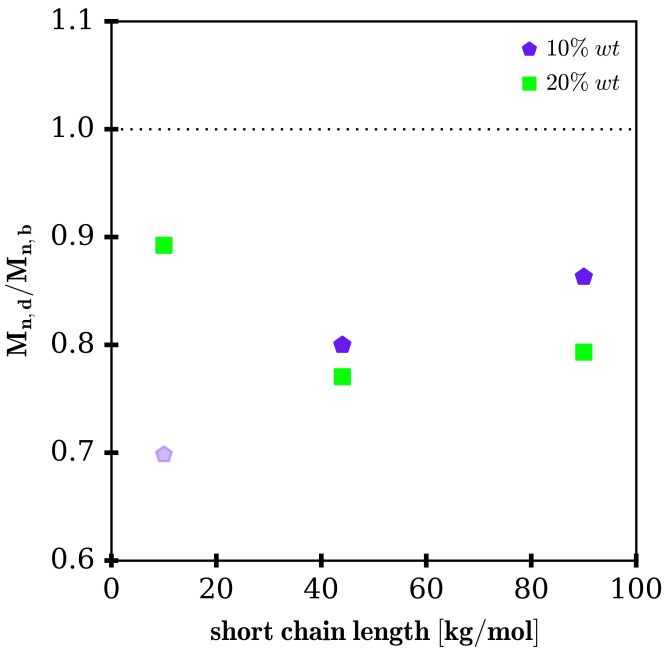

Figure 5.11: Enrichment as a function of chain length, dashed line is the reference material.

A reduction in the value of Mn represents a system enriched by short chains. The impact of doubling the short chain content is clearly seen to enhance surface migration as seen from the lower values of the blends with 20% wt. fractions. This can be attributed to the enhanced relaxation of the melt as shown in Fig. 5.8a. With regard to the effect of the chain length on fractionation, Kwakye-Nimo et al. (2022b) observed in their study that chains with length shorter than Me were depleted. In this study also, even though the shortest chain length incorporated in the blends was far much longer than Me, a look at Fig. 5.10c shows that enrichment was not enhanced at shorter chain lengths levels by the incorporation of short chains but rather, intermediate chains showed a higher level of enrichment. This we believe is attributable to first, a chain being able to compensate for

entropic penalty and then taking advantage of its length to get adsorbed to multiple sites; a capability which decreases as the chain length increases as shown by the upward trends from Fig. 5.11 i.e. starting from blends 336k-44k. It is worth nothing that even though the polymers capability to enrich the surface was decreasing with chain length, but by doubling their content of the short chains the difference between the 10% wt. and 20% wt. fractions get considerably noticeable [see chain length of 90K in Fig.5.11].

Ansari et al. (2013) utilized concepts from the double-reptation theory to develop an expression relating slip velocity of polymers to their M_W and MWD. Using this expression, they showed that migration of shorter chains to the surface significantly increases slip velocity. Similarly, die drool studies previously showed that drool M_W is lower as compared to the bulk. Musil and Zatloukal (2011) showed that, after extrusion of a polydisperse HDPE through a capillary, die drool from this process has a lower weight average molecular weight than the original polymer. We believe that the debris in our experiments is in nature the same as die drool and therefore can be treated as the layer of molecules which ends up as die drool in the capillary flow, though the enrichment mechanisms are not exactly the same. Nonetheless, observations in this study might bring us one step closer to a more comprehensive understanding of some complex behavior of polydisperse systems.

The implications of the observed behavior are versatile. For example, enhanced slip in polydisperse polymer melts in previous studies may be related to the surface enrichment of short/intermediate length chains not purely driven by thermodynamic factors. Also, the experimental data for surface segregation can significantly improve theoretical models (Joshi et al., 2000; Tchesnokov et al., 2005; Ansari et al., 2013). Joshi et al. (2000) modeled wall-slip by using a transient network model to unify various features of the slip phenomenon in one theoretical framework. Underlying physical mechanisms (wall disentanglement, desorption and bulk disentanglement) were incorporated in this model.

Our results indicate that the incorporation of another mechanism related to surface segregation to such a model may be necessary.

5.5 Conclusion

The molecular weight distribution of debris at the polybutadiene-glass interface after strong slip in simple shear flow is presented for the first time. These data represent surface composition attained without the need of chain labeling. Significant enrichment of short and intermediate chains (shorter than the weight average chain length) is observed as compared to the bulk. Enrichment of short chains at the surface is balanced with a depletion of long chains. Our results are in general agreement with predictions from Van der Gucht et al. and Minnikanti et al. enrichment equations; components with molecular weights below the mixture weight-average molecular weight are enriched at the surface while there is a depletion of high molecular weight components (larger than the mixture M_W). The enrichment-depletion transition point was however observed to occur at a value lower than M_W and was found to be independent of the MWD. The debris showed varying levels of enrichment in simple shear flow thereby suggesting the presence of an additional mechanism influencing surface fractionation. The surface enrichment was found to decrease with an increase in the short chain length. Doubling the weight fraction of the chain length enhanced the surface fractionation for all values of N_s but its effect was especially profound for small values of N_s.

Chapter 6

Conclusion and Future Works

6.1 Conclusion

This work aimed at understanding the relationship between the features of the molecular weight distributions and its rheological properties. Attention was also given to understanding surface migration in the absence of bulk shear rates. The conclusion from this work can be summarized as follows:

Chapter 3: Linear viscoelasticity is a useful means of probing the molecular structure of polymers. This usually entails performing experiments to obtain material functions which are subsequently used to calculate the viscometric spectra through complex inversions of mathematical integrals. We showed in this work that the linear viscoelasticity of a melt could be probed approximately using the features of its molecular weight distribution. The features of the MWD showed dependence on rheological parameters in the same manner as rheological properties. The breadth of the MWD was observed to increase the zero-shear viscosity's dependence on the weight average molecular weight. Additionally, the relaxation behavior of a melt was also probed using the same method; the breath of the relaxation spectra was

inferred by just using the bimodal separation and the polydispersity index. Being able to predict rheological behavior without performing experiment from just the shape of its distribution will essentially be useful in industrial processes as a first step in the material design process.

Chapter 4: We showed that at the polymer-wall interface, bulk shear rate gradient is not a pre-requisite for the surface fractionation of a melt and this was under circumstances in which the system was far from thermodynamic equilibrium. Not only was surface fractionation observed in the absence of a bulk shear rate gradient, but it was also shear rate dependent. Chains with molecular weight lower than the molecular weight between entanglement were observed to deplete instead of surface enrich, an observation first in its kind. Additional insight was also provided on the wall slip mechanism. Our results showed that both adhesive slip and cohesive slip could occur at the same time contrary to the notion that a system could exhibit just one of the mechanisms based on the surface energy of the wall.

Chapter 5: With a careful design of molecular weight distributions so as to have a systematic variation in both chain length and volume. Surface enrichment was shown to be enhanced under two scenarios i) with increasing volume in short chain and ii) decreasing short chain length. An enhanced relaxation of the melt was shown to greatly improves the surface enrichment capacities of the melt. The enrichment-depletion transition was also observed to be not constant but seem to be a function of the molecular weight even though we could not establish such correlations with our data.

6.2 Perspectives

Both the relaxation and rheological behaviors of melts were shown to correlate with the bimodal parameters defined in chap 3. The materials used in this study however, were dominated by R_B values that were less than 1. Future works could also investigate such correlations for $R_B > 1$.

Surface fractionation was shown to occur in simple shear for the first time. This calls for new models which would incorporate this phenomenon. But first, experiments needs to be designed to help provide a better understanding of the behavior at the enrichment/depletion transition zone. This could be achieved by using a material other than HDPE but with similar molecular characteristics. Additionally, by using a much wider range of short chain length to obtain blends similar to the concept used in chapter 5 the influence of the chain lengths on the enrichement/depletion transition point could also be investigated.

In chapter 4, the slip plane was observed to move up with increasing shear rate. The reason behind such observation is currently not well understood and needs to be looked at in future studies.

Appendix A

Supplementary information for chapter 3

A.1 Estimation of the zero-shear viscosity

The zero-shear viscosity used in our analysis is estimated in regions where the creep experiment had reached steady state. To identify the steady state region, the rate of change of the creep compliance is plotted as a function of time. Fig A.1 shows such a plot for one of our materials. A constant slope (within experimental limits) is observed after 8 hours for HDPE-3.

A comparison of the zero-shear viscosity (from creep) and that estimated using the combined relaxation spectra is plotted as a function of M_W in Figure A.2. A good agreement can be seen between the values from the two methods for determining η_0. This serves as an additional confirmation of the validity of our relaxation spectra.

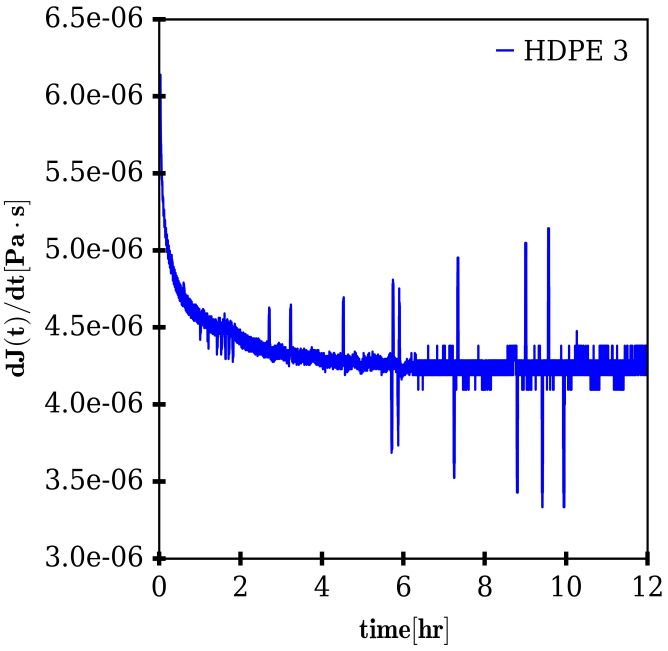

Figure A.1: Rate of change of creep compliance as a function of time. Zero-shear viscosity was evaluated in regions where constant rate of change is observed for all materials.

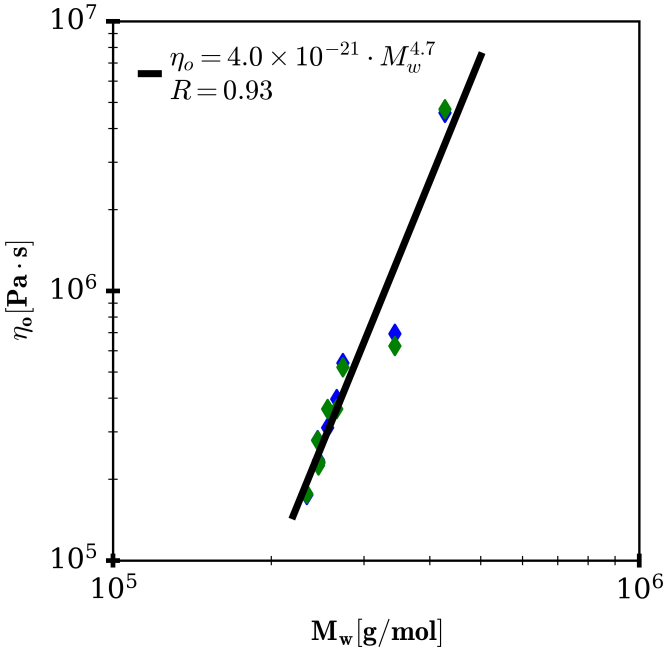

Figure A.2: zero-shear viscosity as a function of the molecular weight. A comparison of two evaluation methods.

A.2 Thermo-rheological analysis

In the estimation of the activation energy, the need for a vertical shift factor was assessed by making use of the Cole-Cole plot. As detailed by Hatzikiriakos (2000), when $G^{''}$ is plotted against $G^{'}$ for different temperatures a vertical shift is not required if the curves superpose. In Figure A.3a we present such a plot for one of our materials indicating that the modulus shift factor is not needed. Superposition was observed for all materials.

We then evaluated the thermo-rheological complexity of our materials using two methods. First by plotting δ versus $|G^*|$, an overlap of the curves obtained at different temperatures signifies thermorheological simplicity as presented in Figure A.3b (Keßner et al., 2009). Finally an activation energy that is independent of the storage modulus is also expected, in the case of thermorheological simplicity (Wood-Adams and Costeux, 2001). This is shown in Figure A.4 for all the experimental materials. From these analyses we conclude that the materials are thermorheologically simple.

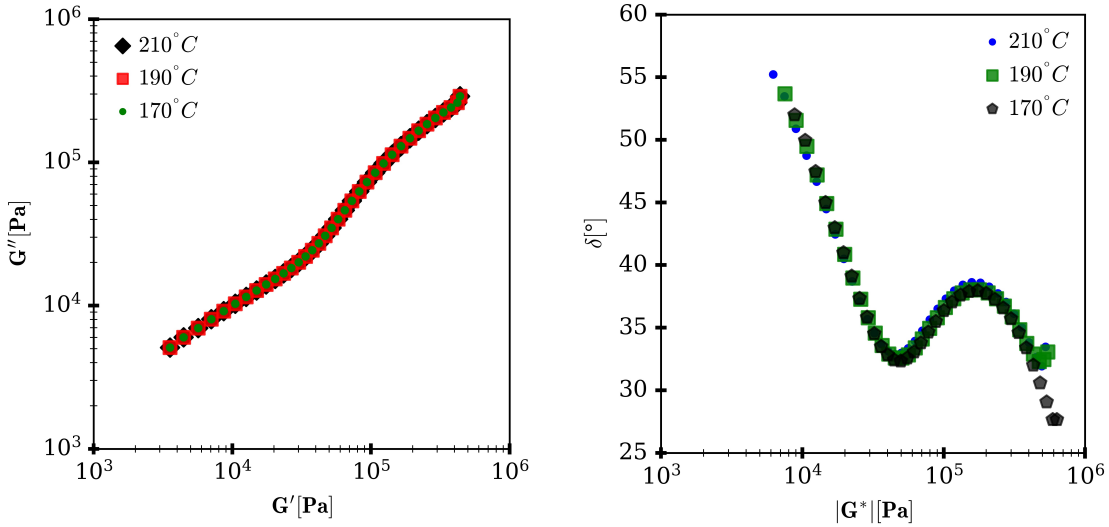

(a) (b)

Figure A.3: Thermo-rheological simplicity curves (a)Cole-Cole plot for HDPE 1, superposition indicates no need for a vertical shift during time-temperature superposition (b) δ versus $|G^*|$, superposition of curves indicates thermorheological simplicity.

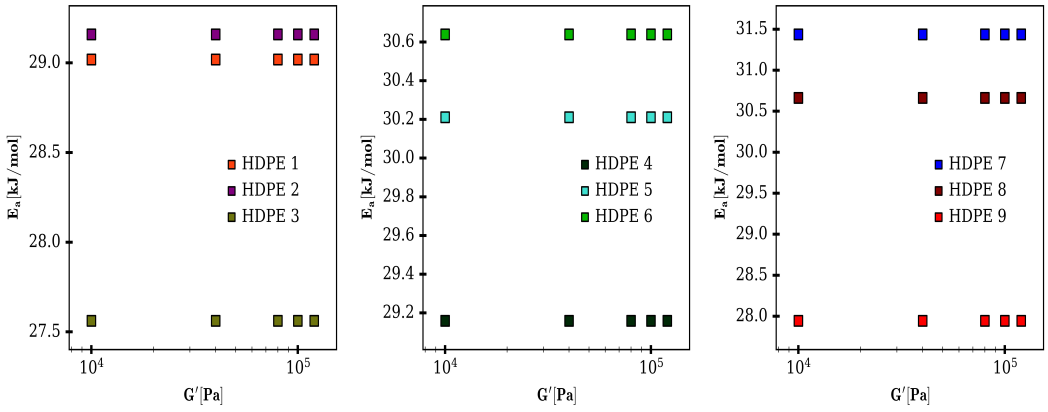

Figure A.4: $E_a(G^{'})$: demonstrating independence of E_a and $G^{'}$ indicating thermorheological simplicity

A.3 Resolved peaks of the MWD

The Gaussian mixture model (McLachlan and Rathnayake, 2014) was used to determine the probability distribution function of the MWD, from which a large number of data points were generated which was subsequently used for clustering of the generated data. The clustering helped determined the number of subpopulations in the distribution which were then grouped in LMW and HMW components. Figure A.5 shows the output of such clustering and in Figure A.6 the resolved peaks are presented.

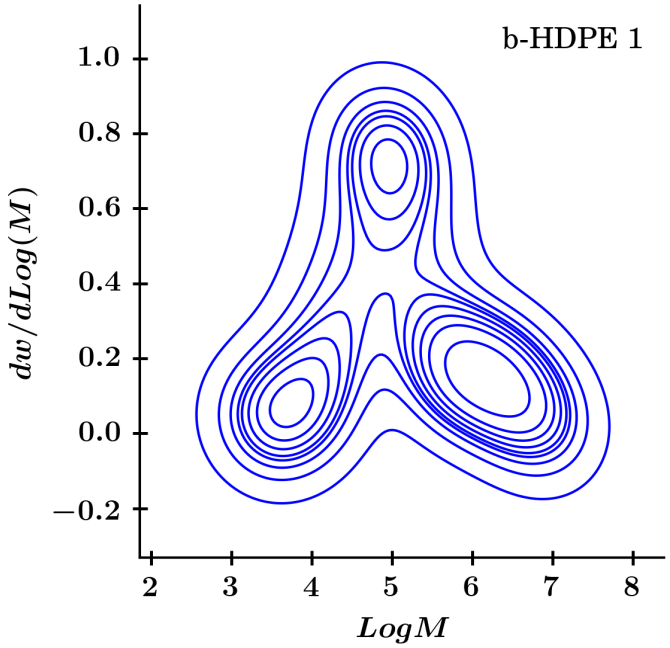

Figure A.5: Surface plot of HDPE-1 showing the subpopulations in the MWD.

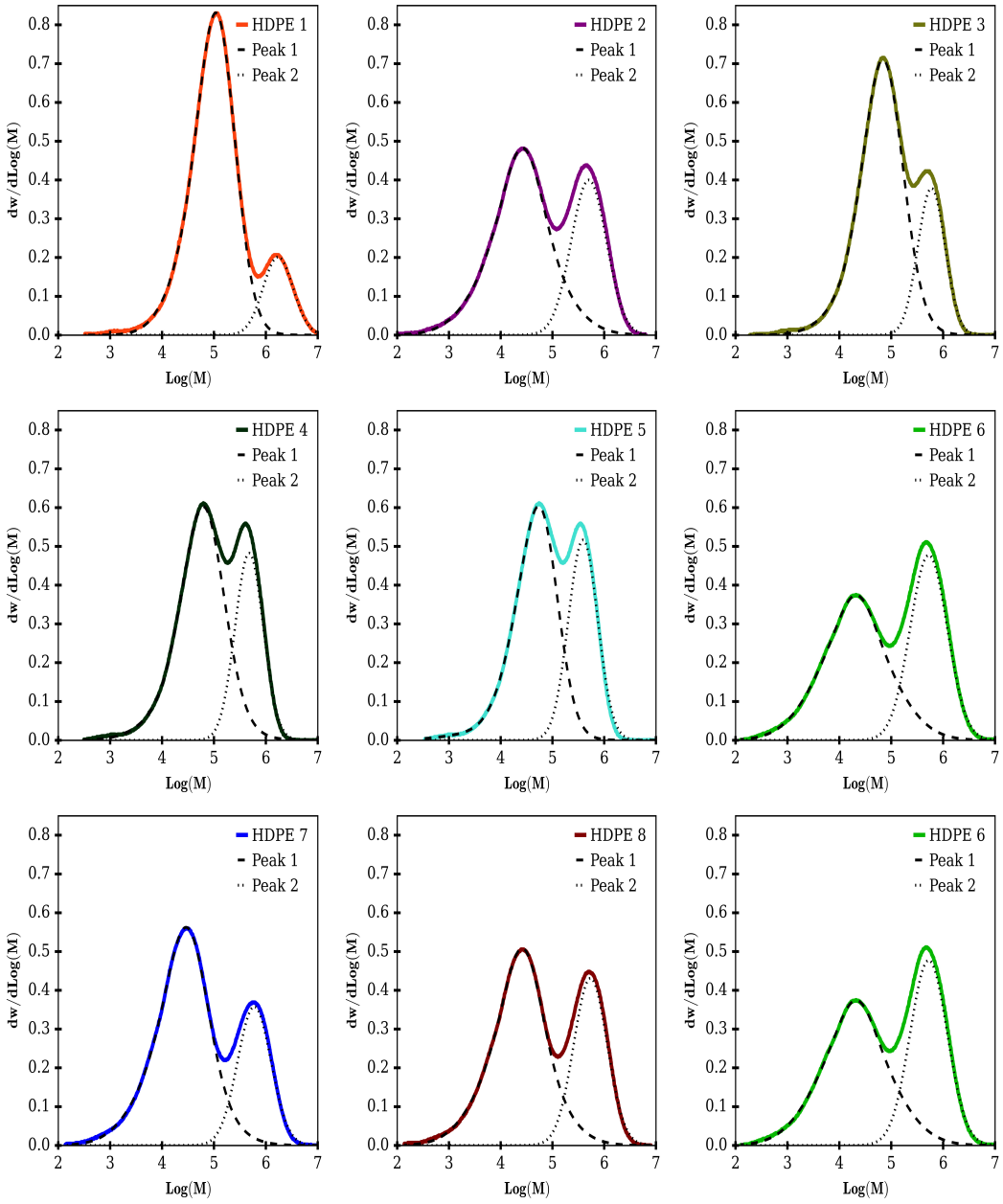

Figure A.6: Resolved peaks of the molecular weight distributions of the studied.

A.4 Weighted relaxation spectra

In Figure A.7, the weighted relaxation spectra of several of our materials are presented.

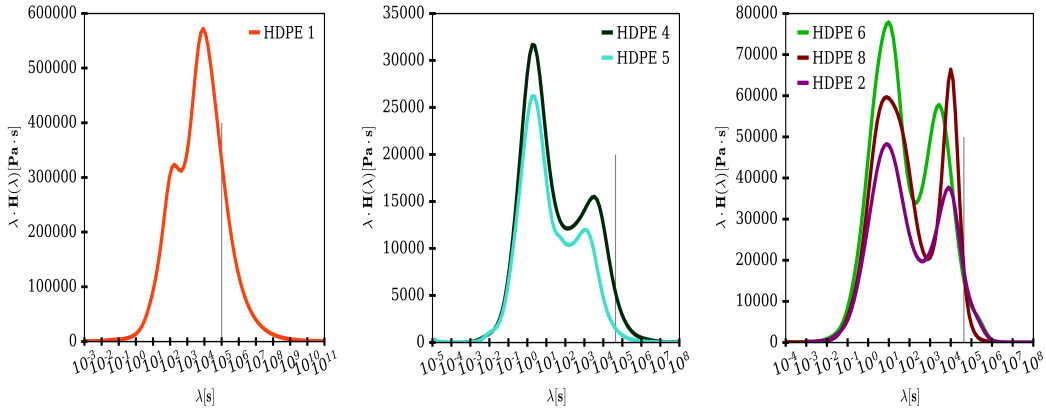

Figure A.7: Weighted relaxation spectra of selected materials.

A.5 Feature Selections

Figure A.8 , A.9 and A.10 shows the scores obtained from the feature selections (Iguyon and Elisseeff, 2000) method. In Figure A.8, the M_W is the principal feature influencing η_0 and not the bimodal parameters.

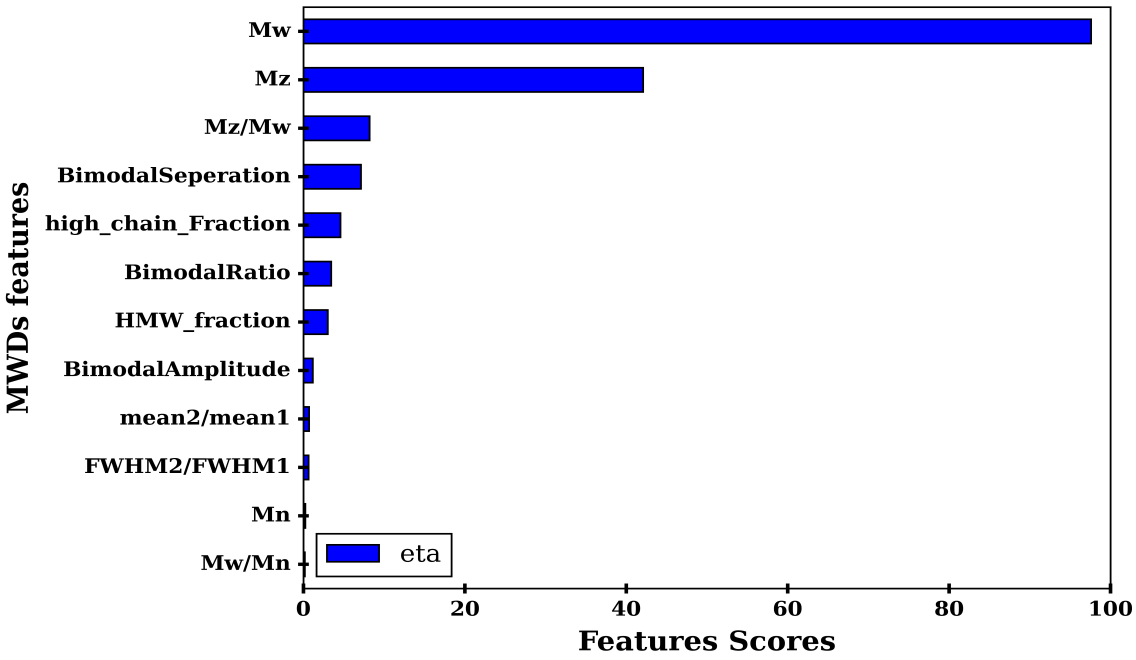

Figure A.8: Scoring output from the feature selection function for η_0

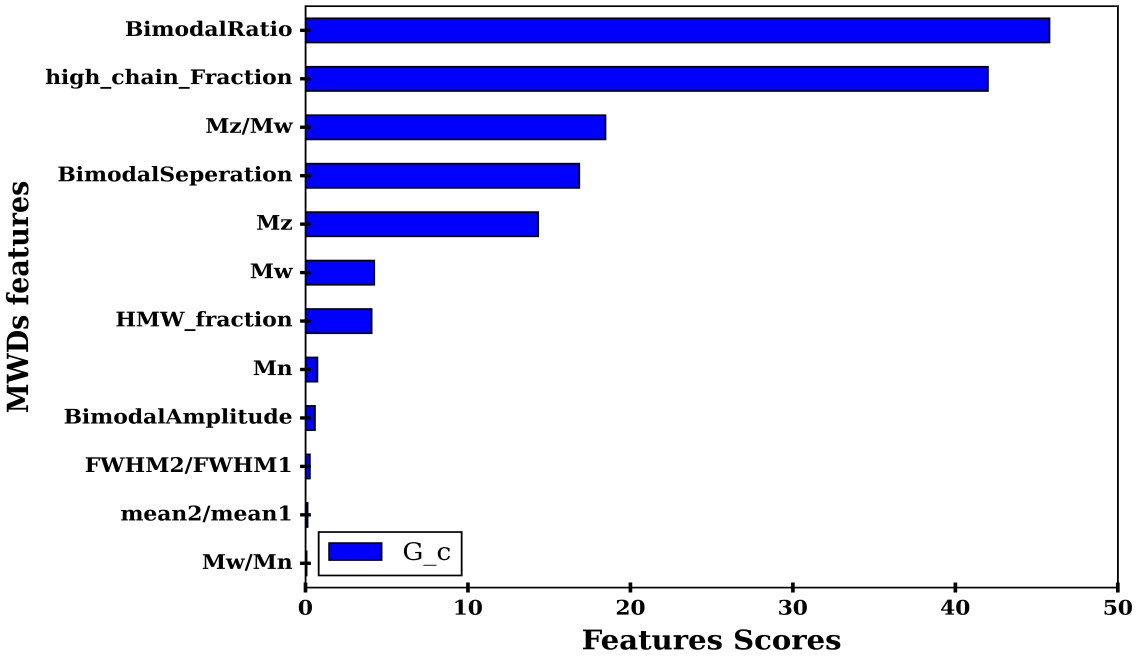

Figure A.9: Scoring output from the feature selection function for G_c.

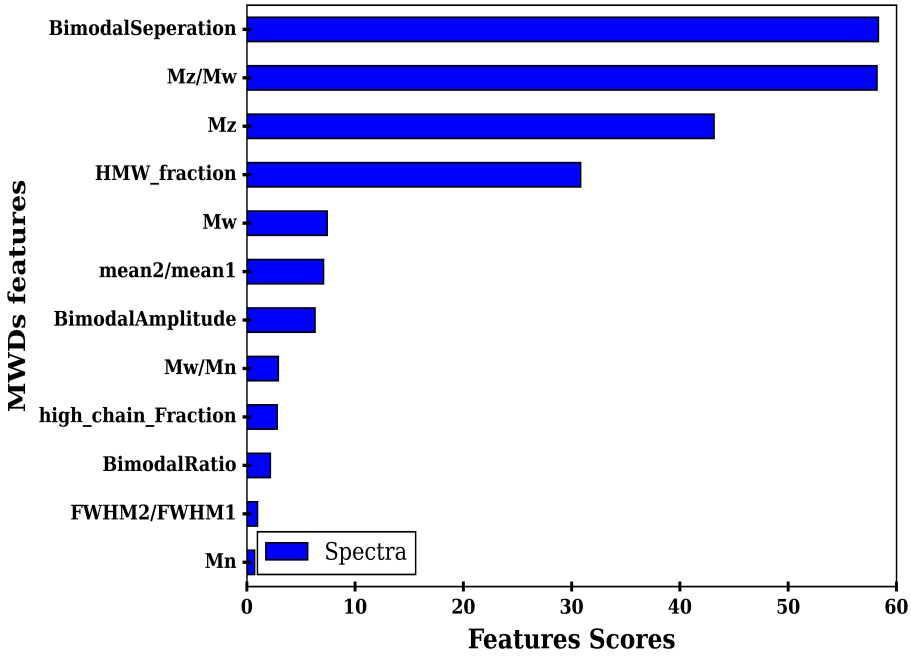

Figure A.10: Scoring output from the feature selection function for RSI_{III}

When two consecutive features have an equivalent score, we determine if those features in question convey the same information by testing their strength of correlation, in which case we choose only 1 of them to include in the model.

A.6 Generalized Linear Model

The correlation between G_c and RSI_{III} with the features of the MWD were carried out using the Generalized Linear model (Nelder and Wedderburn, 1972; Höge et al., 2018). In Table A.1 we present the performance of the model upon addition of new features in the order in which they appear in section A.5. Once the addition of a new feature does not improve the adjusted R-squared then that new feature is not included in the model. In Table A.2 the data input for the GLM correlating RSI_{III} to the features of the distribution is provided and Figure A.11 and A.12 the summary output of the GLM for the crossover modulus and RSI_{III}.

Table A.1: R-Square values used to select the number of features for the model.

	Crossover Modulus		RSI_{III}	
No. Features	R^2	R^2 $Adj.$	R^2	R^2 $Adj.$
1	0.996	0.993	0.955	0.949
2	0.996	0.995	0.990	0.987
3	0.996	0.995	0.991	0.986

All other analysis was performed using Microsoft excel 2019 version.

Table A.2: Input data for the GLM for RSI_{III}

HMW fraction (ϕ)	BimodalSeperation (S_B)	RSI_{III}
0.146616311	0.967067121	2.149702
0.341686503	0.75216727	4.096969
0.248497243	0.714762606	5.792839
0.327908487	0.625623716	9.952996
0.369838648	0.638820727	9.709938
0.427661615	0.733695031	3.948923
0.289123559	0.845427187	4.069804
0.349410932	0.828980535	3.620098
0.258700793	0.858327552	3.633364

OLS Regression Results

Dep. Variable:	G_c	R-squared (uncentered):	0.996
Model:	OLS	Adj. R-squared (uncentered):	0.995
Method:	Least Squares	F-statistic:	889.3
Date:	Wed, 02 Feb 2022	Prob (F-statistic):	3.77e-09
Time:	21:10:13	Log-Likelihood:	-1.6491
No. Observations:	9	AIC:	7.298
Df Residuals:	7	BIC:	7.693
Df Model:	2		
Covariance Type:	nonrobust		

	coef	std err	t	P>|t|	[0.025	0.975]
BimodalRatio	8.0272	0.685	11.711	0.000	6.406	9.648
high_chain_Fraction	-10.6975	0.296	-36.143	0.000	-11.397	-9.998

Figure A.11: Output of the GLM correlating the MWD features to that of the crossover modulus

OLS Regression Results

Dep. Variable:	G_c	R-squared (uncentered):	0.996
Model:	OLS	Adj. R-squared (uncentered):	0.995
Method:	Least Squares	F-statistic:	889.3
Date:	Wed, 02 Feb 2022	Prob (F-statistic):	3.77e-09
Time:	21:10:13	Log-Likelihood:	-1.6491
No. Observations:	9	AIC:	7.298
Df Residuals:	7	BIC:	7.693
Df Model:	2		
Covariance Type:	nonrobust		

	coef	std err	t	P>|t|	[0.025	0.975]
BimodalRatio	8.0272	0.685	11.711	0.000	6.406	9.648
high_chain_Fraction	-10.6975	0.296	-36.143	0.000	-11.397	-9.998

Figure A.12: Output of the GLM correlating the MWD features to that of RSI_{III}

Appendix B

Supplementary information for chapter 4

B.1 Statistical Analysis

B.1.1 Error estimation

We compared the error from the GPC measurements using two method. In the text the standard error of the mean was estimated by drawing several bootstrap replicates. This section compares the output of the estimation using bootstrap replicates to estimating the error from the single experimental data set using its standard deviation and sample size. In Fig. B.1 the error estimated from the two approaches is presented and can be seen to be very comparable. The low margin of error highlights the reproducibility of our experimental results.

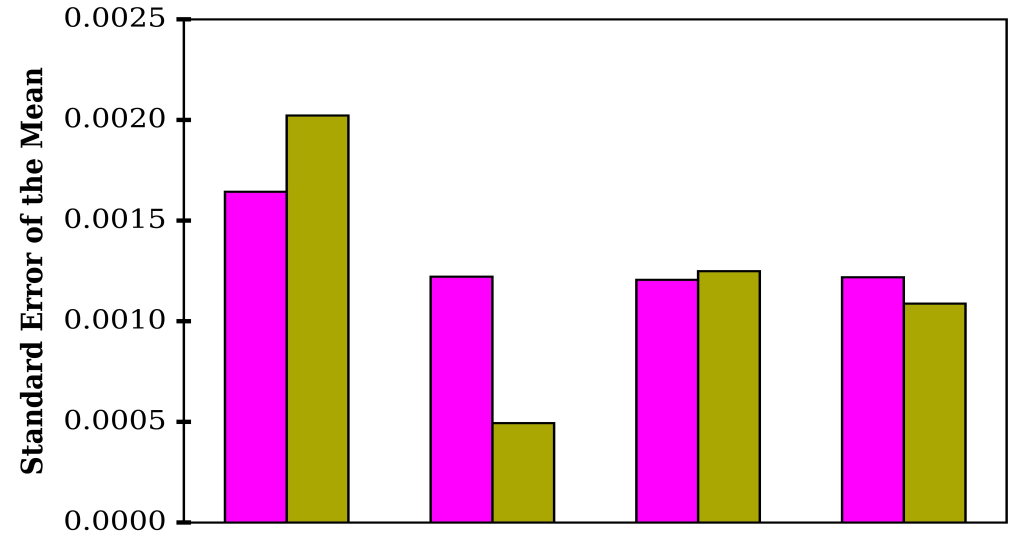

	$3s^{-1}$	$5s^{-1}$	$7s^{-1}$	$9s^{-1}$
experiment	0.00202	0.00049	0.00125	0.00109
simulated	0.00164	0.00122	0.00121	0.00122

Figure B.1: Error analysis, a comparison between estimation from experimental data and simulation

B.1.2 Summary statistics

The MWDs are converted into number fraction distributions, which is subsequently used to calculate the empirical cumulative distribution functions (ECDF). The quartiles of the distribution are next evaluated. Fig. B.2 presents the summary statistics of the MWDs. Both the median chain length and the interquartile range (IQR) of all the debris can be observed to be higher than the bulk. The increase in the median value relative to the bulk signifies a lost of small chains from the debris while the relative increase in IQR also indicates the debris had an increase in chain compositions around its median chain length.

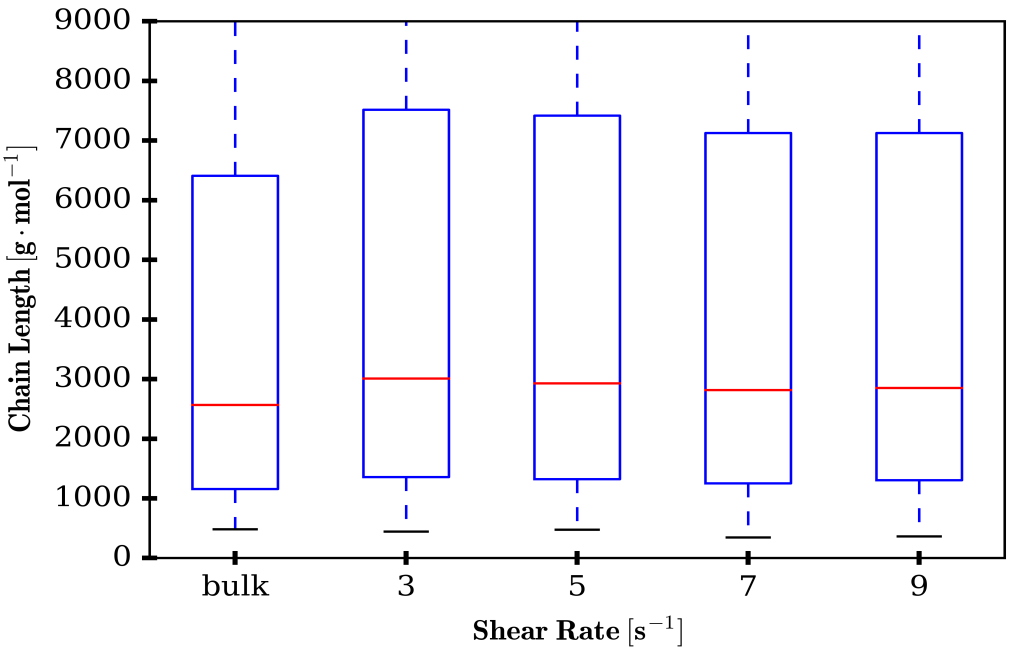

Figure B.2: Summary statistics of the MWDs

B.2 Presence of holes in thin films

Holes were observed on the glass substrate at all experimental shear rates. In Fig. B.3 a pictorial representation of the holes at the different experimental shear rates is shown. Their size and frequency are observed to decrease with shear rate.

Figure B.3: Holes observed on glass substrate. Their size and frequency decreases with shear rate.

Holes were also observed on a much higher surface energy material such as steel as presented in Fig. B.4

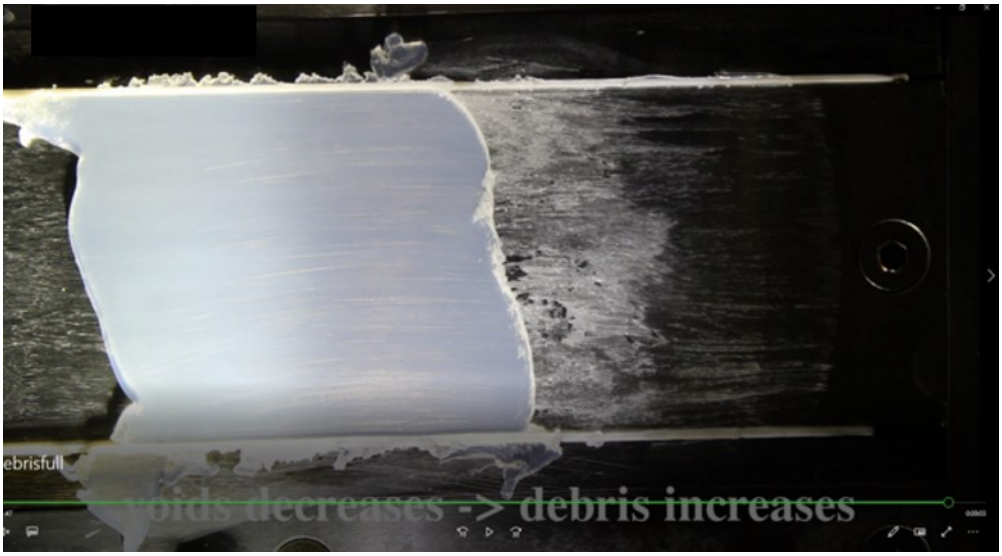

Figure B.4: Holes observed also on steel plate

FTIR Analysis performed on locations where holes were observed did not contain peaks expected for HDPE

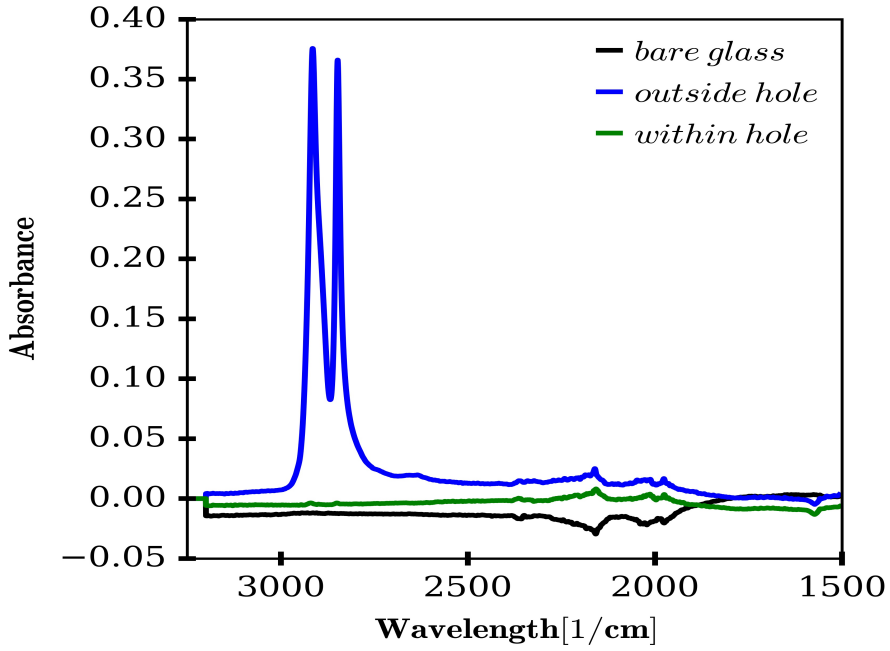

Figure B.5: FTIR on bare glass, location of hole and region with polymer.

B.3 Extensional viscosity measurements

The force required to break the bulk sample when subjected to different extensional strain rates is presented in Fig. B.6. During the simple shear flow experiment, the stress values used to cause the bulk polymer to slide over the tethered chains was much lower than the force required to break the $C - C$ bond of the bulk sample. Hence no chain scission occurred under the experimental conditions used.

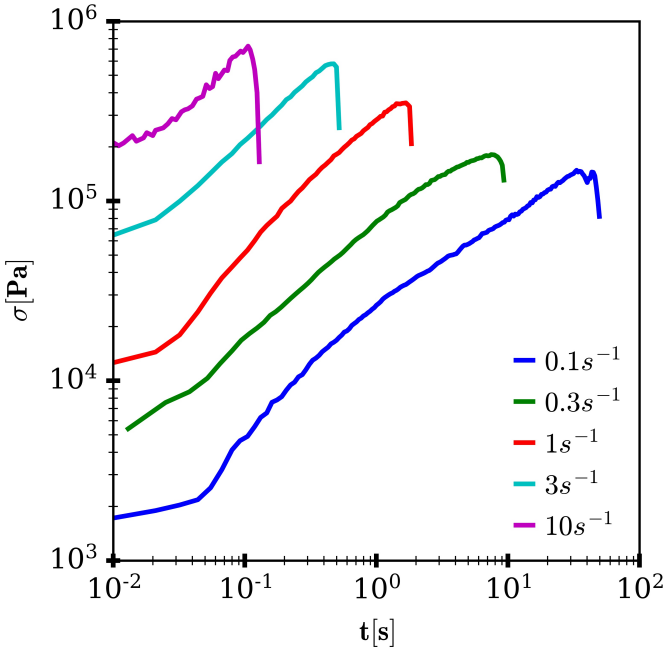

Figure B.6: Stress as function of time from a transient extensional viscosity measurement.

Bibliography

John Paul R. Abbott and Heping Zhu. 3D optical surface profiler for quantifying leaf surface roughness. *Surface Topography: Metrology and Properties*, 7(4), 2019. ISSN 2051672X. doi: 10.1088/2051-672X/ab4cc6. URL https://doi.org/10.1088/2051-672X/ab4cc6.

Armand Adjari, Françoise Brochard-Wyart, Pierre Gilles de Gennes, Ludwik Leibler, Jean Louis Viovy, and Michael Rubinstein. Slippage of an entangled polymer melt on a grafted surface. *Physica A: Statistical Mechanics and its Applications*, 204(1-4): 17–39, 1994. ISSN 03784371. doi: 10.1016/0378-4371(94)90415-4.

Johanna Aho. *Rheological Characterization of polymer melts in Shear and Extension: Measurement Reliability and Data for practical processing*. PhD thesis, Tampere University of Technology, 2011.

A Allal and B Vergnes. Molecular interpretation of the "stick-slip" defect of linear polymers. *Journal of Non-Newtonian Fluid Mechanics*, 164(1-3):1–8, 2009. ISSN 03770257. doi: 10.1016/j.jnnfm.2009.06.007.

Spiros H. Anastasiadis and Savvas G. Hatzikiriakos. The work of adhesion of polymer/wall interfaces and its association with the onset of wall slip. *Journal of Rheology*, 42(4):795–812, jul 1998. ISSN 0148-6055. doi: 10.1122/1.550909. URL http://sor.scitation.org/doi/10.1122/1.550909.

Mahmoud Ansari, Savvas G. Hatzikiriakos, Ashish M. Sukhadia, and David C. Rohlfing. Rheology of Ziegler-Natta and metallocene high-density polyethylenes: Broad molecular weight distribution effects. *Rheologica Acta*, 50(1):17–27, 2011. ISSN 00354511. doi: 10.1007/s00397-010-0503-4.

Mahmoud Ansari, Yong W. Inn, Ashish M. Sukhadia, Paul J. DesLauriers, and Savvas G. Hatzikiriakos. Wall slip of HDPEs: Molecular weight and molecular weight distribution effects. *Journal of Rheology*, 57(3):927–948, 2013. ISSN 0148-6055. doi: 10.1122/1.4801758.

Lynden A Archer. Wall slip: measurement and modeling issues. In *Polymer Processing Instabilities: Control and Understanding*, pages 73—-120. Marcel Dekker New York, 2005.

K.M. Awati, Y. Park, E. Weisser, and M.E. Mackay. Wall slip and shear stresses of polymer melts at high shear rates without pressure and viscous heating effects. *Journal of Non-Newtonian Fluid Mechanics*, 89(1):117–131, 2000. ISSN 03770257. doi: 10.1016/S0377-0257(99)00037-3. URL http://www.sciencedirect.com/science/article/pii/S0377025799000373.

R. C. Ball and T. C.B. McLeish. Dynamic Dilution and the Viscosity of Star Polymer Melts. *Macromolecules*, 22(4):1911–1913, jul 1989. ISSN 15205835. doi: 10.1021/ma00194a066.

Luigi Balzano, Nileshkumar Kukalyekar, Sanjay Rastogi, Gerrit W.M. Peters, and John C Chadwick. Crystallization and dissolution of flow-induced precursors. *Physical Review Letters*, 100(4), 2008. ISSN 00319007. doi: 10.1103/PhysRevLett.100.048302.

Oliver Bäumchen, Ludovic Marquant, Ralf Blossey, Andreas Münch, Barbara Wagner, and Karin Jacobs. Influence of slip on the Rayleigh-Plateau rim instability in dewetting viscous films. *Physical Review Letters*, 113(1), 2014. ISSN 10797114. doi: 10.1103/PhysRevLett.113.014501.

S. Blaber, P. Mahmoudi, R. K.W. Spencer, and M. W. Matsen. Effect of chain stiffness on the entropic segregation of chain ends to the surface of a polymer melt. *Journal of Chemical Physics*, 150(1), jan 2019. ISSN 00219606. doi: 10.1063/1.5064549.

Robert J. Boik. The Fisher-Pitman permutation test: A non-robust alternative to the normal theory F test when variances are heterogeneous. *British Journal of Mathematical and Statistical Psychology*, 40(1):26–42, 1987. ISSN 20448317. doi: 10.1111/j.2044-8317.1987.tb00865.x.

E. Bouchaud and M. Daoud. Polymer Adsorption: Concentration Effects. *Journal de physique Paris*, 48(11):1991–2000, 1987. ISSN 03020738. doi: 10.1051/jphys:0198700480110199100.

I. P. Briedis and L. A. Faitel'son. Rheology and molecular structure of a polyethylene melt. 3. Relaxation spectra and characteristic relaxation time. *Polymer Mechanics*, 12 (2):278–286, 1976. ISSN 15738922. doi: 10.1007/BF00856466.

F. Brochard-Wyart, C. Gay, and P. G. De Gennes. Slippage of polymer melts on grafted surfaces. *Macromolecules*, 29(1):377–382, 1996. ISSN 00249297. doi: 10.1021/ma950753j.

F Brochardt and P G De Gennes. Shear-Dependent Slippage at a Polymer/Solid Interface. *Langmuir*, 8:3033–3031, 1992. URL https://pubs.acs.org/doi/pdf/10.1021/la00048a030.

W. F. Busse. Two decades of high-polymer physics: A survey and forecast. *Physics Today*, 17(9):32–41, 1964. ISSN 19450699. doi: 10.1063/1.3051798.

Christian Carrot and Jacques Guillet. From dynamic moduli to molecular weight distribution: A study of various polydisperse linear polymers. *Journal of Rheology*, 41(5):1203–1220, sep 1997. ISSN 0148-6055. doi: 10.1122/1.550815. URL http://sor.scitation.org/doi/10.1122/1.550815.

Kwang Soo Cho. *Viscoelasticity of Polymers*, volume 241 of *Springer Series in Materials Science*. Springer Netherlands, Dordrecht, 2016. ISBN 978-94-017-7562-5. doi: 10.1007/978-94-017-7564-9. URL http://link.springer.com/10.1007/978-94-017-7564-9.

J. Des Cloizeaux. Relaxation of Entangled Polymers in Melts. *Macromolecules*, 23(17): 3992–4006, 1990. ISSN 15205835. doi: 10.1021/ma00219a021.

R. H. Colby, D C Boris, W E Krause, and S. Dou. Shear thinning of unentangled flexible polymer liquids. In *Rheologica Acta*, volume 46, pages 569–575, 2007. doi: 10.1007/s00397-006-0142-y.

Séverine Coppée, Sylvain Gabriele, Alain M. Jonas, Jacques Jestin, and Pascal Damman. Influence of chain interdiffusion between immiscible polymers on dewetting dynamics. *Soft Matter*, 7(21):9951–9955, nov 2011. ISSN 1744683X. doi: 10.1039/c1sm05486d.

T Cosgrove and P C Griffiths. Nuclear Studies Magnetic of Adsorbed Layers Resonance. *Advances in Colloid and Interface Science*, 42:175–204, 1992.

A. R. Davies and R. S. Anderssen. Sampling localization in determining the relaxation spectrum. *Journal of Non-Newtonian Fluid Mechanics*, 73(1-2):163–179, 1997. ISSN 03770257. doi: 10.1016/S0377-0257(97)00056-6.

P. G. De Gennes. Reptation of a polymer chain in the presence of fixed obstacles. *The Journal of Chemical Physics*, 55(2):572–579, 1971. ISSN 00219606. doi: 10.1063/1.1675789.

Pierre-Gilles De Gennes, Pierre-Gilles Gennes. *Scaling concepts in polymer physics*. Cornell university press, 1979.

A De Virgiliis, A Milchev, V G Rostiashvili, and T A Vilgis. Structure and dynamics of a polymer melt at an attractive surface. *European Physical Journal E*, 35(9), 2012. ISSN 12928941. doi: 10.1140/epje/i2012-12097-6.

J M Dealy and A J Giacomin. Sliding Plate and Sliding Cylinder Rheometers. *Rheological Measurement*, pages 383–404, 1988.

John M. Dealy and Ronald G. Larson. *Structure and Rheology of Molten Polymers: from structure to flow behavior and back again*. Hanser Gardner Publications, Inc, Munchen, 2006.

John M. Dealy and Jian Wang. *Melt Rheology and its application in the plastic industry*. Springer, 2 edition, 2013. ISBN 978-94-007-6394-4.

Jaap den Doelder. Viscosity and compliance from molar mass distributions using double reptation models. *Rheologica Acta*, 46(2):195–210, 2006. ISSN 00354511. doi: 10.1007/s00397-006-0115-1.

Morton M Denn. Extrusion instabilities and wall slip. *Annual Review of Fluid Mechanics*, 33:265–287, 2001. ISSN 00664189. doi: 10.1146/annurev.fluid.33.1.265. URL www.annualreviews.org.

Maziar Derakhshandeh, Mahmoud Ansari, Antonios K Doufas, and Savvas G Hatzikiriakos. Microstructure characterization of polyethylene using thermo-rheological methods. *Polymer Testing*, 60:68–77, 2017. ISSN 01429418. doi: 10.1016/j.polymertesting.2017.03.010. URL http://dx.doi.org/10.1016/j.polymertesting.2017.03.010.

Masao Doi and S. F. Edwards. Dynamics of concentrated polymer systems. Part 1. - Brownian motion in the equilibrium state, 1978a. ISSN 03009238.

Masao Doi and S. F. Edwards. Dynamics of concentrated polymer systems. Part 3. - The constitutive equation, 1978b. ISSN 03009238.

Masao Doi and S. F. Edwards. *The theory of polymer dynamics*. Clarendon, 1986. ISBN 9780198520337.

John Robert Dorgan and Nicholas Andrew Rorrer. Flow induced migration in polymer melts - Theory and simulation. *AIP Conference Proceedings*, 1662, 2015. ISSN 15517616. doi: 10.1063/1.4918880.

Marzieh Ebrahimi, Mahmoud Ansari, and Savvas G. Hatzikiriakos. Wall slip of polydisperse linear polymers using double reptation. *Journal of Rheology*, 59(3):885–901, 2015. ISSN 0148-6055. doi: 10.1122/1.4917543.

Marzieh Ebrahimi, Mahmoud Ansari, Yong W. Inn, and Savvas G. Hatzikiriakos. Surface fractionation effects on slip of polydisperse polymer melts. *Physics of Fluids*, 28(9):093101, 2016. ISSN 1070-6631. doi: 10.1063/1.4962564. URL http://scitation.aip.org/content/aip/journal/pof2/28/9/10.1063/1.4962564.

J. D Ferry. *Viscoelastic Properties of Polymers*. Wiley, New York, 3rd edition, 1980.

P. J. Flory and T. G. Fox. Treatment of Intrinsic Viscosities. *Journal of the American Chemical Society*, 73(5):1904–1908, 1951. ISSN 15205126. doi: 10.1021/ja01149a002.

Fridtjov Irgens. *Rheology and Non-Newtonian Fluids*. Springer, Switzerland, 2014. ISBN 978-3-319-01052-6. doi: 10.1007/978-3-319-01053-3.

Claus Gabriel and Helmut Münstedt. Strain hardening of various polyolefins in uniaxial elongational flow. *Journal of Rheology*, 47(3):619–630, 2003. ISSN 0148-6055. doi: 10.1122/1.1567752.

Claus Gabriel, Joachim Kaschta, and Helmut Münstedt. Influence of molecular structure on rheological properties of polyethylenes I. Creep recovery measurements in shear. *Rheologica Acta*, 37(1):7–20, 1998. ISSN 00354511. doi: 10.1007/s003970050086.

Jesse D. Gander and A. Jeffrey Giacomin. Review of die lip buildup in plastics extrusion. *Polymer Engineering and Science Jul*, 37(7), 1997. URL https://search.proquest.com/docview/218560932?pq-origsite=gscholar.

César A. García-Franco, David J. Lohse, Christopher G. Robertson, and Olivier Georjon. Relative quantification of long chain branching in essentially linear polyethylenes. *European Polymer Journal*, 44(2):376–391, feb 2008. ISSN 00143057. doi: 10.1016/j.eurpolymj.2007.10.030.

Mark Geoghegan and Georg Krausch. Wetting at polymer surfaces and interfaces, 2003. ISSN 00796700. URL www.elsevier.com/locate/ppolysci.

Stefan Gezeck, Burkhart Fischer, and Jens Timmert. Saccadic Reaction Times: a Statistical Analysis of Multimodal Distributions. Technical Report 15, University of Freiburg, 1997.

William W. Graessley. *The entanglement concept in polymer rheology*. Springer Berlin Heidelberg, Berlin, Heidelberg, 1974. ISBN 978-3-540-37860-0. doi: 10.1007/BFb0031037.

H. Gramespacher and J. Meissner. Interfacial tension between polymer melts measured by shear oscillations of their blends. *Journal of Rheology*, 36(6):1127–1141, aug 1992. ISSN 0148-6055. doi: 10.1122/1.550304. URL http://sor.scitation.org/doi/10.1122/1.550304.

Piet Groeneboom and Ronald Pyke. Asymptotic Normality of Statistics Based on the Convex Minorants of Empirical Distribution Functions. *The Annals of Probability*, 11 (2):328–345, 1983.

Andrew Gustafson and David C Morse. A Reptation Model of Slip at Entangled Polymer-Polymer Interfaces. *Macromolecules*, 49(18):7032–7044, 2016. ISSN 15205835. doi: 10.1021/acs.macromol.6b00666. URL https://pubs.acs.org/doi/pdf/10.1021/acs.macromol.6b00666.

Milad Hadaeghnia, Shervin Ahmadi, Ismaeil Ghasemi, and Paula M Wood-Adams. Manipulating the morphology of PA6/POE blends using graphene to achieve balanced electrical and mechanical properties. *Composites Science and Technology*, 200: 108412, 2020. ISSN 02663538. doi: 10.1016/j.compscitech.2020.108412. URL https://doi.org/10.1016/j.compscitech.2020.108412.

Arvind Hariharan, Sanat K Kumar, and Thomas P. Russel. A Lattice Model for the Surface Segregation of Polymer Chains Due to Molecular Weight Effects. *Macromolecules*, 23(15):3584–3592, 1990. ISSN 15205835. doi: 10.1021/ma00217a009. URL https://pubs.acs.org/sharingguidelines.

Arvind Hariharan, Sanat K Kumar, and Thomas P Russell. Surface Segregation in Binary Polymer Mixtures: A Lattice Model. *Macromolecules*, 24(17):4909–4917, 1991. ISSN 15205835. doi: 10.1021/ma00017a030. URL https://pubs.acs.org/sharingguidelines.

Arvind Hariharan, Sanat K. Kumar, and Thomas P. Russell. Reversal of the isotopic effect in the surface behavior of binary polymer blends. *The Journal of Chemical Physics*, 98(5):4163–4173, 1993. ISSN 00219606. doi: 10.1063/1.465024.

S G Hatzikiriakos and J M Dealy. Wall slip of molten high density polyethylene. I. Sliding plate rheometer studies. *Journal of Rheology Journal of Rheology Fluidity Journal of Rheology Journal of Rheology Construction Journal of Rheology Journal of Rheology Journal of Rheology*, 351(10), 1991. URL https://doi.org/10.1122/1.550178http://sor.scitation.org/toc/jor/35/4.

Savvas G. Hatzikiriakos. Long chain branching and polydispersity effects on the rheological properties of polyethylenes. *Polymer Engineering & Science*, 40(11): 2279–2287, nov 2000. ISSN 0032-3888. doi: 10.1002/pen.11360. URL http://doi.wiley.com/10.1002/pen.11360.

Savvas G. Hatzikiriakos. Wall slip of molten polymers. *Progress in Polymer Science (Oxford)*, 37(4):624–643, 2012. ISSN 00796700. doi: 10.1016/j.progpolymsci.2011.09.004. URL http://dx.doi.org/10.1016/j.progpolymsci.2011.09.004.

Savvas G. Hatzikiriakos. Slip mechanisms in complex fluid flows. *Soft matter*, 11(40): 7851–6, 2015. ISSN 1744-6848. doi: 10.1039/c5sm01711d. URL http://pubs.rsc.org/en/content/articlehtml/2015/sm/c5sm01711d.

Chunxia He, Paula Wood-Adams, and John M. Dealy. Broad frequency range characterization of molten polymers. *Journal of Rheology*, 48(4):711–724, 2004. ISSN 0148-6055. doi: 10.1122/1.1763943. URL http://sor.scitation.org/doi/10.1122/1.1763943.

Jens Hepperle, Helmut Münstedt, Peter K. Haug, and Claus D. Eisenbach. Rheological properties of branched polystyrenes: Linear viscoelastic behavior. *Rheologica Acta*, 45(2):151–163, 2005. ISSN 00354511. doi: 10.1007/s00397-005-0033-7.

Jacob A. Hill, Kevin J. Endres, Pendar Mahmoudi, Mark W. Matsen, Chrys Wesdemiotis, and Mark D. Foster. Detection of surface enrichment driven by molecular weight disparity in virtually monodisperse polymers. *ACS Macro Letters*, 7(4):487–492, apr 2018. ISSN 21611653. doi: 10.1021/acsmacrolett.7b00993. URL https://pubs.acs.org/doi/abs/10.1021/acsmacrolett.7b00993.

Marvin Höge, Thomas Wöhling, and Wolfgang Nowak. A Primer for Model Selection: The Decisive Role of Model Complexity. *Water Resources Research*, 54(3):1688–1715, mar 2018. ISSN 19447973. doi: 10.1002/2017WR021902.

J. Honerkamp and J. Weese. A nonlinear regularization method for the calculation of relaxation spectra. *Rheologica Acta*, 32(1):65–73, 1993. ISSN 00354511. doi: 10.1007/BF00396678.

D M Hoyle, D Auhl, O G Harlen, V C Barroso, M Wilhelm, and T. C. B. McLeish. Large amplitude oscillatory shear and Fourier transform rheology analysis of branched polymer melts. *Journal of Rheology*, 58(4):969–997, 2014. ISSN 0148-6055. doi: 10.1122/1.4881467. URL https://sor.scitation.org/toc/jor/58/4.

Shao Hua-feng, Wang Shu-lei, Xia Dong, and He Ai-hua. Linear viscoelastic behaviors of polybutene-1 melts with various structure parameters. *Chinese Journal of Polymer Science (English Edition)*, 34(2):174–184, 2016. ISSN 14396203. doi: 10.1007/s10118-016-1736-1.

Ibnelwaleed A. Hussein, Tayyab Hameed, and Michael C. Williams. Influence of molecular structure on the rheology and thermorheology of metallocene polyethylenes. *Journal of Applied Polymer Science*, 102(2):1717–1728, oct 2006. ISSN 00218995. doi: 10.1002/app.24353. URL http://doi.wiley.com/10.1002/app.24353.

Isabelle Iguyon and André Elisseeff. 10.1162/153244303322753616. *CrossRef Listing of Deleted DOIs*, 1:1157–1182, 2000. ISSN 0003-6951. doi: 10.1162/153244303322753616.

Yongwoo Inn. Melt fracture and wall slip of metallocene-catalyzed bimodal polyethylenes in capillary flow. *Journal of Rheology*, 57(2):393–406, mar 2013. ISSN 0148-6055. doi: 10.1122/1.4774397. URL http://scitation.aip.org/content/sor/journal/jor2/57/2/10.1122/1.4774397.

Yongwoo Inn. Melt fracture, wall slip, and flow-induced fractionation of bimodal polyethylenes. *AIP Conference Proceedings*, 1662, 2015. ISSN 15517616. doi: 10.1063/1.4918879.

Yongwoo Inn and David C. Rohlfing. Application of creep test to obtain the linear viscoelastic properties at low frequency range for polyethylene melts. *Applied Rheology*, 22(1):1–8, 2012. ISSN 14306395. doi: 10.3933/ApplRheol-22-15260.

Natalia Janiszewska, Joanna Raczkowska, Andrzej Budkowski, Katarzyna Gajos, Yurij Stetsyshyn, MacIej Michalik, and Kamil Awsiuk. Dewetting of Polymer Films Controlled by Protein Adsorption. *Langmuir*, 36(40):11817–11828, oct 2020. ISSN 15205827. doi: 10.1021/ACS.LANGMUIR.0C01718/SUPPL_FILE/LA0C01718_SI_001.PDF. URL /pmc/articles/PMC7584358//pmc/articles/PMC7584358/?report=abstracthttps://www.ncbi.nlm.nih.gov/pmc/articles/PMC7584358/.

Richard A.L. Jones and Randal W. Richards. *Polymers at Interfaces*. Cambridge University Press, Cambridge, 1999.

Yogesh M. Joshi, Ashish K. Lele, and R. A. Mashelkar. Slipping fluids: A unified transient network model. *Journal of Non-Newtonian Fluid Mechanics*, 89(3):303–335, mar 2000. ISSN 03770257. doi: 10.1016/S0377-0257(99)00046-4.

Yogesh M. Joshi, Ashish K. Lele, and R. A. Mashelkar. Molecular model for wall slip: Role of convective constraint release. *Macromolecules*, 34(10):3412–3420, 2001. ISSN 00249297. doi: 10.1021/ma001020o.

Dilhan M. Kalyon and Halil Gevgilili. Wall slip and extrudate distortion of three polymer melts. *Journal of Rheology Journal of Rheology Journal of Rheology Construction Journal of Rheology Journal of Rheology I. Sliding plate rheometer studies Journal of Rheology*, 47(101):12011122–210, may 2003. ISSN 0148-6055. doi: 10.1122/1.1562156. URL https://doi.org/10.1122/1.1562156http://sor.scitation.org/toc/jor/47/3http://sor.scitation.org/doi/10.1122/1.1562156.

J. Kaschta and F. R. Schwarzl. Calculation of discrete retardation spectra from creep data - I. Method. *Rheologica Acta*, 33(6):517–529, 1994a. ISSN 00354511. doi: 10.1007/BF00366337.

J. Kaschta and F. R. Schwarzl. Calculation of discrete retardation spectra from creep data - II. Analysis of measured creep curves. *Rheologica Acta*, 33(6):530–541, 1994b. ISSN 00354511. doi: 10.1007/BF00366337.

I. B. Kazatchkov, N. Bohnet, S. K. Goyal, and S. G. Hatzikiriakos. Influence of molecular structure on the rheological and processing behavior of polyethylene resins. *Polymer Engineering and Science*, 39(4):804–815, 1999. ISSN 00323888. doi: 10.1002/pen.11468.

Ute Keßner, Joachim Kaschta, and Helmut Münstedt. Determination of method-invariant activation energies of long-chain branched low-density polyethylenes. *Journal of Rheology*, 53(4):1001–1016, jul 2009. ISSN 0148-6055. doi: 10.1122/1.3124682.

Jack Kirk, Martin Kröger, and Patrick Ilg. Surface Disentanglement and Slip in a Polymer Melt: A Molecular Dynamics Study. *Macromolecules*, 51(21):8996–9010, nov 2018. ISSN 15205835. doi: 10.1021/acs.macromol.8b01865. URL https://pubs.acs.org/doi/abs/10.1021/acs.macromol.8b01865.

Jacob Klein. Dynamics of Entangled Linear, Branched, and Cyclic Polymers. *Macromolecules*, 19(1):105–118, 1986. ISSN 00255416. doi: 10.1016/0025-5416(70)90078-9. URL https://pubs.acs.org/sharingguidelines.

Vassilis Kontogiorgos. Calculation of relaxation spectra from mechanical spectra in MATLAB. *Polymer Testing*, 29(8):1021–1025, 2010. ISSN 01429418. doi: 10.1016/j.polymertesting.2010.09.007. URL http://dx.doi.org/10.1016/j.polymertesting.2010.09.007.

François Koran and John M. Dealy. Wall slip of polyisobutylene: Interfacial and pressure effects. *Journal of Rheology*, 43(5):1291–1306, aug 1999. ISSN 0148-6055. doi: 10.1122/1.551025. URL https://sor.scitation.org/doi/abs/10.1122/1.551025.

M. Kraft, J. Meissner, and J. Kaschta. Linear Viscoelastic Characterization of Polymer Melts with Long Relaxation Times †. *Macromolecules*, 32(3):751–757, 1999. ISSN 0024-9297. doi: 10.1021/ma980730f. URL http://pubs.acs.org/doi/abs/10.1021/ma980730f.

van Dirk Willem Krevelen and Nijenhuis K. Te. Properties of Polymers. In *Properties of Polymers: their correlation with chemical structure; their numerical estimation and prediction from additive group contributions*, chapter Typology o, pages 7–45. Elsevier, 2009. ISBN 978-0-08-054819-7.

Qin Kuang, Xue Wang, Zhiyuan Jiang, Zhaoxiong Xie, and Lansun Zheng. High-energy-surface engineered metal oxide micro- and nanocrystallites and their applications. *Accounts of Chemical Research*, 47(2):308–318, feb 2014. ISSN 00014842. doi: 10.1021/ar400092x.

Shadrach Kwakye-Nimo, Yongwoo Inn, Youlu Yu, and Paula M. Wood-Adams. Linear viscoelastic behavior of bimodal polyethylene. *Rheologica Acta*, 61(6):373–386, apr 2022a. ISSN 14351528. doi: 10.1007/s00397-022-01340-5. URL https://link.springer.com/10.1007/s00397-022-01340-5.

Shadrach Kwakye-Nimo, Yongwoo Inn, Youlu Yu, and Paula M. Wood-Adams. Polymer Fractionation at an Interface in Simple Shear with Slip. *Macromolecules*, 55(15):6609–6619, aug 2022b. ISSN 0024-9297. doi: 10.1021/ACS.MACROMOL.2C01102. URL https://pubs.acs.org/doi/10.1021/acs.macromol.2c01102.

Martin Laun, Dietmar Auhl, Rüdiger Brummer, Dirk J. Dijkstra, Claus Gabriel, Marc A. Mangnus, Maximilian Rüllmann, Wim Zoetelief, and Ulrich A. Handge. Guidelines

for checking performance and verifying accuracy of rotational rheometers: Viscosity measurements in steady and oscillatory shear (IUPAC Technical Report). *Pure and Applied Chemistry*, 86(12):1945–1968, dec 2014. ISSN 13653075. doi: 10.1515/pac-2013-0601.

Alexei E Likhtman, Tom C B Mcleish, Likhtman A E, and McLeish T C B. Quantitative Theory for Linear Dynamics of Linear Entangled Polymers. *Macromolecules*, 35(16): 6332–6343, jul 2002. doi: 10.1021/ma0200219. URL https://pubs.acs.org/sharingguidelines.

Chenyang Liu, Jin Wang, and Jiasong He. Rheological and thermal properties of m-LLDPE blends with m-HDPE and LDPE. *Polymer*, 43(13):3811–3818, apr 2002. ISSN 00323861. doi: 10.1016/S0032-3861(02)00201-X.

Chenyang Liu, Jiasong He, Evelyne van Ruymbeke, Roland Keunings, and Christian Bailly. Evaluation of different methods for the determination of the plateau modulus and the entanglement molecular weight, jun 2006. ISSN 00323861.

Gustavo Luengo, Franz Josef Schmitt, Robert Hill, and Jacob Israelachvili. Thin film rheology and tribology of confined polymer melts: Contrasts with bulk properties. *Macromolecules*, 30(8):2482–2494, 1997. ISSN 00249297. doi: 10.1021/ma9519122. URL https://pubs.acs.org/sharingguidelines.

J. Lyklema and T. Van Vliet. Polymer-stabilized free liquid films. *Faraday Discussions of the Chemical Society*, 65:25–32, 1978. ISSN 03017249. doi: 10.1039/DC9786500025.

P. Mahmoudi and M. W. Matsen. Segregation of chain ends to the surface of a polymer melt: Effect of surface profile versus chain discreteness. *European Physical Journal E*, 39(8), 2016. ISSN 1292895X. doi: 10.1140/epje/i2016-16078-5.

P. Mahmoudi and M. W. Matsen. Entropic segregation of short polymers to the surface of a polydisperse melt. *European Physical Journal E*, 40(10):1–9, 2017. ISSN 1292895X. doi: 10.1140/epje/i2017-11575-7.

P Mahmoudi, W. S.R. Forrest, T M Beardsley, and M W Matsen. Testing the Universality of Entropic Segregation at Polymer Surfaces. *Macromolecules*, 51(3):1242–1247, 2018. ISSN 15205835. doi: 10.1021/acs.macromol.7b02474. URL https://pubs.acs.org/sharingguidelines.

G. Marin, J. J. Labaig, and Ph Monge. Dynamic viscoelasticity of entangled polymers. *Polymer*, 16(3):223–226, 1975. ISSN 00323861. doi: 10.1016/0032-3861(75)90058-0.

G. Marin, J. P. Montfort, and Ph Monge. Reptation and tube renewal: Experimental and numerical simulation. *Journal of Non-Newtonian Fluid Mechanics*, 23(C):215–228, 1987. ISSN 03770257. doi: 10.1016/0377-0257(87)80019-8.

G. Marrucci. Relaxation By Reptation and Tube Enlargement: a Model for Polydisperse Polymers. *Journal of polymer science. Part A-2, Polymer physics*, 23(1):159–177, 1985. ISSN 04492978. doi: 10.1002/pol.1985.180230115.

Yuichi Masubuchi, Hiroshi Watanabe, Giovanni Ianniruberto, Francesco Greco, and Giuseppe Marrucci. Comparison among slip-link simulations of bidisperse linear polymer melts. *Macromolecules*, 41(21):8275–8280, 2008. ISSN 00249297. doi: 10.1021/ma800954q.

M. W. Matsen and P. Mahmoudi. Segregation of chain ends to the surface of a polymer melt. *European Physical Journal E*, 37(8):1–8, aug 2014. ISSN 1292895X. doi: 10.1140/epje/i2014-14078-1.

Geoffrey J. McLachlan and Suren Rathnayake. On the number of components in a Gaussian mixture model. *Wiley Interdisciplinary Reviews: Data Mining and Knowledge Discovery*, 4(5):341–355, sep 2014. ISSN 1942-4795. doi: 10.1002/WIDM.1135. URL https://onlinelibrary.wiley.com/doi/full/10.1002/widm.1135https://onlinelibrary.wiley.com/doi/abs/10.1002/widm.1135https://onlinelibrary.wiley.com/doi/10.1002/widm.1135.

Joachim Meissner. Combined Constant Strain Rate and Stress Relaxation Test for Linear Viscoelastic Studies. *J Polym Sci Polym Phys Ed*, 16(5):915–919, 1978. ISSN 00981273. doi: 10.1002/pol.1978.180160515.

Vijay Mhetar, L. A. Archer, Vijay Mhetar And, and L. A. Archer*. Slip in Entangled Polymer Melts. 1. General Features. *Macromolecules*, 31(24): 8607–8616, dec 1998. ISSN 0024-9297. doi: 10.1021/ma980163w. URL https://pubs.acs.org/doi/abs/10.1021/ma980163whttp://pubs.acs.org/doi/abs/10.1021/ma980163whttp://pubs.acs.org/doi/pdf/10.1021/ma980163w.

K. B. Migler, H. Hervet, and L. Leger. Slip transition of a polymer melt under shear stress. *Physical Review Letters*, 70(3):287–290, jan 1993. ISSN 0031-9007. doi: 10.1103/PhysRevLett.70.287. URL https://link.aps.org/doi/10.1103/PhysRevLett.70.287.

S. T. Milner and T. C.B. Mc Leish. Reptation and contour-length fluctuations in melts of linear polymers. *Physical Review Letters*, 81(3):725–728, 1998. ISSN 10797114. doi: 10.1103/PhysRevLett.81.725.

Scott T. Milner. Relating the shear-thinning curve to the molecular weight distribution in linear polymer melts. *Journal of Rheology*, 40(2):303–315, mar 1996. ISSN 0148-6055. doi: 10.1122/1.550742.

Venkatachala S Minnikanti, Qian Zhenyu, and Lynden A Archer. Surface segregation and surface tension of polydisperse polymer melts. *Journal of Chemical Physics*, 126 (14):144905, 2007. ISSN 00219606. doi: 10.1063/1.2721542. URL https://doi.org/10.1063/1.2721542.

J P Montfort, G Marin, and Ph Monge. Molecular Weight Distribution Dependence of the Viscoelastic Properties of Linear Polymers: The Coupling of Reptation and Tube-Renewal Effects. *Macromolecules*, 19(2):1980–1988, 1986. URL https://pubs.acs.org/sharingguidelines.

Jean Pierre Montfort, Gérard Marin, and Philippe Monge. Effects of Constraint Release on the Dynamics of Entangled Linear Polymer Melts. *Macromolecules*, 17(8):1551–1560, 1984. ISSN 15205835. doi: 10.1021/ma00138a022.

Samantha L. Morelly and Nicolas J. Alvarez. Characterizing long-chain branching in commercial HDPE samples via linear viscoelasticity and extensional rheology. *Rheologica Acta*, 59(11):797–807, 2020. ISSN 14351528. doi: 10.1007/s00397-020-01233-5.

Faith A. Morrison. *Understanding Rheology*. Oxford University press, New York, 1 edition, 2001. ISBN 978-0-19-514166-5.

P. Müller-Buschbaum and M Stamm. Correlated roughness, long-range correlations, and dewetting of thin polymer films. *Macromolecules*, 31(11):3686–3692, 1998. ISSN 00249297. doi: 10.1021/ma971486f. URL https://pubs.acs.org/sharingguidelines.

A. Munoz-Escalona, P. Lafuente, J. F. Vega, and A. Santamariacute;a. Rheology of metallocene-catalyzed monomodal and bimodal polyethylenes. *Polymer Engineering and Science*, 39(11):2292–2303, nov 1999. ISSN 00323888. doi: 10.1002/pen.11617.

H Münstedt and H M Laun. Elongational properties and molecular structure of polyethylene melts. *Rheologica Acta*, 20(3):211–221, 1981. ISSN 00354511. doi: 10.1007/BF01678022.

Jan Musil and Martin Zatloukal. Experimental investigation of flow induced molecular weight fractionation during extrusion of HDPE polymer melts. *Chemical Engineering Science*, 66(20):4814–4823, 2011. ISSN 00092509. doi: 10.1016/j.ces.2011.06.047. URL http://dx.doi.org/10.1016/j.ces.2011.06.047.

Marina Najm and Savvas G. Hatzikiriakos. Flow-induced fractionation effects on slip of polydisperse polymer melts. *Physics of Fluids*, 32(7):073109, jul 2020. ISSN 10897666. doi: 10.1063/5.0017996. URL https://aip.scitation.org/doi/abs/10.1063/5.0017996.

J. A. Nelder and R. W. M. Wedderburn Wedderburn. Generalized Linear Models. *Journal of the Royal Statistical Society A*, 135(3):370–384, 1972.

Andrew Keong Ng, Kai Keng Ang, and Cuntai Guan. Automatic selection of neuronal spike detection threshold via smoothed Teager energy histogram. *International IEEE/EMBS Conference on Neural Engineering, NER*, pages 1437–1440, 2013. ISSN 19483546. doi: 10.1109/NER.2013.6696214.

Jon Otegui, Javier Ramos, Juan F Vega, and Javier Martínez-Salazar. Effect of high molar mass species on linear viscoelastic properties of polyethylene melts. *European Polymer Journal*, 49(9):2748–2758, 2013. ISSN 00143057. doi: 10.1016/j.eurpolymj.2013.06.015. URL http://dx.doi.org/10.1016/j.eurpolymj.2013.06.015.

Hee Eon Park, Sung Taek Lim, Fabricio Smillo, John M. Dealy, and Christopher G. Robertson. Wall slip and spurt flow of polybutadiene. *Journal of Rheology*, 52(5):1201, 2008. ISSN 01486055. doi: 10.1122/1.2964199. URL http://dx.doi.org/10.1122/1.2964199.

C. Pattamaprom and R. G. Larson. Predicting the linear viscoelastic properties of monodisperse and polydisperse polystyrenes and polyethylenes. *Rheologica Acta*, 40(6):516–532, 2001. ISSN 00354511. doi: 10.1007/s003970100196.

Cattaleeya Pattamaprom, Ronald G. Larson, and Timothy J. Van Dyke. Quantitative predictions of linear viscoelastic rheological properties of entangled polymers. *Rheologica Acta*, 39:517–531, mar 2000. ISSN 0035-4511. doi: 10.1007/s003970050015. URL http://link.springer.com/10.1007/s003970050015.

Cattaleeya Pattamaprom, Ronald G Larson, and Anuvat Sirivat. Determining polymer molecular weight distributions from rheological properties using the dual-constraint model. *Rheologica Acta*, 47(7):689–700, 2008. ISSN 00354511. doi: 10.1007/s00397-008-0264-5.

Coussot Philippe. *Rheophysics: Matter in aall its states*. Springer, 2014. doi: 10.1007/978-3-319-06148-1.

D. H.S. Ramkumar, J. M. Caruthers, H. Mavridis, and R. Shroff. Computation of the linear viscoelastic relaxation spectrum from experimental data. *Journal of Applied Polymer Science*, 64(11):2177–2189, 1997. ISSN 00218995. doi: 10.1002/(sici)1097-4628(19970613)64:11⟨2177::aid-app14⟩3.3.co;2-l.

Devulapalli H.S. Ramkumar and John M. Wiest. Molecular weight distributions from linear viscoelastic measurements. *Rheologica Acta*, 35(4):356–363, 1996. ISSN 00354511. doi: 10.1007/BF00403536.

C Redon, F Brochard-Wyart, and F Rondelez. Dynamics of dewetting. *Physical Review Letters*, 66(6):715–718, 1991. ISSN 00319007. doi: 10.1103/PhysRevLett.66.715.

Günter Reiter and Ashutosh Sharma. Auto-Optimization of Dewetting Rates by Rim Instabilities in Slipping Polymer Films. *Physical Review Letters*, 87(16):166103, oct 2001. ISSN 0031-9007. doi: 10.1103/PhysRevLett.87.166103. URL https://link.aps.org/doi/10.1103/PhysRevLett.87.166103.

Ben Robertson, Ian M Robinson, D Stocks, and Richard L Thompson. Shear processing maps: a new design guide for melt processors. *Plastics, Rubber and Composites*, 51 (5):217–239, 2022. ISSN 17432898. doi: 10.1080/14658011.2020.1796082. URL https://doi.org/10.1080/14658011.2020.1796082.

Nicholas A Rorrer and John R Dorgan. Molecular-scale simulation of cross-flow migration in polymer melts. *Physical Review E - Statistical, Nonlinear, and Soft Matter Physics*, 90(5):52603, 2014. ISSN 15502376. doi: 10.1103/PhysRevE.90.052603.

Michael Rubinstein, Eugene Helfand, and Dale S. Pearson. Theory of Polydispersity Effects on Polymer Rheology: Binary Distribution of Molecular Weights. *Macromolecules*, 20(4):822–829, 1987. ISSN 15205835. doi: 10.1021/ma00170a021.

S. Mostafa Sabzevari, Itai Cohen, and Paula M. Wood-Adams. Wall Slip of Tridisperse Polymer Melts and the Effect of Unentangled versus Weakly Entangled Chains. *Macromolecules*, 47(22):8033–8040, 2014a. ISSN 15205835. doi: 10.1021/ma501320d. URL http://pubs.acs.org/doi/pdf/10.1021/ma501320d.

S Mostafa Sabzevari, Joshua D Mcgraw, Karin Jacobs, and Paula Wood-Adams. Sacrificial mica substrates influence the slip boundary condition of dewetting polymer films. *Polymer*, 78:202–207, 2015a. doi: 10.1016/j.polymer.2015.08.038. URL https://ac.els-cdn.com/S0032386115301774/1-s2.0-S0032386115301774-main.pdf?{_}tid=2baaa762-01f3-11e8-8663-00000aab0f6c{&}acdnat=1516900636{_}babbc2fc7e8e3a2bc25d17800483cb8b.

S Mostafa Sabzevari, Joshua D Mcgraw, and Paula Wood-Adams. Short chains enhance slip of highly entangled polystyrenes during thin film dewetting. *Royal Society of Chemistry*, 6:91163–91170, 2016. doi: 10.1039/c6ra15606a. URL http://pubs.rsc.org/-/content/articlepdf/2016/ra/c6ra15606a.

Seyed Mostafa Sabzevari, Satu Strandman, and Paula Marie Wood-Adams. Slip of polydisperse polymers: Molecular weight distribution above and below the plane of slip. In *AIP Conference Proceedings*, volume 1662, page 030003. AIP Publishing LLC, apr 2015b. doi: 10.1063/1.4918878. URL http://aip.scitation.org/doi/abs/10.1063/1.4918878.

S.M. Mostafa Sabzevari, Itai Cohen, and Paula M. P.M. Wood-Adams. Wall slip of bidisperse linear polymer melts. *Macromolecules*, 47(9):3154–3160, 2014b. ISSN 15205835. doi: 10.1021/ma500451g.

Sadowski, S Czarnecki, and J Hoła. Evaluation of the height 3D roughness parameters of concrete substrate and the adhesion to epoxy resin. *International Journal of Adhesion and Adhesives*, 67:3–13, 2016. ISSN 01437496. doi: 10.1016/j.ijadhadh.2015.12.019. URL http://dx.doi.org/10.1016/j.ijadhadh.2015.12.019.

G. H. Sambrook Smith, A. P. Nicholas, and R. I. Ferguson. Measuring and defining bimodal sediments: Problems and implications. *Water Resources Research*, 33(5): 1179–1185, 1997. ISSN 00431397. doi: 10.1029/97wr00365.

Mohammadali Sattari, Yongwoo Inn, and Paula M. Wood-Adams. Wall Slip of Bimodal Polyethylene. *Macromolecules*, 55(11):4568–4577, jun 2022. ISSN 0024-9297. doi: 10.1021/acs.macromol.2c00331.

J M Scheutjens and G J Fleer. Statistical Theory of the Adsorption of Interacting Chain Molecules. 2. Train, Loop, and Tail Size Distribution. *J. Phys. Chem*, 84:178–190, 1980. URL https://pubs.acs.org/sharingguidelines.

J. M. H. M. Scheutjens and G. J. Fleer. Scientific bases for the preparation of heterogeneous catalysts. In *The Journal of Physical Chemistry*, volume 83, pages 1619–1635, 1979. doi: 10.1595/147106707X169786. URL https://pubs.acs.org/sharingguidelines.

Andrew M. Schmalzer and A. Jeffrey Giacomin. Die drool theory. *Journal of Polymer Engineering*, 33(1):1–18, 2013. ISSN 03346447. doi: 10.1515/polyeng-2012-0044.

H. P. Schreiber and S. H. Storey. Molecular fractionation in capillary flow of polymer fluids. *Journal of Polymer Science Part B: Polymer Letters*, 3(9):723–727, 1965. ISSN 04492986. doi: 10.1002/pol.1965.110030908.

H. P. Schreiber, S. H. Storey, and E. B. Bagley. Molecular Fractionation in the Flow of Polymeric Fluids. *Transactions of the Society of Rheology*, 10(1):275–297, jul 1966. ISSN 0038-0032. doi: 10.1122/1.549047. URL https://sor.scitation.org/doi/abs/10.1122/1.549047.

F. R. Schwarzl. Numerical calculation of storage and loss modulus from stress relaxation data for. Technical report, 1971.

Stéphanie Senet. Plastic production on the rise worldwide but slowing in Europe, 2021. URL https://www.euractiv.com/section/energy-environment/news/while-global-plastic-production-is-increasing-worldwide-it-is-slowi

Martin Sentmanat, Benjamin N. Wang, and Gareth H. McKinley. Measuring the transient extensional rheology of polyethylene melts using the SER universal testing platform. *Journal of Rheology*, 49(3):585–606, may 2005. ISSN 0148-6055. doi: 10.1122/1.1896956.

A. P. Sgouros and D. N. Theodorou. Atomistic simulations of long-chain polyethylene melts flowing past gold surfaces: structure and wall-slip. *Molecular Physics*, 118(9-10), jun 2020. ISSN 13623028. doi: 10.1080/00268976.2019.1706775. URL https://www.tandfonline.com/doi/abs/10.1080/00268976.2019.1706775.

Vahid Shaayegan, Paula Wood-Adams, and Nicole Raymonde Demarquette. Linear viscoelasticity of immiscible blends: The application of creep. *Journal of Rheology*, 56(5):1039–1056, 2012. ISSN 0148-6055. doi: 10.1122/1.4720081. URL http://sor.scitation.org/doi/10.1122/1.4720081.

M. David Shelby and George B. Caflisch. Shear field induced diffusion and molecular weight fraetionation during polymer processing. *Polymer Engineering and Science*, 44(7):1283–1294, 2004. ISSN 00323888. doi: 10.1002/pen.20124. URL https://search.proquest.com/docview/218618298?pq-origsite=gscholar.

Asheesh Shukla, Sachin Shanbhag, and Yogesh M. Joshi. Analysis of linear viscoelasticity of aging soft glasses. *Journal of Rheology*, 64(5):1197–1207, 2020. ISSN 0148-6055. doi: 10.1122/8.0000099. URL https://doi.org/10.1122/8.0000099.

F. J. Stadler, A. Nishioka, J. Stange, K. Koyama, and Helmut Münstedt. Comparison of the elongational behavior of various polyolefins in uniaxial and equibiaxial flows. *Rheologica Acta*, 46(7):1003–1012, 2007. ISSN 00354511. doi: 10.1007/s00397-007-0190-y.

Florian J. Stadler. Effect of incomplete datasets on the calculation of continuous relaxation spectra from dynamic-mechanical data. *Rheologica Acta*, 49(10):1041–1057, oct 2010. ISSN 0035-4511. doi: 10.1007/s00397-010-0479-0. URL http://link.springer.com/10.1007/s00397-010-0479-0.

Florian J. Stadler and Tahmineh Mahmoudi. Evaluation of relaxation spectra of linear, short, and long-chain branched polyethylenes. *Korea Australia Rheology Journal*, 25(1):39–53, 2013. ISSN 1226119X. doi: 10.1007/s13367-013-0005-x.

Florian J. Stadler, Christian Piel, Joachim Kaschta, Sascha Rulhoff, Walter Kaminsky, and Helmut Münstedt. Dependence of the zero shear-rate viscosity and the viscosity function of linear high-density polyethylenes on the mass-average molar mass and polydispersity. *Rheologica Acta*, 45(5):755–764, 2006. ISSN 00354511. doi: 10.1007/s00397-005-0042-6.

Rüdiger Stark, Michael Kappl, and Hans Jürgen Butt. Interaction of solid surfaces across binary mixtures of polymer melts. *Macromolecules*, 40(11):4088–4091, 2007. ISSN 00249297. doi: 10.1021/ma070024r. URL https://pubs.acs.org/sharingguidelines.

StatisticsCanada. Manufacturing - Canadian Industry Statistics, 2022. URL https://www.ic.gc.ca/app/scr/app/cis/manufacturing-fabrication/3261.

Pavlos S. Stephanou and Vlasis G. Mavrantzas. Quantitative predictions of the linear viscoelastic properties of entangled polyethylene and polybutadiene melts via modified versions of modern tube models on the basis of atomistic simulation data. *Journal of Non-Newtonian Fluid Mechanics*, 200:111–130, 2013. ISSN 03770257. doi: 10.1016/j.jnnfm.2013.04.003. URL http://dx.doi.org/10.1016/j.jnnfm.2013.04.003.

Pavlos S. Stephanou, Chunggi Baig, Georgia Tsolou, Vlasis G. Mavrantzas, and Martin Kröger. Quantifying chain reptation in entangled polymer melts: Topological and dynamical mapping of atomistic simulation results onto the tube model. *Journal of Chemical Physics*, 132(12):124904, 2010. ISSN 00219606. doi: 10.1063/1.3361674.

Pavlos S. Stephanou, Chunggi Baig, and Vlasis G. Mavrantzas. Projection of atomistic simulation data for the dynamics of entangled polymers onto the tube theory: Calculation of the segment survival probability function and comparison with modern tube models. *Soft Matter*, 7(2):380–395, 2011. ISSN 1744683X. doi: 10.1039/c0sm00327a. URL www.rsc.org/softmatter.

T. Strauch, L. Yelash, and W. Paul. A coarse-graining procedure for polymer melts applied to 1,4-polybutadiene. *Physical Chemistry Chemical Physics*, 11(12):1942–1948, 2009. ISSN 14639076. doi: 10.1039/b818271j.

Mark J. Struglinski and William W. Graessley. Effects of Polydispersity on the Linear Viscoelastic Properties of Entangled Polymers. 1. Experimental Observations for Binary Mixtures of Linear Polybutadiene. *Macromolecules*, 18(12):2630–2643, 1985. ISSN 15205835. doi: 10.1021/ma00154a046.

L. Szántó, Y. Feng, and C. Friedrich. Extensional hardening of multimodal, linear PE with high amounts of UHMWPE. *Journal of Rheology*, 65(3):371–380, 2021. ISSN 0148-6055. doi: 10.1122/8.0000197.

Levente Szántó, Yukang Feng, Fan Zhong, Timo Hees, Evelyne van Ruymbeke, Rolf Mülhaupt, and Christian Friedrich. Ultra-broad molecular weight distribution effects on viscoelastic properties of linear multimodal PE. *Journal of Rheology*, 63(5):773–784, 2019. ISSN 0148-6055. doi: 10.1122/1.5109481.

Keiji Tanaka, Atsushi Takahara, and Tisato Kajiyama. Effect of polydispersity on surface molecular motion of polystyrene films. *Macromolecules*, 30(21):6626–6632, 1997. ISSN 00249297. doi: 10.1021/ma970057e. URL https://pubs.acs.org/sharingguidelines.

Keiji Tanaka, Tisato Kajiyama, Atsushi Takahara, and Seiji Tasaki. A novel method to examine surface composition in mixtures of chemically identical two polymers with different molecular weights. *Macromolecules*, 35(12):4702–4706, jun 2002. ISSN 00249297. doi: 10.1021/ma011960o.

Roger I. Tanner. *Engineering Rheology*. Oxford University press, New York, 2 edition, 2000. ISBN 0198564732.

M. A. Tchesnokov, J. Molenaar, J. J.M. Slot, and R. Stepanyan. A molecular model for cohesive slip at polymer melt/solid interfaces. *Journal of Chemical Physics*, 122 (21):214711, jun 2005. ISSN 00219606. doi: 10.1063/1.1915327. URL https://aip.scitation.org/doi/abs/10.1063/1.1915327.

Vasileios Touloupidis, Christof Wurnitsch, Alexandra Albunia, and Girish Galgali. Connecting Linear Polymers Molecular Structure to Viscoelastic Properties and Melt Flow Index. *Macromolecular Theory and Simulations*, 25(4):392–402, 2016. ISSN 15213919. doi: 10.1002/mats.201600028.

S Trinkle and C. Freidrich. Van Gurp-Palmen-plot: A way to characterize polydispersity of linear polymers. *Rheologica Acta*, 40(4):322–328, 2001. ISSN 00354511. doi: 10.1007/s003970000137. URL https://link.springer.com/content/pdf/10.1007/s003970000137.pdf.

B. Utracki, L. A., Schlund. Linear low density polyethylenes and their blends: Part 2. Shear flow of LLDPE's. *Polymer Engineering & Science*, 27(5):380–386, 1987. ISSN 15482634. doi: 10.1002/pen.760270511.

Jasper Van der Gucht, N. A.M. Besseling, and G. J. Fleer. Chain-length dependence of the polymer surface excess near the adsorption/depletion transition. *Macromolecules*, 35(7):2810–2816, mar 2002a. ISSN 00249297. doi: 10.1021/ma010540w. URL https://pubs.acs.org/doi/abs/10.1021/ma010540w.

Jasper Van der Gucht, N. A.M. Besseling, and G. J. Fleer. Surface segregation in polydisperse polymer melts. *Macromolecules*, 35(17):6732–6738, 2002b. ISSN 00249297. doi: 10.1021/ma010964q.

E. Van Ruymbeke, R. Keunings, V. Stéphenne, A. Hagenaars, and C. Bailly. Evaluation of reptation models for predicting the linear viscoelastic properties of entangled linear polymers. *Macromolecules*, 35(7):2689–2699, mar 2002a. ISSN 00249297. doi: 10.1021/ma011271c. URL https://pubs.acs.org/sharingguidelines.

Evelyne Van Ruymbeke, Roland Keunings, and Christian Bailly. Determination of the molecular weight distribution of entangled linear polymers from linear viscoelasticity data. *Journal of Non-Newtonian Fluid Mechanics*, 105(2-3):153–175, 2002b. ISSN 03770257. doi: 10.1016/S0377-0257(02)00080-0.

Evelyne Van Ruymbeke, C.-Y Chen-Yang Liu, Christian Bailly, Evelyne Van Ruymbeke, C.-Y Chen-Yang Liu, and Christian Bailly. Quantitative Tube Model Predictions for the Linear Viscoelasticity of Linear Polymers. *Rheology Reviews*, 2007(January):53–134, 2007. URL http://www.bsr.org.uk.

Fathollah Varnik and Kurt Binder. Multiscale modeling of polymers at interfaces. *International Journal of Materials Research*, 100(11):1494–1502, 2009. ISSN 18625282. doi: 10.3139/146.110209.

J. F. Vega, A. Muñoz-Escalona, A. Santamaría, M. E. Muñoz, and P. Lafuente. Comparison of the rheological properties of metallocene-catalyzed and conventional high-density polyethylenes-comment. *Macromolecules*, 29(3):8280–8281, jan 1996. ISSN 00249297. doi: 10.1021/ma9504633. URL https://pubs.acs.org/sharingguidelines.

J. F. Vega, M. Aguilar, and J. Martınez-Salazar. Model linear metallocene-catalyzed polyolefins: Melt rheological behavior and molecular dynamics. *Journal of Rheology*, 47(6):1505–1521, nov 2003. ISSN 0148-6055. doi: 10.1122/1.1621422. URL http://sor.scitation.org/doi/10.1122/1.1621422.

J. F. Vega, S. Rastogi, G. W. M. Peters, and H. E. H. Meijer. Rheology and reptation of linear polymers. Ultrahigh molecular weight chain dynamics in the melt. *Journal of Rheology*, 48(3):663–678, 2004. ISSN 0148-6055. doi: 10.1122/1.1718367.

Juan F. Vega, Jon Otegui, Javier Ramos, and Javier Martínez-Salazar. Effect of molecular weight distribution on Newtonian viscosity of linear polyethylene. *Rheologica Acta*, 51(1):81–87, jan 2012. ISSN 00354511. doi: 10.1007/s00397-011-0594-6. URL https://link.springer.com/article/10.1007/s00397-011-0594-6.

Manfred H Wagner, Víctor Hugo Rolón-Garrido, Kyu Hyun, and Manfred Wilhelm. Analysis of medium amplitude oscillatory shear data of entangled linear and model comb polymers. *Journal of Rheology*, 55(3):495–516, 2011. ISSN 0148-6055. doi: 10.1122/1.3553031. URL https://sor.scitation.org/toc/jor/55/3.

Shanfeng Wang, Shi Qing Wang, A. Halasa, and W. L. Hsu. Relaxation dynamics in mixtures of long and short chains: Tube dilation and impeded curvilinear diffusion. *Macromolecules*, 36(14):5355–5371, 2003. ISSN 00249297. doi: 10.1021/ma0210426.

S. H. Wasserman, G.N. Foster, and D.J. Yacka. Dynamic melt rheometry used to study degradation of metallocene polyethylene. In *Soc. Plastics Engineers Ann. Tech. Conf. (ANTEC) Tech. Papers*, pages 992–996, 1998.

Scott H. Wasserman and William W. Graessley. Prediction of linear viscoelastic response for entangled polyolefin melts from molecular weight distribution. *Polymer Engineering and Science*, 36(6):852–861, 1996. ISSN 00323888. doi: 10.1002/pen.10472.

Geoffrey M. Wise, Morton M. Denn, Alexis T. Bell, Jimmy W. Mays, Kunlun Hong, and Hermis Iatrou. Surface mobility and slip of polybutadiene melts in shear flow. *Citation: Journal of Rheology*, 44(3):549–567, may 2000. ISSN 0148-6055. doi: 10.1122/1.551100. URL https://doi.org/10.1122/1.551100http://sor.scitation.org/toc/jor/44/3http://sor.scitation.org/doi/10.1122/1.551100.

Paula Wood-Adams and Stéphane Costeux. Thermorheological behavior of polyethylene: Effects of microstructure and long chain branching. *Macromolecules*, 34(18): 6281–6290, aug 2001. ISSN 00249297. doi: 10.1021/ma0017034. URL https://pubs.acs.org/sharingguidelines.

Paula M. Wood-Adams, John M. Dealy, A. Willem DeGroot, and O. David Redwine. Effect of molecular structure on the linear viscoelastic behavior of polyethylene. *Macromolecules*, 33(20):7489–7499, 2000. ISSN 00249297. doi: 10.1021/ma991533z.

Philip J. Wyatt. Light scattering and the absolute characterization of macromolecules. *Analytica Chimica Acta*, 272(1):1–40, 1993. ISSN 00032670. doi: 10.1016/0003-2670(93)80373-S.

R Xie, A Karim, J F Douglas, C C Han, and R A Weiss. Spinodal dewetting of thin polymer films. *Physical Review Letters*, 81(6):1251–1254, 1998. ISSN 10797114. doi: 10.1103/PhysRevLett.81.1251.

Junke Xu, Stéphane Costeux, John M. Dealy, and Mark N. De Decker. Use of a sliding plate rheometer to measure the first normal stress difference at high shear rates. *Rheologica Acta*, 46(6):815–824, jun 2007. ISSN 0035-4511. doi: 10.1007/s00397-006-0156-5. URL http://link.springer.com/10.1007/s00397-006-0156-5.

Longjian Xue and Yanchun Han. Pattern formation by dewetting of polymer thin film, 2011. ISSN 00796700.

Youlu Yu, Paul J Deslauriers, and David C Rohlfing. SEC-MALS method for the determination of long-chain branching and long-chain branching distribution in polyethylene. *Polymer*, 46(14):5165–5182, 2005. ISSN 00323861. doi: 10.1016/j.polymer.2005.04.036. URL www.elsevier.com/locate/polymer.

Yong Hua Zang, René Muller, and Daniel Froelich. Influence of molecular weight distribution on viscoelastic constants of polymer melts in the terminal zone. New blending law and comparison with experimental data. *Polymer*, 28(9):1577–1582, 1987. ISSN 00323861. doi: 10.1016/0032-3861(87)90362-4.

Chidong Zhang, Brian E. Mapes, and Brian J. Soden. Bimodality in tropical water vapour. *Quarterly Journal of the Royal Meteorological Society*, 129(594):2847–2866, 2003. ISSN 00359009. doi: 10.1256/qj.02.166.

Hui Zhao, Ying Xu, Zhen Luo, Cui-Ran Gong, Yang-Qing Zheng, and Li-Ming Yu. Rational Design of Waterborne Polyurethane Pressure Sensitive Adhesives for Different Working Temperatures. *Materials*, 15(6):2011, 2022. doi: 10.3390/ma15062011. URL https://doi.org/10.3390/ma15062011.

W. Zhao, X Zhao, M. H. Rafailovich, J Sokolov, R J Composto, S D Smith, M Satkowski, T P Russell, W. D. Dozier, and T Mansfield. Segregation of Chain Ends to Polymer Melt Surfaces and Interfaces. *Macromolecules*, 26(3):561–562, 1993. ISSN 15205835. doi: 10.1021/ma00055a026. URL https://pubs.acs.org/sharingguidelines.

Bruno H. Zimm and RALPH W. KILB. Dynamics of Branched Polymer Molecules in Dilute Solution. *Phase Equilibrium in Mixtures*, XXXVII:203–270, 1969. doi: 10.1016/b978-0-08-012301-1.50009-6.

Bruno H. Zimm and Walter H. Stockmayer. The dimensions of chain molecules containing branches and rings. *The Journal of Chemical Physics*, 17(12):1301–1314, 1949. ISSN 00219606. doi: 10.1063/1.1747157.